DISSERTATION

RGS4, CD95L and B7H3: Targeting evasive resistance and the immune privilege of glioblastoma

Philipp-Niclas Pfenning

2011

DISSERTATION

submitted to the

Combined Faculties for the Natural Sciences and for Mathematics

of the Ruperto-Carola University of Heidelberg, Germany

for the degree of

Doctor of Natural Sciences

presented by

Diplom-Biologe Philipp-Niclas Pfenning
born in Heidelberg, Germany

Oral Examination: 06.05.2011

RGS4, CD95L and B7H3: Targeting evasive resistance and the immune privilege of glioblastoma

Referees: Prof. Dr. Hilmar Bading
Prof. Dr. Wolfgang Wick

Dedicated to my wife

Acknowledgements

I wish to express my deepest gratitude to my thesis supervisor Prof. Dr. Wolfgang Wick for his constant support and encouragement, his confidence and dynamism as well as for the excellent working conditions.

I am thankful to Prof. Dr. Hilmar Bading for examination and for evaluation of my thesis, to PD Dr. Karin Müller-Decker and Dr. Marius Lemberg for examination and to Prof. Dr. Andreas von Deimling for being a member of my PhD Thesis Advisory Committee.

My sincere thanks go to Dr. Markus Weiler for introducing me to the exciting field of glioma research and for his supervision and scientific support. I would also like to thank Dr. Dieter Lemke for sharing the project and for his precious ideas. Furthermore, I appreciate the additional tutorship of Prof. Dr. Michael Platten and his ideas and suggestions.

I am very grateful to all my collaboration partners at the German Cancer Research Center, at the University Hospital Heidelberg and at Apogenix GmbH for their valuable support and fruitful contributions to the different projects of my thesis.

Special thanks go to Ulli Litzenburger for scientific and also not so scientific discussions as well as the fun we had during the time we spent together in the lab and in the 'outside world'.

I would like to thank all present and former lab members of the 'G370 and G160' for the good working atmosphere, for scientific and practical support and all the things that would take up too much space to be mentioned here. Special thanks in this regard to Jonas Blaes for being such a great office mate. My thanks also go to Dr. Regine Garcia-Boy for critical reading of the manuscript.

Further, I would like to thank my family and friends for encouragement throughout my PhD thesis.

Finally, I am deeply grateful to my beloved wife Katja for cheering me up over and over again and for being the most supportive person in my life.

Summary

Glioblastoma are the most common primary brain tumors in adults with a median survival of one year even with multimodal therapy including surgical resection, radiotherapy, and chemotherapy. Important hallmarks of these tumors are vascular proliferation, diffuse invasion of tumor cells into the surrounding brain tissue and effective suppression of the immune system. The efficacy of resection and current radiochemotherapy treatment regimens are therefore extremely limited. Both the genesis and development as well as the progression of malignant gliomas are highly dependent on angiogenic processes, the formation of new blood vessels from pre-existing vessels. Current treatment strategies tested in clinical trials targeting tumor angiogenesis have so far not been proven to increase survival of the patients. In addition to the insufficiency of clinical trials done, this has been attributed to several potent evasion strategies occurring at disease progression and recurrence, including increasing infiltrative tumor growth, commonly referred to as 'evasive resistance'. These invasive growth patterns occur in addition as responses to radiotherapy and essentially trigger disease progression and have a strong influence on patients' survival.

Parts of the work presented here address the challenge of targeting the evasive resistance in glioblastoma in order to develop novel treatment strategies for a clinical application which combine anti-angiogenic with radio-enhanced anti-invasive modalities. Several strategies, focusing on different molecular targets, were undertaken: (1) Activation of the PI3K/AKT/mTOR signaling pathway is relatively common in human glioblastoma and is associated with poor survival. A clinically relevant radiation-enhanced inhibition of this pathway, using the mTOR inhibitor CCI-779, resulted in the dual control of angiogenesis and excessive invasiveness. This is mediated by a combined disrupture of the VEGF/VEGFR-2 angiogenic signaling axis on glioblastoma as well as on endothelial cells and suppression of RGS4, which was identified to be a key driver of glioblastoma invasiveness. (2) Following compelling evidence, proving that invasiveness is mediated in apoptosis-resistant glioblastoma in part by the CD95 death receptor system, antagonism of the receptor-ligand interaction was accomplished by the CD95-ligand inhibitor APG101. Clinically relevant administration of this novel compound resulted in inhibition of invasion-driving effector molecules, reduced unwanted radiotherapy-induced invasiveness, and prolonged survival of glioma-bearing mice.

In addition to increased angiogenesis and invasive growth, glioblastoma effectively inhibit antitumor immune responses. Impaired recognition and attack by the immune system is effectively achieved by creating an immunosuppressive microenvironment through expression and secretion of several factors. In order to identify potential immunotherapy related targets, the costimulatory molecule B7H3 was investigated for its role in glioblastoma immunobiology. Expression correlates with grades of glioma malignancy and is associated with poor patients' survival. Cell-bound and secreted B7H3 was identified to suppress tumor attacks by the immune system as well as to mediate invasiveness of glioblastoma cells.

From the findings presented in this thesis, several therapeutic options emerge for targeting unwanted adaptive evasive escape and immunosuppression and should be considered for further clinical investigation in glioblastoma therapy.

Zusammenfassung

Das Glioblastom ist der im Erwachsenenalter am häufigsten auftretende Gehirntumor. Durch die derzeitige multimodale Standardtherapie bestehend aus chirurgischer Entfernung, Strahlentherapie und adjuvanter Chemotherapie kann meist nur eine mittlere Überlebensdauer von etwas mehr als einem Jahr erreicht werden. Gekennzeichnet ist das Glioblastom durch eine verstärkte Neubildung von Blutgefäßen, einem infiltrierenden, diffusen Wachstum in das umliegende Gehirngewebe und einer effektiven Unterdrückung des Immunsystems. Die Ausbildung eines Tumorblutgefäßsystems (Angiogenese) zur ausreichenden Versorgung des Tumors mit Nährstoffen, ist ein essentieller Bestandteil für das Wachstum des Glioblastoms. Derzeitige in der klinischen Erprobung befindliche, gegen die Angiogenese gerichtete Behandlungsstrategien, konnten bisher das Überleben der Patienten nicht signifikant verlängern. Neben dem insuffizienten Studiendesign ist dies ist zum Teil auf Resistenzmechanismen zurückzuführen, durch die der Tumor seine infiltrative Ausbreitung als Antwort auf die gefäßnormalisierende und reduzierende Therapie verstärkt. Dieses als „ausweichende Resistenz“ beschriebene Verhalten des Tumors wurde auch als Resistenzmechanismus auf die Strahlentherapie beschrieben und bestimmt in großem Maße den malignen Verlauf dieser Tumorerkrankung.

Große Teile dieser Arbeit beschäftigen sich demnach mit der Entwicklung von gezielten, auf die evasive Resistenz ausgerichteten Therapieformen, durch die sowohl das invasive Wachstum wie auch die Angiogenese unterdrückt werden sollen. (1) Die Aktivierung des PI3K/AKT/mTOR Signalweges ist in malignen Gliomen sehr häufig nachweisbar und assoziiert mit einem schlechteren Überleben der Patienten. Durch die kombinierte Anwendung von ionisierender Strahlung und eines spezifischen pharmakologischen Inhibitors des mTOR-Proteinkomplexes wurden sowohl die Angiogenese als auch das invasive Tumorwachstum kontrolliert und reduziert. Dies wurde durch eine duale Inhibierung des VEGF/VEGF-Rezeptor 2 Signalweges in Glioblastom- und Endothelzellen, sowie durch eine Unterdrückung von RGS4, einem in dieser Arbeit identifizierten, für die Invasion sehr bedeutsamen Schlüsselmoleküls, vermittelt. (2) Neueren Hinweisen zufolge führt die Stimulierung des CD95-Todesrezeptors in Apoptose-resistenten Zellen zu einem Anstieg der Invasion einzelner, isolierter Glioblastomzellen. Diese CD95-vermittelte Invasion konnte im Rahmen dieser Arbeit durch eine Inhibierung des CD95-Liganden mittels eines neuen Wirkstoffes (APG101) effektiv verhindert werden. Die Anwendung von APG101 in einem etablierten Glioblastommodell der Maus resultierte zudem in einem verlängerten Überleben und geringerer Ausbildung strahleninduzierter Tumorsatelliten im umliegenden Gewebe.

Neben der Angiogenese und einem verstärkten infiltrativen Wachstum erschwert eine effektive Unterdrückung des Immunsystems die Behandlung von Glioblastomen. Durch die Expression und Präsentierung verschiedener immunsuppressiver Moleküle sind diese Tumore in der Lage sich der Erkennung und des Angriffs durch das Immunsystem zu entziehen. Mit dem Ziel, potentielle Moleküle für eine Immuntherapie zu charakterisieren, wurde die Rolle des kostimulatorischen Proteins 4IgB7H3 in Glioblastomen untersucht. Die Expression korreliert hierbei mit dem Grad der Malignität verschiedener Gliome und ist assoziiert mit einem schlechteren Überleben. Zudem konnte für Glioblastom-assoziiertes 4IgB7H3 erstmals eine duale Rolle in der Vermittlung der Immunsuppression und der Invasion nachgewiesen werden. Die in dieser Arbeit über die Biologie maligner Gliome gewonnenen Erkenntnisse liefern vielfältige Ansatzpunkte für die klinische Entwicklung verschiedener zielgerichter und kombinierter Therapieformen zur Behandlung der evasiven Resistenz und Immunsuppression bei Glioblastomen.

List of Publications

Pfenning P*, Weiler M*, Thiepold A, Jestaed L, Gronych J, Dittman L, Berger B, Jugold M, Combs S, Platten M, Wick W. (2010). *Novel anti-invasive and anti-angiogenic mechanisms of mTOR inhibition in glioblastoma*. Proceedings of the 101st Annual Meeting of the American Association for Cancer Research; Washington DC: AACR, 2010. Abstract nr. 1308. *Authors contributed equally.

Weiler M*, **Pfenning PN***, Thiepold A, Jestaed L, Gronych J, Dittman L, Berger B, Jugold M, Kosch M, Weller M, Combs S, von Deimling A, Bendszus M, Platten M, Wick W. (2011). *Suppression of invasion-driving RGS4 by mTOR inhibition optimizes glioma treatment.* Manuscript submitted for publication. *Authors contributed equally.

Pfenning PN, Weiler M, Merz C, Jugold M, Haberkorn U, Abdollahi A, Rieken S, Gieffers C, Platten M, Fricke H, Wick W. (2011). *Inhibition of CD95 signalling by APG-101 enhances efficacy of radiotherapy (RT) and reduces RT-induced tumor satellite formation in glioblastoma.* Proceedings of the 102nd Annual Meeting of the American Association for Cancer Research; Orlando/FL: AACR, 2011.

Lemke D*, **Pfenning PN***, Sahm F, Klein AC, Kempf T, Warnken U, Schnölzer M, Tudoran RI, Weller M, Platten M, Wick W. (2011). *Co-stimulatory protein 4IgB7H3 drives the malignant phenotype of glioblastoma by* mediating *immune escape and invasiveness*. Manuscript submitted for publication. *Authors contributed equally.

Related publications, not included in the thesis:

Berger B, Capper D, Lemke D, **Pfenning PN**, Platten M, Weller M, von Deimling A, Wick W, Weiler M (2010). *Defective p53 antiangiogenic signaling in glioblastoma*. Neuro Oncology 12: 894-907.

Table of Contents

1. Introduction

1.1 Tumors of the central nervous system

The mammalian central nervous system (CNS), consisting of the brain and the spinal cord, is comprised of two major cell populations, which are neurons and glia. The latter, discovered in 1846 by Rudolf Virchow, can be divided into two different subgroups, macroglia and microglia. Macroglia are further divided into several subpopulations with different functions and morphologies: astrocytes, oligodendrocytes and ependymal cells. Astrocytes are the most abundant type of macroglial cells and fulfill various important functions. These include the support of neurons by regulating synapse formation and synapse transmission, the induction of neurogenesis and the initiation of immune responses. Oligodendrocytes are the myelin-synthesizing cells in the CNS. Tumors of the CNS are relatively common with annually more than 8,000 newly diagnosed tumors in Germany and more than 40,000 in the United States. Although only 2% of newly diagnosed cancers are CNS tumors, they represent the third leading cause of death from cancer in adults [1]. Classification of CNS tumors is roughly based on the distinction between gliomas and non-gliomas. The latter group consists of benign tumors, such as meningiomas, as well as malignant tumors, such as medulloblastomas, neuroblastomas and CNS lymphomas [1]. Gliomas are defined as primary CNS tumors originating from macroglial cells or their precursors and include various histologic grades of astrocytoma, oligodendroglioma, ependymoma and oligoastrocytic tumors.

1.2 Classification and biology of gliomas

The group of gliomas consists of three different tissue types: astrocytomas, oligodendrogliomas, and ependymomas. The most common gliomas - around 80% of all primary malignant brain tumors [2] are astrocytomas, by morphological and rough genetic definition tumors that arise from astrocytes after malignant transformation and proliferation. The grading system of the World Health Organisation (WHO) categorises astrocytic tumors based on their grade of malignancy, which is determined by key histological features, like increased cellularity, mitoses, endothelial proliferation, and necrosis (Table 1).

As a group, gliomas include tumors with a wide range of histological forms, from benign to highly malignant: WHO grade I astrocytomas display a circumscribed growth and retain their well-differentiated histological features, whereas tumors of grade II-IV are de-differentiated and tend to infiltrate diffusely into the surrounding brain tissue.

Table 1. Grading system of astrocytomas according to "The 2007 WHO grading of tumors of the central nervous system" [3] and corresponding patient survival rates [2].

Grade	Denotation	Histological Criteria	5-year survival rate
I	Pilocytic astrocytoma	Circumscribed morphology, non-infiltrating	80%
II	Diffuse astrocytoma	Diffusely infiltrating, nuclear atypia	47%
III	Anaplastic astrocytoma	As grade II + increased cellularity, mitotic activity	30%
IV	Glioblastoma	As grade III + nuclear atypia, mitotic activity, endothelial proliferation, tumor necrosis	4%

Transformation of low-grade (WHO grade II) astrocytoma into a higher grade after 4-5 years is frequently observed.

Common presenting symptoms of gliomas include headache, seizures, altered mental status and focal neurological symptoms and are related to mass effects and tissue destruction. Tumor diagnosis comprises besides a neurological examination different imaging methods, such as Computed X-ray Tomography (CT), Magnetic Resonance Imaging (MRI) and Positron Emission Tomography (PET). Typical ranges of survival are 10 years from the time of diagnosis for pilocytic astrocytoma (WHO grade I), more than 5 years for diffuse astrocytoma (WHO grade II), 2-5 years for patients with anaplastic astrocytomas (WHO grade III) and less than 1 year for patients with glioblastoma (WHO grade IV). Treatment strategies differ in their composition with respect to the diagnosed tumor grade. Standard treatment of newly diagnosed low-grade gliomas consists of maximal surgical resection, whereas in high-grade gliomas, like glioblastoma, radiotherapy alone or together with concomitant and adjuvant chemotherapy are usually applied immediately in addition to tumor resection. Recurrence occurs at high frequency in all WHO grade II-IV gliomas due to the extensive invasive growth behavior and therapy resistance. Taken this into account, one major focus of current anti-glioma research lays in the development of novel therapeutic approaches targeting glioma invasion.

1.3 Clinical characteristics and standard therapy of glioblastoma

Glioblastoma or glioblastoma multiforme (GBM), a WHO grade IV astrocytoma, is the most common and most malignant form of the primary brain tumors in adults [4] accounting for approximately 50% of all glial tumor types [5]. Prognosis of glioblastoma patients remains poor, given the fact that without therapeutic intervention, patients die within 3 months. Survival can be extended by optimal therapy, including resection, radiation therapy, and chemotherapy to approximately 12-15 months, with fewer than 25% of patients surviving up to two years [5]. Average age at tumor diagnosis is 55

years, with a slight predominance of males over females [6]. The pathological characteristics of these tumors include increased cellularity, nuclear atypia, frequent mitosis, areas of necrosis and endothelial proliferation [7]. Glioblastoma can be classified as primary or secondary. Primary glioblastoma manifest without clinical evidence of a pre-existing, less-malignant precursor lesion and account for 80-90% of cases. Secondary glioblastoma develop through malignant progression from low-grade or anaplastic astrocytoma (WHO grade II and III; [8]).

The characteristic molecular lesions of primary glioblastoma are epidermal growth factor receptor (EGFR) amplifications or mutations as well as phosphatase and tensin homologue deleted on chromosome 10 (PTEN). Whereas secondary glioblastoma are characterized by p53 and isocitrate dehydrogenase (IDH) mutations. Other common characteristic genetic alterations in glioblastoma are (I) loss of heterozygosity (LOH) on chromosome arm 10q, which harbours PTEN, (II) losses of 9p with the CDKN2A locus and (III) gains on chromosomes 7q and 12p [9-13]. However, none of these genetic changes associated with the pathogenesis of gliomas are able to predict response to current treatment standards [14].

In 2006, three novel subclasses of high-grade gliomas were defined, which are characterized by distinct clinical and molecular characteristics [15]. The identified tumor subclasses show a prognostic value and delineate a pattern of disease progression, as the proneural (PN) signature was significantly over represented among less aggressive forms of high-grade gliomas, while the proliferative (Prolif) and mesenchymal (Mes) signatures overlapped with poor risk disease [15, 16].

Standard treatment of glioblastoma currently consists of maximal surgical resection, radiotherapy, and concomitant and adjuvant chemotherapy. Post-operative radiation treatment, commonly administered to a total dose of 60 Gy delivered in 2 Gy fractions over 30 days, is routinely performed and significantly improves survival of glioblastoma patients [1]. In order to control tumor growth and maintain a good quality of life for these patients, the use of chemotherapy is well established for the treatment of glioblastoma.

The chemotherapeutic standard of care for patients with newly diagnosed glioblastoma only changed back in 2005, when the concomitant and adjuvant application of the alkylating agent Temozolomide (TMZ) proved to increase median and 2-year survival of patients when added to radiation therapy [17]. TMZ is an orally available prodrug which penetrates into the brain and methylates guanine residues in the DNA, leading to base/base mismatches which result in cell death. Unfortunately, resistance to this drug is mediated by the DNA repair protein O^6-methylguanine-DNA methyltransferase (MGMT), through its ability to remove methyl/alkyl groups from the O^6 -position of guanine and thereby preventing TMZ-induced DNA damage. Approximately 50% of the patients,

namely those with a methylated/epigenetically silenced *MGMT* promoter, i.e. no expression of MGMT benefit from temozolomide whereas those with an unmethylated *MGMT* promoter do not [18]. DNA methylation of MGMT is therefore considered to be a predictive marker for benefit from TMZ treatment. Other treatments for glioblastoma either upfront or at recurrence include the use of alkylating agents (e.g. lomustine or carmustine), procarbazine,topoisomerase inhibitors and at least in several countries, antiangiogenic treatments like the antibody against vascular endothelial growth factor (VEGF), bevacizumab [19].

Taken together and despite all study activity, the need for a research-based effective glioblastoma therapy is evident, given the fact that only half of the glioblastoma patients response to current standard therapy and that this response is only in the range of two months.

1.4 Biological properties of glioblastoma

Despite some proven beneficial impacts on patient's survival, current treatment results are still unsatisfactory. This is in large part due to certain key biological features of glioblastoma, such as rapid cellular proliferation, increased invasive growth, potent angiogenic signaling, and resistance against radiation. These biological factors will be discussed in the following chapter.

1.4.1 Invasiveness

One of the main reasons for the highly malignant phenotype and the dismal prognosis of glioblastoma is invasion of isolated tumor cells into the surrounding brain tissue. This limits the feasibility of local treatment like surgical tumor resection and involved-field radiotherapy to a massive extent. Moreover, gliomas tend to disseminate along myelinated fibre tracts of white matter, which may even results in the spreading of tumor cells through the corpus callosum into the contralateral hemisphere [20].

1.4.1.1 Cellular processes involved in glioma invasion

Invasion of tumor cells involves four independent but highly coordinated processes [21,22]:

(I) Detachment from the tumor mass, involving downregulation of neural cell adhesion molecules (NCAMs) and E-cadherin as well as upregulation of CD44, a glycoprotein which functions as an adhesion molecule. (II) Attachment to extracellular matrix (ECM), mediated by integrins and tenascin-C. (III) Degradation and remodelling of the ECM, including the activity of matrix metalloproteinases (MMPs), and (IV) Migration, requiring cytoskeletal rearrangements and formation of lamellipodia and filopodia (Figure 1).

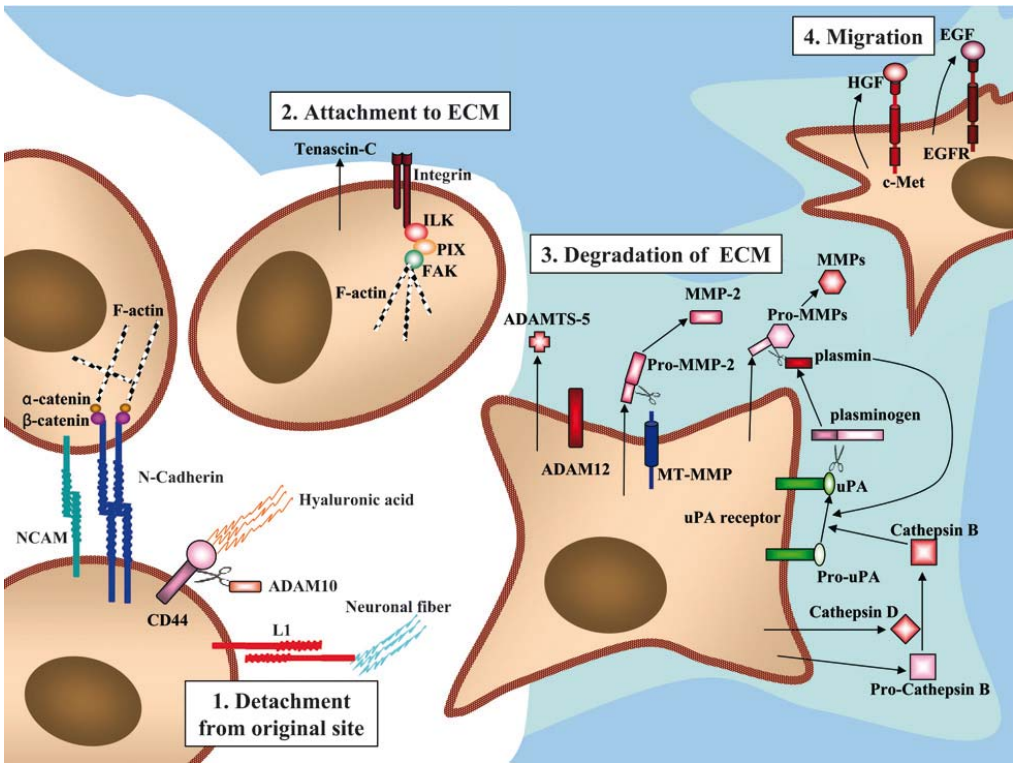

Figure 1. Underlying intracellular and extracellular mechanisms of glioma cell invasion [21]

Attachment of tumor cells to the extracellular matrix is mediated by integrins, a family of heterodimeric transmembrane proteins [23]. Combinations of different alpha and beta subunits form at least 22 different receptors. Integrins are promising targets in glioblastoma therapy, given that $\alpha_V\beta_3$ and $\alpha_V\beta_5$ integrins are overexpressed on both glioma cells as well as on the tumor vasculature [24]. Cilengitide (EMD 121974) is a specific inhibitor of the above mentioned integrin receptors overexpressed in glioblastomas and is currently under clinical investigation for its potential to synergize with standard radiochemotherapy (CENTRIC study).

The process of invasion includes the degradation and destruction of extracellular matrix components by proteases. Protease expression studies in glioblastoma revealed upregulation of serine protease urokinase-type plasminogen activator (uPA), its receptor uPAR and matrix metalloproteinases MMP-2 and MMP-9 [25-27]. MMPs are Zn^{2+}-dependent endopeptidases that are essential for an ECM turnover under normal and pathological conditions [26]. They mediate the breakdown of the basal membrane and create and maintain a microenvironment that facilitates tumor cell survival [28]. Strong correlations have been reported not only between MMP expression, especially MMP-2 and MMP-9, and glioma cell invasion [29] but also with poor prognosis in glioma patients [21, 30]. A promising approach to inhibit increased MMP production by invading tumor cells involves targeting the signaling-transduction mechanisms that mediate their induction. Unfortunately, MMP-2/-9 inhibition is resulting in serious side effects and efficacy is not yet proven in brain tumors [31-33].

1.4.1.2 Signaling-mechanisms driving glioma invasion and progression

Glioma invasiveness is mediated for the most part by genetic alterations, which are commonly found in these tumors, leading to activation of invasion-related signal transduction pathways. This includes mutated or deleted tumor suppressor genes, such as PTEN or overexpression of oncogenes, such as *epidermal growth factor receptor (EGFR).*

I. Epidermal growth factor receptor (EGFR) and the PI3K/AKT/mTOR pathway

The epidermal growth factor receptor (EGFR) is a member of the EGFR receptor family of receptor tyrosine kinases. It plays an important role in regulating proliferation, angiogenesis, migration, tumorigenesis and metastasis. Overexpression as well as mutations of the EGFR contribute to aberrant activation of downstream effectors in various tumor entities [34]. In glioblastoma, activation of EGFR is present in 40–60% of all tumors [35] and correlates with a poor outcome in patients [36, 37]. Induction of receptor phosphorylation is mediated through binding of several ligands, including EGF and transforming growth factor α (TGF-α), and leads to the activation of a complex downstream signaling network [38]. In glioma, a number of pro-invasive effector molecules are upregulated through EGFR-stimulation, including MMPs and other proteases [39].

The canonical EGFR signaling pathway leads to downstream activation of the phosphatidylinositol 3-kinase (PI3K)/protein kinase B (AKT)/mammalian target of rapamycin (mTOR) signaling axis (Figure 2). Upregulation of the PI3K/AKT/mTOR pathway is relatively common in brain tumors as a result of EGFR amplification or excessive stimulation by growth factor receptors [30, 40] and leads to cell cycle progression, neovascularization, escape from apoptosis, and inhibition of autophagy. For gliomas, aberrant activation of the pathway is significantly associated with increasing glioma tumor grade and an adverse clinical outcome [41]. The mammalian target of rapamycin (mTOR) is an AKT-dependent protein kinase and part of two distinct multi-protein complexes, called mammalian target of rapamycin complex 1 and 2 (mTORC1 and mTORC2 [42-45]. The mTor signaling pathway integrates both intracellular and extracellular signals and serves as a central regulator of cell metabolism, growth, proliferation and survival (Figure 2). Activation occurs during various cellular processes, for example tumor formation and angiogenesis, insulin resistance and T-lymphocyte activation and is commonly deregulated in human diseases such as cancer and type 2 diabetes [46].

mTORC1 is a protein kinase complex that consists of five components: mTOR, which is the catalytic subunit of the complex, regulatory-associated protein of mTOR (Raptor), mammalian lethal with Sec13 protein 8 (mLST8, also known as GβL), proline-rich AKT substrate 40 kDa (PRAS40), and DEP-domain-containing mTOR-interacting protein (Deptor; [47]). Regulation of cell growth by mTORC1 is modulated by various processes, including protein synthesis, ribosome biogenesis and autophagy

[47, 48]. Important molecular downstream effectors of mTORC1 are regulators of translation such as 4EBP1 (eukaryotic translation initiation factor 4E binding protein 1) and S6K1 (ribosomal S6 kinase 1). mTORC2 comprises six different proteins, of which several are common to mTORC1 and mTORC2: mTOR; rapamycin-insensitive companion of mTOR (Rictor), mammalian stress-activated protein kinase interacting protein (mSIN1), protein observed with Rictor-1 (Protor-1) mLST8, and Deptor. In glioma, TORC2 is hyperactivated and leads to promotion of tumor cell invasion via Rictor [47].

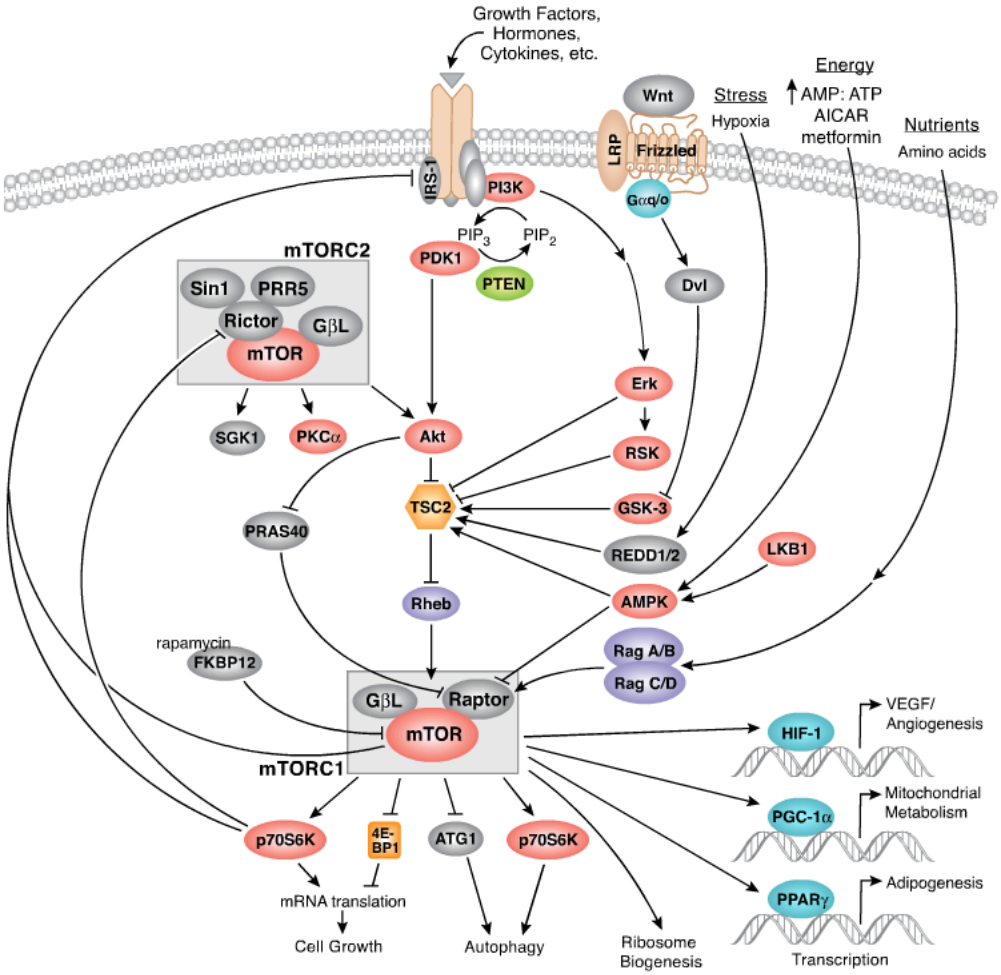

Figure 2. The mTOR signaling pathway

mTORC1 is composed of mTOR, Raptor, GβL (mLST8), and Deptor and is partially inhibited by rapamycin. mTORC1 integrates multiple signals to promote either cellular growth when conditions are favorable or catabolic processes during cellular stress. Growth factors and hormones (e.g. insulin) signal to mTORC1 via AKT, which inactivates TSC2 to prevent inhibition of mTORC1. Active mTORC1 has a number of downstream biological effects including translation of mRNA via the phosphorylation of downstream targets (4E-BP1 and p70 S6 Kinase), suppression of autophagy, ribosome biogenesis, and activation of transcription leading to mitochondrial metabolism or adipogenesis. **mTORC2** is composed of mTOR, Rictor, GβL, Sin1, PRR5/Protor-1, and Deptor and promotes cellular survival by activating AKT mTORC2 also regulates cytoskeletal dynamics and regulates ion transport and growth (adapted from Cell Signaling Technology, Inc.).

Rapamycin (also known as sirolimus), a macrolide that was originally discovered as an antifungal agent, is a potent inhibitor of the mTOR-complex 1. Temsirolimus (CCI-779), the mTOR-inhibitor used in this study, is a soluble ester analog of rapamycin, formulated for intravenous application. After bioconversion to sirolimus, it binds to the cytosolic immunophilin FK506-binding protein 12 (FKBP12), and this protein-drug complex inhibits mTOR-mediated phosphorylation of S6K1 and 4E-BP1 [49].

The PI3K/AKT/mTOR pathway has several forms of regulation, the most important one is mediated by PTEN. PTEN is a tumor suppressor and acts as a lipid phosphatase. By dephosphorylating phosphatidylinositol (3,4,5)-trisphosphate (PIP_3), PTEN antagonizes PI3K activity and thereby several downstream effectors like AKT and mTOR (Figure 2). In non-malignant cells with a functioning *PTEN* gene, PIP_3-mediated activated AKT is held on a low level, whereas in PTEN-deficient tumor cells AKT is highly activated and able to promote tumor cell growth via its numerous downstream effectors. Importantly, in gliomas increasing malignancy is correlated with decreased *PTEN* transcript levels [50]. This is also reflected by findings from Wang *et al.* [51] who detected mutated or deleted *PTEN* genes in 30% to 40% of glioblastoma patients.

II. Transforming growth factor beta (TGF-β)

Transforming growth factor-β (TGF-β) is a cytokine involved in cell growth, differentiation, and immune response modulation [52, 53]. The TGF-β protein is released into the intercellular space, where it is stored in the extracellular matrix [28]. Signaling cascades are initiated by binding of TGF-β to three different receptors, TGF-βRI–III. TGF-βRI and -II are serine-threonine protein kinases that form complexes and phosphorylate the Smad transcription factors [28, 54]. TGF-β signaling exhibits strong effects on migration and invasion of glioma cells [55, 56] based on upregulated $\alpha v b_3$ integrin expression [57] and induction of MMP-2 and MMP-9 expression paralleled by downregulation of endogenous MMP inhibitors [28].

III. CD95 death receptor

CD95 (APO-1/Fas) is a prototype death receptor that regulates tissue homeostasis by the induction of apoptosis, upon binding of its ligand CD95L and subsequent formation of a death-inducing signaling complex (DISC; [58, 59]). Due to a suppressed CD95-induced apoptosis in cancer cells, increase of apoptosis sensitivity by pharmacological stimulation of the CD95/CD95L-system has long been in the focus of anticancer research. Treatment with anticancer drugs leads to an increase in CD95L expression which stimulates the receptor in an autocrine or paracrine manner [60-62].

However, there is growing evidence in recent years that CD95 is able to promote tumor growth through intracellular non-apoptotic signaling mechanisms, besides its pro-apoptotic role [63, 64]. Regardless of the CD95 apoptosis sensitivity, tumor progression depends on constitutive activity of

CD95, stimulated by cancer-produced CD95L. This autocrine mediated growth-promoting role of the CD95/CD95L-system has recently been described also for glioblastoma [65, 66]. In this regard activation of CD95 by CD95L stimulates AKT kinase and beta-catenin depending cascades (Figure 3), irrespective of a DISC-formation [65]. This leads to invasive growth and migration by an increased expression of MMPs, which are key mediators of glioma invasion, as discussed above.

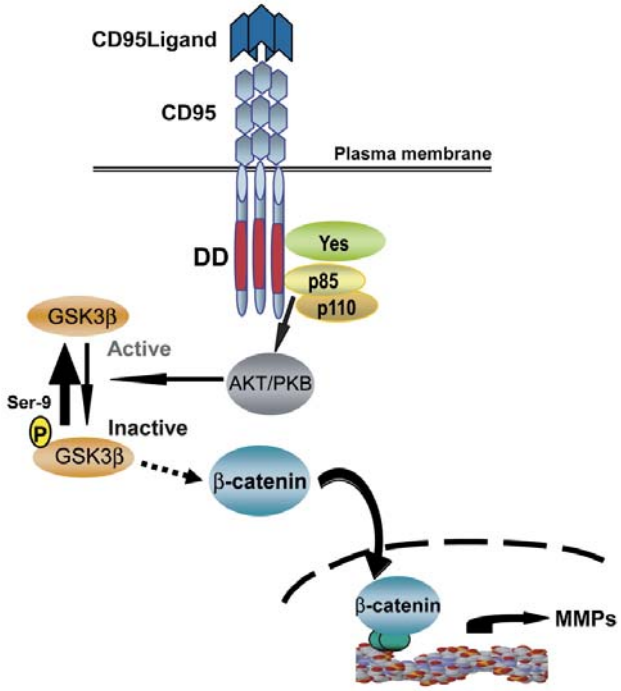

Figure 3. The CD95 induced signaling pathway leading to glioma cell invasion by the induction of MMP
CD95L induces recruitment of the Src family member Yes and the p85 subunitof PI3K (depicted here by its two subunits: p85 and p110) to CD95, thereby activating AKT. Activated AKT phosphorylates and inactivates GSK3β, allowing β-catenin translocation into the nucleus, where it induces transcription of MMPs [65].

In order to inhibit this CD95-mediated pro-invasive signaling and to transfer this concept into the clinic, a CD95L inhibitor was developed: APG101 (Apogenix GmbH Heidelberg) is a fusion protein, consisting of the extracellular domain of the human CD95 receptor and the Fc- region of human immunoglobulin G. Due to this composition an effective receptor signaling blockage can be achieved through specific binding of the CD95 ligand. Furthermore, the compound can be utilized in the clinic due to its ability to reach the tumor site via the blood brain barrier.

IV. Ionizing radiation

Radiation therapy after neurosurgical tumor resection is an effective clinically treatment modality [24]. However, ionizing radiation has been shown to increase invasiveness of glioma cells [67, 68]. This is mediated by the stimulation of MMP-2 and MMP-9 expression through activation of the EGFR and subsequent stimulation of the PI3K/AKT pathway [69]. Taken into account that radiochemotherapy is the standard of care in high-grade gliomas, these responses are exceedingly unwanted and need to be overcome.

V. Hypoxia

Glioblastoma invasion is not only triggered by genetic aberrations but also by signals that dispose tumor cells to evade the tumor mass. Hypoxia, defined as deprived oxygen supply to the tumor mass, is therefore one of the key drivers of glioma cell invasion, since glioblastoma are highly hypoxic tumors. One of the master regulator of different cellular responses to hypoxia is the hypoxia-inducible factor 1 (HIF-1). It is a heterodimeric transcription factor composed of a α and β subunit. The α-subunit is unstable and degraded by the proteasome under limited oxygen conditions (normoxia). In hypoxic conditions upon stabilization of the α subunit, HIF-1 translocates into the nucleus and induces transcription of its different downstream target genes [70, 71]. Activation of the PI3K/AKT/mTOR pathway by receptor tyrosine kinases has been shown to increase HIF-1α by modulating its stability and enhancing *HIF* gene expression (Figure 2; [72]).

HIF-1α acts as a strong activator and driver for angiogenesis, the formation of new blood vessels from existing vessels. This issue will be discussed in detail in the following chapter dealing with the principles of angiogenesis in glioma.

Glioblastoma cells, found at the invasive tumor front, have upregulated HIF-1α expression levels, hinting at a role of HIF in the regulation of invasion and migration. Indeed, HIF-1α promotes invasion by regulating the expression of MMP-2 in glioma cells [70, 73].

VI. Autocrine signals

Besides different paracrine stimuli which drive glioma cell invasion, glioblastoma cells themselves secrete several factors for an autocrine motility signaling. In this regard, the cell surface chemokine receptor 4 (CXCR4) and its ligand chemokine ligand 12 (CXCL12) have been shown to be involved in an invasive phenotype in malignant gliomas [74]. Additional autocrine driven receptor-ligand pairs playing a role in glioma invasiveness are the hepatocyte growth factor/scatter factor (HGF/SF) and its receptor, Met tyrosine kinase receptor (Met) as well as the platelet derived growth factor (PDGF) and its receptor PDGFR [75, 76].

1.4.2 Angiogenesis

Since mammalian cells require oxygen and nutrients for their survival, they are located within 0.1–0.2 mm to blood vessels, which is the diffusion limit for oxygen [77, 78]. However, proliferating tumor cells quickly grow beyond this oxygen diffusion distance and are then restricted in their growth potential due to the lack of an efficient blood supply. In order to spread further distances they have to recruit new blood vessels from pre-existing vessels by a process defined as angiogenesis [79-81]. The induction of angiogenesis in the vasculature is described as the 'angiogenic switch' [82] and is caused by a misbalance of anti- and pro-angiogenic factors [83].

Tumors are able to shift the balance between pro- and anti-angiogenic regulators to the pro-angiogenic side. This results in a failure of the sprouting endothelium to maturate and become quiescent. Similarly to normal and controlled angiogenesis, which occurs during embryogenesis and in tissue repair mechanisms, the vascular basement membrane and the extracellular matrix are locally degraded [84] and endothelial cell sprouts migrate into the perivascular space. New vessels are formed and perivascular cells are recruited.

Both the development as wells as the progression of malignant gliomas are highly dependent on angiogenic processes. Due to a very potent pro-angiogenic signaling, glioblastomas are among the best vascularized human tumors, whereas microvascular proliferation cannot be observed in low-grade gliomas. Angiogenic factors like vascular endothelial growth factor (VEGF), basic fibroblast growth factor (bFGF) and platelet derived growth factor (PDGF) released by glioblastoma cells effectively stimulate the endothelial cells of the surrounding brain vasculature system (Figure 4). In comparison to normal blood vessels this pro-angiogenic signaling results in a significantly altered blood vessel structure, which is characterized by immature, disorganized, highly permeable and leaky vessels with larger diameters and thicker basement membranes. Of note, the high vascularization of gliomas is also the basis for tumor visualization by MRI in patients and animals models. Following intravenous injection, the paramagnetic contrast medium gadolinium is distributed throughout the blood stream, accumulates in tumors, and disturbs the magnetic field in regions of high vascularization, resulting in enhanced MRI signals [78].

VEGF is perhaps the most important and best investigated angiogenic factor that is released by tumor cells in order to stimulate endothelial cell sprouting. VEGF, a 45kDa glycoprotein, belongs to a family of growth factors that includes VEGF-A to E, with VEGF-A as the predominant form. Expression of VEGF is increased in response to hypoxia and is mediated by activation of VEGF gene transcription through HIF-1α [70, 85]. In glioma VEGF-A is upregulated and regulates endothelial cell survival, proliferation and migration by binding to the vascular endothelial growth factor receptor 2 (VEGFR-2; Figure 5).

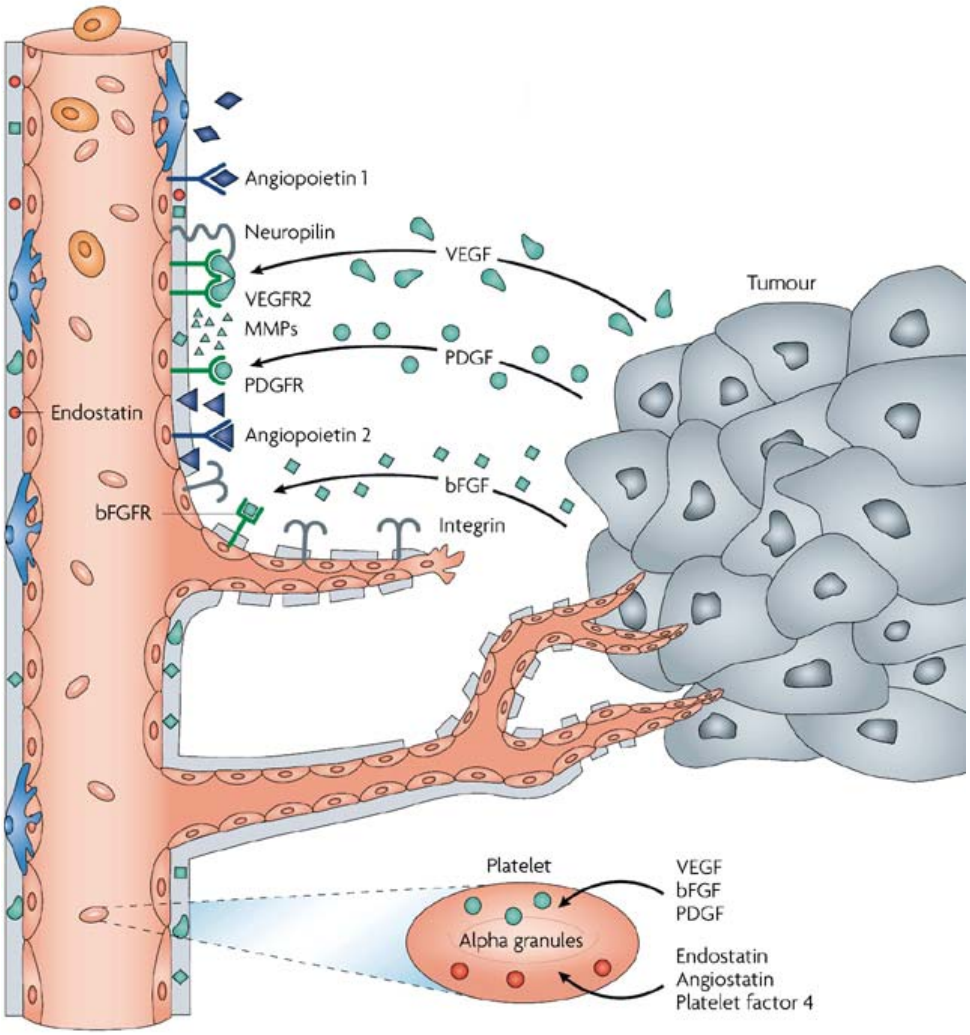

Figure 4. Key steps in tumor angiogenesis

Vascular endothelial growth factor **(VEGF)** is secreted by tumour cells and binds to its receptor **VEGFR2** on endothelial cells. Matrix metalloproteinases **(MMPs)** are released from tumour cells, but also by VEGF-stimulated endothelial cells. MMPs mobilize pro-angiogenic proteins from stroma. Tumour cells secrete **angiopoietin 2** (ANGPT2), which competes with ANGPT1 for binding to the endothelial TIE2 receptor. ANGPT2 increases the degradation of vascular basement membrane and migration of endothelial cells, therefore facilitating sprout formation. Platelet-derived growth factor **(PDGF)**, an angiogenic protein secreted by some tumours, can upregulate its own receptor PDGFR on endothelial cells. Basic fibroblast growth factor **(bFGF)** is secreted by other tumours. **Integrins** facilitate endothelial cell binding to extracellular membranes. Endothelial growth factors are not all delivered to the local endothelium directly from tumour cells. Some angiogenic regulatory proteins are scavenged by platelets, stored in alpha granules and seem to be released within the tumour vasculature [86].

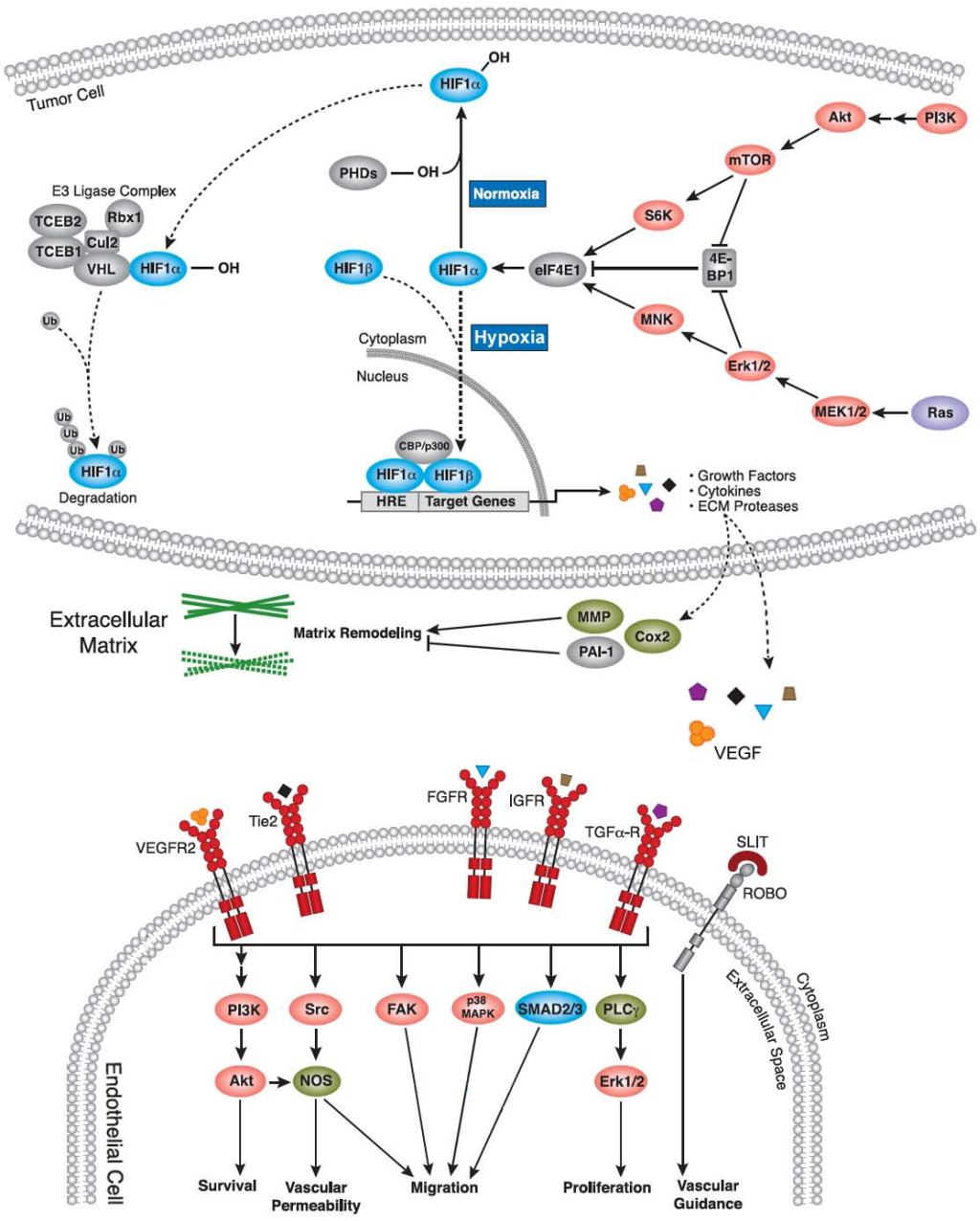

Figure 5. Principles of angiogenic signaling mechanisms

Hypoxia-inducible factor (HIF) is a transcription factor that responds to changing intracellular oxygen concentration. Under normix conditions HIF is degraded. During hypoxia, HIF accumulates and is transported to the nucleus where it induces expression of numerous target genes for secreted growth factors, which induce signaling pathways in endothelial cells, such as proliferation, increase of vascular permeability and cell migration. In addition to hypoxia, PI3K and Ras pathways can increase HIF expression by promoting HIF translation. In addition, Extracellular matrix proteases and regulators induce tissue matrix remodeling in preparation for migration of endothelial cells from existing vessels (adapted from Cell Signaling Technology, Inc.).

Taken into account that glioblastoma are paradigmatic for both massively increased angiogenesis and invasive growth, two major reasons for poor prognosis of glioblastoma patients [87], inhibition of angiogenesis seems to be an attractive target for glioma therapy [86, 88-90]. One of the most best established anti-angiogenic cancer treatment modality in general is bevacizumab (Avastin, Roche), a monoclonal antibody against VEGF-A, which prevents binding of VEGF to its receptor. Bevacizumab is approved for recurrent glioblastoma in the USA since 2009, in the EU approval was rejected [91, 92].
In addition to antibody-based approaches targeting free VEGF, compounds have been developed to target the functioning of the VEGF receptor. An example of this class of inhibitors is cediranib (Recentin/AZD2171; Astra-Zeneca), an indole-ether quinazoline that inhibits tyrosine kinase receptors, particularly all subtypes of the VEGF receptor, and has some activity against the PDGF and c-Kit receptors In gliomas cediranib was shown to induce normalization of the vasculature by inhibiting pathological proliferation of endothelial cells and immature vessel [92-95]. Additional anti-angiogenic therapies currently tested in clinical trials are summarized in Table 2.

Table 2. **Anti-angiogenic agents currently tested in high-grade glioma clinical trials [94]**

Compound	Class	Molecular Target
Bevacizumab	Antibody	VEGF-A
Cediranib	Tyrosine Kinase Inhibitor	VEGFR / PDGFR
Imatinib	Tyrosine Kinase Inhibitor	PDGFR
Enzastaurin	Signal Pathway Inhibitor	Protein Kinase C
Temsirolimus	Signal Pathway Inhibitor	mTOR
Cilengitide	Receptor Blockage	Integrins

However, the proven beneficial effects of angiogenesis inhibitors targeting the VEGF signaling pathway have not been translated into a survival benefit of similar extent [89, 92, 94]. Especially for treatment with bevacizumab, it has been reported that recurrence after therapy is more likely to be diffuse and distant to the primary tumor location [96]. Referring to this, increasing evidence suggests that impaired angiogenesis promotes infiltrative tumor growth (Figure 6). Impaired angiogenesis is therefore supposed to act as ‘detrimental driving force’ for enhanced tumor cell invasion into the surrounding tissue, a process commonly referred to as ‘evasive resistance’ [97-101].

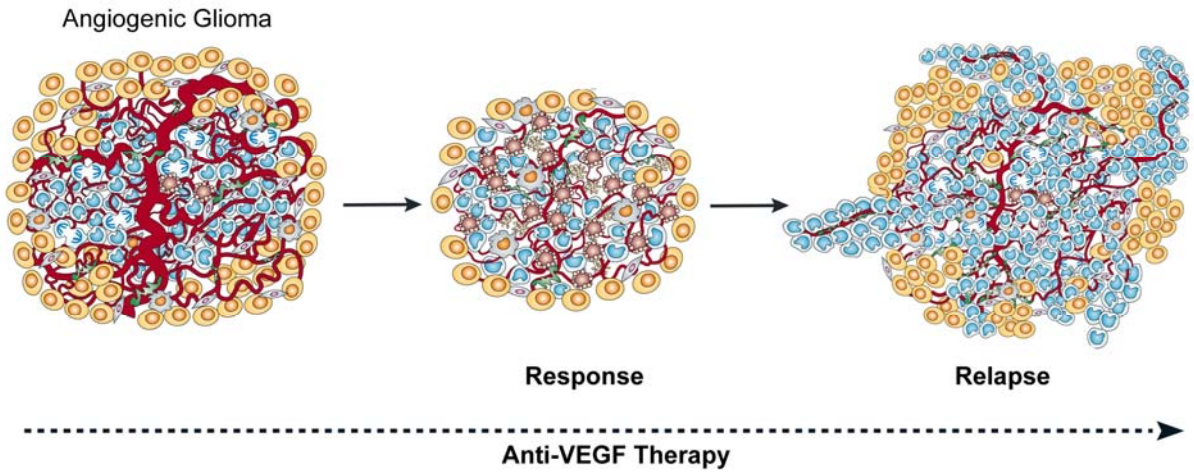

Figure 6. Evasive resistance mediated by tumor cell invasion in response to anti-angiogenic therapy. (adapted and modified from [102]).

Multiple adaptive mechanisms are supposed to be responsible for the evasive phenotype of increased invasiveness. Tumors may increase the activity of an invasion program that was prior to anti-angiogenic treatment not the main driving force of invasive tumor growth. Alternatively tumors may switch to a different invasive growth program [102].

In addition, anti-angiogenic therapy further increases hypoxia in the remaining tumor cells by constricting blood supply [92, 103]. This in turn activates survival pathways like AKT/PI3K/mTOR and promotes glycolytic energy metabolism and autophagy [92, 103, 104]. Alternatively, anti-angiogenic therapy induces altered tumor cell invading patterns. For example, untreated glioblastoma cells often diffusely invade as single cells into the surrounding brain tissue, whereas angiogenic impaired cells tend to invade as multicellular layers along blood vessels which is described as 'perivascular invasion' or 'vascular cooption' [99-102].

Of note, increased invasion is not the only mediator of 'evasive resistance' to angiogenesis inhibitors. Several others, all resulting in renewed angiogenesis and tumor growth are described as (I) activation and upregulation of alternative pro-angiogenic signaling effectors (e.g. fibroblast growth factor (FGF), angiopoietins), (II) recruitment of vascular progenitor cells from the bone marrow, and (III) increased pericyte coverage mediated blood vessel protection [102].

Recently, a novel mechanism for irradiation treatment induced evasive resistance was described by Kioi *et al*. [105] by suggesting that that vasculogenesis and not angiogenesis is the key process of revascularization that occurs during glioma recurrence after irradiation treatment. For this it is important to mention, that in general two processes are responsible for the formation of new blood vessels: angiogenesis and vasculogenesis. The latter describes the process of a *de novo* formation of new blood vessels from endothelial precursor cells or bone marrow-derived hematopoietic cells (BMDCs), whereas angiogenesis involves the formation of new blood vessels by sprouting of local

pre-existing vessels via proliferation of endothelial cells. Prior to irradiation, tumor growth is mainly directed by angiogenesis. After irradiation, the tumor becomes more hypoxic due to a radiation-damaged vasculature, which leads to increased HIF-1 activity and subsequent CXCR4/SDF-1 mediated recruitment of BMDCs into the tumors to form new vessels [105, 106]. Taken this into account the concept of anti-angiogenic treatment in recurrent glioblastoma needs to be reconsidered and probably more oriented on the signaling pathways involved in vasculogenesis (e.g. CXCR4/SDF-1 inhibitors) in order to counteract angiogenesis-stimulating side effects of radiation therapy.

Taken together, an approach to overcome the problem of increasing infiltrative tumor growth lies in treatment modalities which combine anti-angiogenic and anti-invasive mechanisms. Applying such drugs, targeting evasive resistance mechanisms, are therefore promising options in modern glioblastoma therapy, since they comprise the probability to reach sustained efficacy of glioma treatment.

1.4.3 Immunosuppression

Besides tumor cell invasion and potent pro-angiogenic signaling, the ability of suppressing the immune system is one of the key biological features of glioblastoma.

The brain is an immunologically specialized organ. Under physiological conditions, the brain contains different immune cell populations: Microglial cells, macrophages, dendritic cells (DCs) and T-cells which are found in perivascular zones, the choroid plexuses, and the meninges. Due to its composition the blood-brain-barrier regulates the selective entry of immune cells to the brain parenchyma [107], leading to a prevented immune recognition of glial tumors at the onset of tumor growth. However at later stages, the blood-brain-barrier is disorganised, destructed, and leaky which makes the gliomas accessible to components of the immune system leading to infiltration of immune cell infiltrates [108]. Attraction of these immune cells (e.g. microglial cells, macrophages, DCs and T cells) is mediated by a number of molecules, which are mainly produced by oxygen-deprived tumor cells surrounding necrosis. HIF-1α for example has been identified as a key factor in gliomas promoting the release of chemoattractants for immune cells, such as CXCL12/SDF-1.

In general, the generation of an effective anti-tumor response by the immune system is a multistep process which requires presentation and interaction of tumor antigens by an antigen-presenting cell (e.g., dendritic cell or macrophage) in a major histocompatibility complex (MHC) to T-cell receptors on $CD4^+$-T-helper cells. In addition, costimulator activity is provided by cell surface molecules including B7 and by soluble factors including cytokines like interleukin-1 (IL-1). Activated $CD4^+$-T-helper cells trigger cytotoxic $CD8^+$-T-cells, via release of cytokines like IL-2, interferon-γ (IFN-γ) and tumor necrosis factor-α (TNF-α), to recognize tumor antigen expressed in association with

MHC class I antigen. Tumor cells can then be destroyed by cytotoxic immune effector cells using and Fas/APO-1 receptor-mediated apoptosis [53].

This general model of anti-tumor immune response is efficiently impaired and suppressed in malignant gliomas, leading to the fact that these tumors are extremely immune privileged. Malignant glioma cells express and secrete a variety of substances that suppress antitumor immunity [53, 108, 109] and are therefore responsible for the impaired recognition and attack of the glioma cells by the immune system (Figure 7).

In general, malignant gliomas are characterized by the presence of a large number of immunosuppressive soluble factors, such as IL-10 and TGF-β, whereas immunostimulatory molecules, such as IL-12, IL-18, and INF-γ, are lacking.

One of the strongest mediators of glioma-induced immunosuppression is TGF-β. TGF-β is a cytokine with marked known immunosuppressive activity. Tumor-released TGF-β suppresses the host's immune response by induction of growth suppression and apoptosis in immune cells, by suppression of activity and cytokine release of immune cells, by autocrine and paracrine downregulation of putative tumor antigen expression and expression of costimulatory factors like B7 and by changes in the cytokine release profiles of non-immune cells [28, 52]. Another soluble factor is known as glioma-derived T-cell suppressive factor (G-TsF) which inhibits proliferation and IL-2 production by T cells [109].

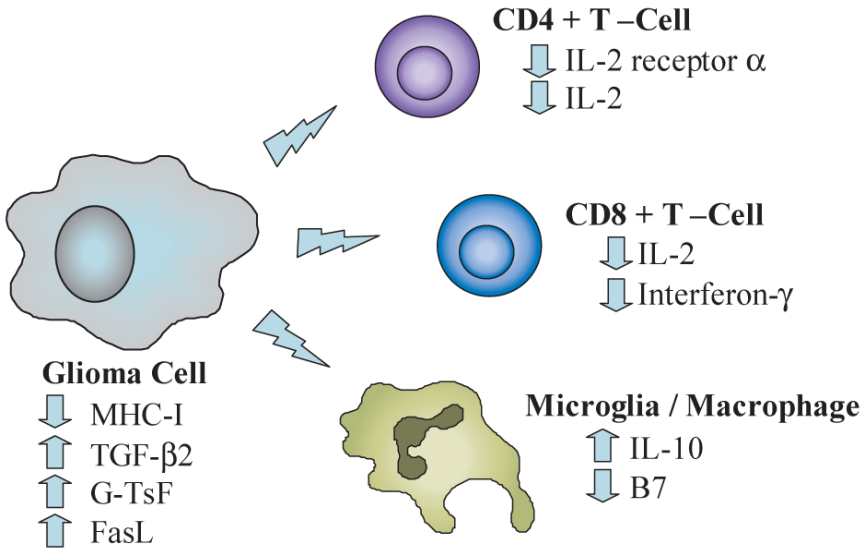

Figure 7. Immunosuppressive mediators of the glioma immune privilege

Glioma cells secrete a number of different immunosuppressive mediators that inhibit antitumor immunity (IL = interleukin, G-TsF = glioma-derived T-cell suppressor factor, TGF-β = transforming growth factor beta) Adapted from [109].

In addition, increased expression of apoptosis-inducing Fas ligand (FasL or CD95L) has been shown to been capable of killing T cells directly and thereby inhibiting immune response [110, 111].

Inhibitory cytokine signaling molecules such as signal transducers and activators of transcription 3 (Stat3) are known to be constitutively activated in human glioma promoting tumor cell growth and survival [108, 112, 113]. Furthermore, several enzymes as for example Indoleamine 2,3-dioxygenase (IDO) have been described to be overexpressed in glioma and to mediate immunesuppression. IDO is a kynurenine pathway enzyme catalyzing oxidation of the essential amino acid tryptophan and is thought to be involved in the immune resistance of malignant tumors through T-cell inactivation caused by tryptophan depletion [114-116].

In general, an optimal T cell response is achieved by a combination of signals delivered through the antigen-specific T cell receptor and costimulatory signals that are stimulatory or inhibitory [117]. By interacting with counterreceptors on T cells, the members of the B7 family of costimulatory molecules play a critical role in the control and fine-tuning of antigen-specific immune responses. Recently, B7-family member H3 (B7H3) was identified as a novel member of the B7-family of costimulatory proteins with its two isoformsm2IgB7H3 and 4IgB7H3 [118]. The latter is more widely expressed in human maturating dendritic cells (DC), T-cells and many human tumor cell lines. 4IgB7H3 was initially supposed to only convey T-cell activation and to induce IFN-γ production [118], but more recent evidence suggests that 4IgB7H3 is expressed by different human malignancies. In this regard 4IgB7H3 mediates suppression of natural killer (NK) cell and cytotoxic $CD8^+$-T-cells [119], hinting at role for B7H3 in mediating immunosuppressive tumor effects. In addition, high expression of 4IgB7H3 is associated with a poor prognosis in different tumor entities [120-122]. Apart from the expression on tumor cells, 4IgB7H3 is also specifically upregulated on tumor endothelia [123]. The ligand for 4IgB7H3 has not been identified yet, but it has been postulated that it is expressed on activated T-cells [118]. A soluble form of 4IgB7H3 is expressed by human immune cells and by a variety of different tumor cells. This soluble form which is cleaved by MMP from the cell surface was detected in increased levels in the serum of patients with non small cell lung carcinoma compared with healthy controls and correlated with the tumor burden [124].

Taken together, differentiation, maturation and function of tumor-infiltrating cells, as well as the generation and activation of immune effector cells are markedly suppressed in the tumor microenvironment of malignant gliomas due to expression and secretion of immunosuppressive factors. In order to overcome the effective immunosuppresion in gliomas, therapeutic treatment modalities need to provided additional immune stimulation or antagonize tumor-derived immune inhibition.

2. Materials and Methods

2.1 Reagents and methods for *in vitro* studies

2.1.1 Cell culture

I. Glioma cell lines

The human malignant glioma cell lines LN-308, LN-229, LN-428 and LN-18 were kindly provided by N. de Tribolet (Lausanne, Switzerland). LN-229 cells still harbor the wild-type *TP53* gene and were therefore renamed LNT-229 (T for Tuebingen) for clarification. U87-MG and T98G glioma cells were purchased from the American Type Culture Collection (Manassas, VA, USA). The human glioma cell line NCH-89 was provided by Ana Martin-Villalba (Heidelberg, Germany). The murine glioma cell line SMA-560 was provided by D.D. Bigner (Durham, NC, USA). Glioma cells were maintained in Dulbecco's Modified Eagle's Medium (DMEM) containing 10% fetal bovine serum (FBS; Perbio, Bonn, Germany) and 100 IU/mL penicillin and 100 mg/mL streptomycin (PAA Laboratories, Pasching, Austria).

II. Glioma-initiating cells (GIC)

For the generation of GIC cultures T269 and T325, tumor samples were obtained from adult patients diagnosed with primary glioblastoma after informed consent. GIC culture methods were modified according to [125] as described previously [126]. Briefly, cells were cultured in neural sphere cell medium (NSCM) containing DMEM:F12 growth medium (Invitrogen, Karlsruhe, Germany) enriched with B27 supplement (Invitrogen), 20 ng/mL basic fibroblast growth factor (bFGF; Invitrogen), 20 ng/mL epidermal growth factor (EGF; Invitrogen) and 20 ng/mL leukemia inhibitory factor (LIF; Millipore, Temecula, CA, USA).

III. Endothelial cells (EC)

Human umbilical vein endothelial cells (HUVEC) were purchased from PromoCell (Heidelberg, Germany) and cultured in endothelial cell growth medium (ECGM) supplemented with Promocell Supplement Mix C-39215, 10% FBS, 100 IU/mL penicillin and 100 mg/mL streptomycin.

The human brain capillary endothelial cell line hCMEC/D3 was kindly provided by Pierre-Olivier Couraud (Institut Cochin, Université René Descartes, Paris, France) and grown in EBM-2 (Lonza, Basel, Switzerland) supplemented with EGM-2 MV SingleQuots (Lonza, Basel, Switzerland), HEPES (PAA Laboratories, Pasching, Austria), 100 IU/mL penicillin and 100 mg/mL streptomycin in cell culture dishes coated with rat tail collagen I (BD Biosciences, Heidelberg, Germany). Irradiation of cells was performed in a GE Healthcare Buchler (Braunschweig, Germany) radiation device OB58 using a

caesium-137 source. For hypoxia experiments, cells were cultured at 1% O_2 in a nitrogen-supplied C42 hypoxia incubator (Labotect, Goettingen, Germany).

2.1.2 Reagents, inhibitors and drugs

CCI-779 (Temsirolimus/Torisel®) was provided by Wyeth Pharma (Muenster, Germany) a member of the Pfizer company and dissolved in dimethyl sulfoxide (DMSO). The PKC beta inhibitor enzastaurin (ENZA) was purchased from Selleck Chemicals LLC (Houston, TX, USA) and dissolved in DMSO. The soluble CD95 ligand (CD95L) inhibitor APG101 and the CD95L were kindly provided by Apogenix GmbH (Heidelberg, Germany). Phorbol 12-myristate 13-acetate (PMA) was purchased from Sigma-Aldrich (Taufkirchen, Germany) and diluted in DMSO. The synthetic furin inhibitor, decanoyl-Arg-Val-Lys-Arg-chloromethylketone (dec-RVKR-cmk) was purchased from Bachem (Heidelberg, Germany) and dissolved in methanol. The MMP inhibitor Ilomastat was purchased from Chemicon International (Temecula, CA, USA).

2.1.3 Modulation of gene expression

I. si-RNA mediated knock down

The ON-TARGET-plus SMART-pool siRNA by Dharmacon RNA Technologies (Lafayette, CO, USA) was used to knock-down *RGS4* (NM_005613; Smartpool No. L-009900), *Rictor* (NM_152756; Smartpool No. L-016984) and *Raptor* (NM_020761; Smartpool No. L-004107). ON-TARGET-plus siControl Nontargeting Pool (D-001810-10-05, Dharmacon) and a transfection without siRNA were used as negative controls. Cells were transfected using the Lipofectamine™ RNAiMAX Transfection Reagent (Invitrogen). Briefly, 3×10^5 cells were resuspended in Lipofectamine RNAiMAX solution, mixed with 50 nM of siRNA and plated into 6-well plates containing DMEM and 10% FBS. Following 48 – 72 h of incubation, cells were harvested and analyzed for transient gene knockdown by qRT-PCR and immunoblot.

II. Gene overexpression

Stable overexpression of RGS4 in human LN308 glioma cells was achieved by transfecting the pCR3.0 eukaryotic expression vector (Invitrogen) harboring *RGS4*-encoding cDNA (pCR3.0-RGS4; provided by Prof. Thomas Wieland, University of Heidelberg, Mannheim, Germany) using the Fugene HD Transfection Reagent (Roche, Mannheim, Germany) and selecting with G418 (Sigma-Aldrich, Taufkirchen, Germany). pCR3.0 served as an empty vector control.

III. Lentiviral knock-down

Lentiviral knock-down of 4IgB7H3 and control knock-down cells were produced with lentiviral sh 4IgB7H3 and control particles from Santa Cruz Biotechnology (Santa Cruz, CA, USA; Cat. no.: sc-45444-V and sc-108080).

2.1.4 Sequencing

Sequence analysis of PTEN-specific cDNAs derived from human LNT-229, LN-428, LN-18, LN-308, T98G and U87MG glioma cell lines, from T269 and T325 GIC cultures or from the murine SMA-560 astrocytoma cell line was performed by Dr. Markus Weiler.

Total RNA was isolated from cells that had been cultured for 48 h and harvested according to the RNeasy RNA isolation kit (Qiagen, Hilden, Germany). cDNA synthesis was carried out following the instructions of the QuantiTect Reverse Transription Kit (Qiagen). A 1497-bp stretch of cDNA containing the entire coding region of the human *PTEN* gene was amplified by polymerase chain reaction (PCR) using the primer pair 5'-GCATCAGCTACCGCCAAGTC-3' and 5'-GTGTCAAAACCCTGTGGATG-3'. Homologous mouse sequences, 1514 bp of length, were PCR-amplified from SMA-560-derived cDNA using the primers 5'-GCATCAGCGACCGCCAAGTC-3' and 5'-GTGTCAAAACCCTGTGGATG-3'. The PCR products were separated on a 1% agarose gel, extracted from the gel, sequenced, and analyzed for mutations by comparison with the respective database entries for human or mouse *PTEN* mRNAs.

2.1.5 Quantitative Reverse Transcription PCR

Total RNA was extracted using the Qiagen RNeasy RNA isolation kit (Qiagen, Hilden, Germany). cDNA was prepared from RNA using the High-Capacity cDNA Reverse Transcription Kit (Applied Biosystems, Darmstadt, Germany). Gene expression analysis was performed in triplicates in an ABI Prism 7000 Sequence Detection System (Applied Biosystems, Darmstadt, Germany) using the SYBR Green Master Mix (Eurogentec, Cologne, Germany). Standard curves were generated for each transcript demonstrating 90-100% amplification efficiency, and relative quantification of gene expression was determined by comparison of threshold values. Primers were purchased from Sigma-Aldrich (Taufkirchen, Germany). Primer sequences are given in Table 3.

Table 3. **List of qRT-PCR primers and genes used for normalization of expression results**

Target	Forward primer	Reverse primer	Normalization gene
RGS-4	5'-GCTTCTTGCTTGAGGAGTGC-3'	5'-GGGAAGAATTGTGTTCACAGG-3'	GAPDH
VEGFR-2	5'-GCGTGGTCAGGCAGCTCACA-3'	5'-GGGGATTCCCAGATGCCGTGC-3'	β-Actin
Raptor	5'-TAGTTTTGTGCCTGAATGTTGGT-3'	5'-GAGCTTTCTGAGGACCCATCG-3'	eEF1
Rictor	5'-CGAGTACGAGGGCGGAATG-3'	5'-TCAGATGGCCTAGCTTTCTCATA-3'	eEF1
4IgB7H3	5'-AGAGGGCCGTGCGGTTGGCA-3'	5'-CATCACACCCCAGAGAAGCC -3'	GAPDH
CD95L	5'-TCTCAGACGTTTTTCGGCTT-3'	5'-CCTCCATTTGTCTGGCTCAT-3'	GAPDH

2.1.6 cRNA microarray analysis

For gene expression analyses, total RNA was extracted using the RNeasy Kit (Qiagen). RNA integrity was assessed with a 2100 Bioanalyzer (Agilent Technologies, Santa Clara, CA, USA). Only samples with an RNA integrity number (RIN) above seven were used for further processing. Sample labeling with the Low RNA Input Linear Amplification Kit and hybridization on 4 x 44K Whole Human Genome Microarrays (Agilent) were performed according to the manufacturer´s protocol. In brief, 1 µg of total RNA was subjected to reverse transcription and subsequent cRNA synthesis and labeling with Cy3- or Cy5-CTP, respectively. Samples were hybridized against universal human reference RNA (Agilent), dye swap experiments were included. Data processing was performed using ChipYard (http://www.dkfz.de/genetics/ChipYard/), an in-house developed R-based platform. Normalized data was further analyzed using the open source platform Chipster (http://chipster.sourceforge.net/). Differentially expressed genes were identified using the implemented empirical Bayes method with adjustment for multiple testing according to Benjamini-Hochberg and a significance threshold of $p<0.05$. Functional annotation of genes was performed using Ingenuity Pathway Analysis (Ingenuity Systems, Redwood City, CA, USA). Array data are available at Gene Expression Omnibus accession no. GSE24232 (http://www.ncbi.nlm.nih.gov/geo/). cRNA Microarray analysis was performed by the group of Prof. Peter Lichter, German Cancer Research Center, Heidelberg, Germany.

2.1.7 Promoter methylation analysis

Methylation-specific PCR (MSP) was used to analyze the *PTEN* promoter region for potential methylation-mediated epigenetic silencing and was conducted by Dr. Markus Weiler.

One microgram of genomic DNA derived from human LNT-229, LN-428, LN-18, LN-308, T98G and U87MG glioma cell lines, from T269 and T325 GIC cultures or from the murine astrocytoma cell line SMA-560 was each treated with sodium bisulfite using the Qiagen EpiTect Kit (Qiagen). The primer sequences used to detect methylated human *PTEN* promoter sequences were

5'-GTTTGGGGATTTTTTTTTCGC-3' and 5'-AACCCTTCCTACGCCGCG-3'. This primer combination amplifies a 178-base pair (bp) fragment from methylated human DNA. The primer sequences used to detect unmethylated human *PTEN* promoter sequences were 5'-TATTAGTTTGGGGATTTTTTTTTTGT-3' and 5'-CCCAACCCTTCCTACACCACA-3'. This primer combination amplifies a 186-bp fragment from unmethylated human DNA. The primer sequences used to detect methylated murine *PTEN* promoter sequences were 5'-TTGGGGATTTTTCGCGTTAGC-3' and 5'-CCCTCTCTTACCGAATCG-3'. This primer combination amplifies a 177-bp fragment from methylated murine DNA. The primer sequences used to detect unmethylated murine *PTEN* promoter sequences were 5'-ATAGTTTGGGGATTTTTTGTGTTAGT-3' and 5'-AACCCCTCTCTTACCAAATCA-3'. This primer combination amplifies a 185-bp fragment from unmethylated murine DNA. After an initial denaturation step at 95°C for 10 min, 38 PCR cycles were run using the following conditions: denaturation, 94°C for 30 s; annealing, 55°C for 60 s; extension, 72°C for 55 s; followed by a final extension at 72°C for 10 min. As positive or negative controls for methylation, CpGenome Universal methylated or unmethylated DNA, Vial A, (Millipore) were used. In addition, a control reaction without any template DNA was performed for both PCR experiments. The PCR products were separated on a 3% agarose gel. MSP primers were purchased from Eurofins MWG Operon (Ebersberg, Germany).

2.1.8 Immunoblot analyses

Preparations of cell lysates were performed as follows: cells were lysed in 50 mM Tris–HCl (pH 8) containing 120 mM NaCl, 5 mM EDTA, 0.5% Nonidet P-40, 2 µg/mL aprotinin, 10 µg/mL leupeptin (Sigma-Aldrich), and 100 µg/mL phenylmethylsulfonyl fluoride (PMSF). Protein levels were analyzed by immunoblot following SDS-PAGE using 20 µg of protein per lane. Antibodies used for immunoblot analyses are given in Table 4.

2.1.9 Flow cytometry

All flow cytometry work was carried out on a BD FACSCanto II flow cytometer (BD Biosciences), and results were analyzed using FACSDiva 6.1 software (BD Biosciences). Final data were processed with the help of FlowJo flow cytometry analysis software (Tree Star, Ashland, OR, USA). Specific fluorescence intensity (SFI) was calculated by using the mean fluorescence signal of B7H3 divided by the mean fluorescence isotype signal.

I. Proliferation and cell cycle distribution

For studies of proliferation and cell cycle distribution, cells were treated as indicated and then incubated with 5-bromo-2-deoxyuridine (BrdU) at 10 µmol/L for 45 min, fixed with methanol, treated

with 0.5% Triton X-100-containing 0.1 mol/L HCL and stained with a FITC-conjugated anti-BrdU antibody (1:50; BD Biosciences) to mark actively cycling S-phase cells. Cell cycle distributions were assessed after DNA staining with DAPI at 488 nm and 405 nm, respectively.

Table 4. List of primary and secondary antibodies used for immunoblotting

Target	Source	Concentration	Company	2nd antibody
Pathscan Multiplex Cocktail I (Phospho-AKT^{S473}, Phospho-RPS6, eIF4E)	rabbit	1:200	Cell Signaling, Danvers, MA, USA	+
RPS6	mouse	1:1000		#
Phospho-mTOR^{S2481}	rabbit			+
VEGFR-2				
Phospho-GSK-3β^{S9}				
GSK-3β				
Phospho-AKT^{T308}				
Phospho-AKT^{S473}				
AKT				
PTEN	rabbit	0.1 µg/mL	R&D Systems, Minneapolis, MN, USA	+
RGS4 (C17)	goat	1 µg/mL	Santa Cruz Biotechnologies, Santa Cruz, CA, USA	*
HIF-1α	mouse	2 µg/mL	Novus Biologicals, Littleton, CO, USA	#
4IgB7H3	goat	1:100	R&D Systems, Minneapolis, MN, USA	*
GAPDH	goat	1:1000	Abcam, Cambridge, UK	*
β-Actin	rabbit	1:1000	Cell Signaling, Danvers, MA, USA	+
α-Tubulin	mouse	1:5000	Sigma-Aldrich, Taufkirchen, Germany	#
Secondary Antibodies (horseradish peroxidase-coupled)				
* Anti-Goat	donkey	1:2000	GE Healthcare, UK	
+ Anti-Rabbit				
# Anti-Mouse	sheep			

II. Autophagy

Flow cytometric analyses of autophagy were performed as described before (3) After indicated treatments, cells were stained with acridine orange (Polyscience, Warrington, PA, USA) at 1 µg/mL for 20 min in phenol red-lacking DMEM supplemented with 10% FBS. Cells were then washed and harvested with accutase (PAA Laboratories, Pasching, Austria). Acridine orange staining was assayed

by measuring the green and red fluorescence emission of 10^4 cells. Percentage of five was set as the autophagic baseline level in vehicle-treated control cells.

III. Apoptosis

Apoptotic response to drugs and irradiation was measured by annexin V-FITC (AnxV-FITC) staining. Cells were harvested, washed, resuspended in $CaCl_2$-containing PBS and incubated with AnxV-FITC (Biocat, Heidelberg, Germany). After incubation for 15 min at room temperature, DNA was stained with DAPI and cells were analyzed flow cytometrically at 488 nm.

2.1.10 Mass spectrometry analysis

I. Probe preparation

Protein bands were excised from SDS-PAGE. Gel pieces were consecutively washed with water and 50% acetonitrile, reduced with 10 mM DTT at 56°C for 1 h and alkylated with 55 mM iodoacetamide (Sigma Aldrich) at 25°C for 30 min in the dark. After alkylation, gel plugs were repeatedly washed with water and 50% acetonitrile, dehydrated with 100% acetonitrile and air-dried. The dried gel plugs were reswollen in 40 mM ammonium bicarbonate containing 17ng/µl sequencing grade modified trypsin (Promega, Mannheim, Germany). Following enzymatic digestion overnight at 37°C, peptides were repeatedly extracted with 0.1% TFA and acetonitrile/0.1% TFA 50:50 (v/v). The combined solutions were dried in a speed-vac for 2 h at 37°C. Peptides were redissolved in 5 µl 0.1% TFA by sonication for 10 min and applied for ESI-MS/MS analysis.

II. Orbitrap Mass spectrometry analysis

NanoLC-MS/MS analysis was performed using the nanoACQUITY (Waters, Eschborn, Germany) coupled to a nanoESI-LTQ-Orbitrap mass spectrometer (Thermo Scientific, Bremen, Germany) using a stepped linear acetonitrile/water gradient ranging from 5% to 90% within 45 minutes. Peptide masses obtained from an *in silico* trypsin digestion of the protein of interest using a MS-Digest tool from the online ProteinProspector v5.7.2 software (UCSF, San Francisco, USA) were isolated and fragmented by the Orbitrap. Processed data were searched against the NCBInr database using the Mascot algorithm version v2.2.0 (Matrix Science Ltd., London, UK). The taxonomy *homo sapiens* was selected for Mascot searches. Mass spectrometry analysis was performed by the group of Dr. Martina Schnölzer, DKFZ Heidelberg.

2.1.11 Cell viability assays

I. Trypan blue dye exclusion

Glioma cells were seeded in cell culture flasks at $2x10^5$ cells suspended in cell culture medium and treated as indicated. Cells were harvested after 72 h and stained with trypan blue (Gibco Life Technologies, Karlsruhe, Germany). Unstained viable and trypan blue-positive dead cells were counted automatically using the Beckman Coulter Vi-Cell XR cell viability analyzer (Krefeld, Germany).

II. Crystal violet staining.

For crystal violet staining, glioma cells were seeded in culture medium at 1x104 cells per well in 96-well plates and treated as indicated. Medium including floating dead cells was removed and viable cells were fixed with 1% glutaraldehyde (Sigma-Aldrich) and stained with crystal violet. After destaining with 0.2% Triton-X-100, optical density OD590 was measured using a microplate reader.

2.1.12 Cell invasion assays

I. Matrigel invasion assay

Invasion of glioma cells *in vitro* was assessed in Boyden chamber assays (BD Biosciences), where upper and lower wells are separated by a porous membrane (8 µm pore size) coated with matrigel matrix. Following pretreatment as indicated, subconfluent glioma cells were harvested in enzyme-free cell dissociation buffer (Gibco Life Technologies) and added in triplicates at a total of 4×10^4 cells suspended in culture medium to each upper chamber. NIH 3T3-conditioned medium (0.5ml) was used as a chemoattractant in the bottom well. Cell invasion was evaluated by counting the number of cells that had migrated across the membrane within 20 h in five random microscopic fields, and photographs of representative microscopical fields were taken at 100-fold magnification. To rule out that invasion was biased by differences in cell proliferation among experimental conditions, invasion raw data were normalized to respective cell viability as assessed in parallel by crystal violet staining. Data were expressed as percentage of invasion relative to the respective control condition.

II. Collagen invasion assay

Following indicated pre-treatments glioma cells were harvested and added in quadruplets at a total of 4 x 104 suspended cells to each upper chamber of an xCELLigence Real-Time Cell-Analyzer system (RTCA; Roche Diagnostics, Mannheim, Germany). Invasion was monitored in real-time by the RTCA system for 24 h and growth curves were analyzed using the RTCA software 1.2. The dimensionless Cell Index (CI), derived as a relative change in measured electrical impedance caused by migrated cells, reflects the invasive behavior of monitored cells.

III. Spheroid invasion assay

Multicellular glioma spheroids of glioma cell lines were obtained as described previously [127] by seeding glioma cells ($3x10^4$ cells/mL) in 96-well plates that were base coated with 1% Noble Agar (Difco Laboratories, Detroit, MI, USA) prepared in DMEM and culturing for 4 days until spheroids had formed. For the generation of GIC spheroids, 1×10^6 GIC were seeded in neural sphere cell medium (NSCM; Invitrogen, Karlsruhe, Germany) and kept in culture until spheroids had formed spontaneously. Extracellular matrix gel was prepared as described previously [127]. Spheroids were seeded in triplicates into the collagen gel solution in a 24-well plate. After gelation, the gel was covered with medium and cultured in a humidified atmosphere (37°C; 5% CO_2). For quantification of cell invasion, the radial distance from the center of each spheroid was measured for 40 representative migrated cells at 0, 24, 48, and 72 h after implantation.

2.1.13 Clonogenicity and GIC sphere formation assays

Clonogenic capacity was assessed by seeding glioma cells suspended in culture media containing 500 cells per well in a 6-well plate. Cells were treated as indicated. Macroscopically visible colonies were counted after 10-12 days following crystal violet staining.

Sphere formation capacity of GIC was determined by seeding dissociated single cells derived from sphere-forming GIC cultures at 100 cells/well in a 96-well plate. Indicated drugs and respective controls were added. The GIC growth factors bFGF and EGF (20 ng/mL) were refreshed every 48 h. GIC. Number and size of microscopically visible spheres were determined after approximately 14 days in culture.

2.1.14 Angiogenesis assays

I. Endothelial cell viability assay

Viability assays using both primary HUVEC and brain-derived hCMEC/D3 were performed as described previously [128]. In brief, 2,000 cells were seeded into 96-well plates, and absorbance of viable endothelial cells was colorimetrically measured in a plate reader (Thermo Scientific, Karlsruhe, Germany) at 490 nm using 3-(4,5-dimethylthiazol-2-yl)-5-(3-carboxymethoxyphenyl)-(4-sulfophenyl)-2H-tetrazolium (MTS) as a substrate provided in the CellTiter 96™ Aqueous One Solution Cell Proliferation Assay (Promega, Madison, WI, USA) according to the manufacturer's instructions.

II. HUVEC sprouting assay

Spheroid formation and sprouting of HUVEC was carried out as described previously [128]. Briefly, spheroids were generated by resuspending HUVEC in culture medium containing 0.24% (w/v) carboxymethylcellulose (Sigma-Aldrich) followed by an incubation for 24 h as hanging drops. Spheroids were embedded into collagen gels consisting of 8 volumes of rat tail collagen equilibrated to 2 mg/mL in 0.1% acidic acid with 1 volume Medium 199 (Sigma-Aldrich) and ~1 volume 0.2 M NaOH and 1 M HEPES buffer (Roth, Karlsruhe, Germany). Endothelial cell basal medium (Promocell, Heidelberg, Germany) containing 25 ng/mL VEGF 165 (R&D Systems) was added on top of each spheroid-containing gel after polymerization at 37°C. After incubation for 24 h, inhibition of endothelial cell function was quantified by measuring the lengths of the sprouts grown out of each HUVEC spheroid (at least n = 25 per experimental group) using the National Institutes of Health (NIH) ImageJ software (Bethesda, MD, USA). The average cumulative sprout length of all spheroids belonging to one treatment group was calculated.

III. VEGF-ELISA

VEGF concentrations in cell culture supernatants were quantified using the enzyme-linked immunosorbent assay (ELISA) Quantikine kit from R&D Systems (Minneapolis, MN, USA) according to the manufacturer's instructions. The assay was performed by Dr. Benjamin Berger. Following indicated treatment cell culture supernatants were collected, freed from debris, nonadherent and dead cells by centrifugation (3 min; 4370 × g), and used in the ELISA. The absorbance at 450 nm was determined for each probe using a 96-well plate reader (Thermo Scientific, Karlsruhe, Germany) and used to calculate the respective VEGF concentration (in pg/mL) based on a standard curve generated from defined standard samples.

2.1.15 Mixed leukocyte reaction

Peripheral blood mononuclear cells (PBMC) were isolated from whole blood samples of healthy donors after informed consent by Ficoll-Hypaque density gradient centrifugation (PAA, Pasching, Austria). The mixed leukocyte reaction was performed as described previously (5). Briefly, 2×10^5 irradiated (30 Gy) PBMC as stimulators and 2×10^5 unirradiated PBMC derived from two unrelated donors as responders were mixed in a 96-well plate. After incubating the cells for six days as indicated, cultures were pulsed with [^{3}H]-methylthymidine (Amersham Radiochemical Centre, Buckinghamshire, U.K.) for 18 h. The cells were then harvested (Tomtec Cell Harvester, Tomtec, Hamden, CT, USA) and radionuclide incorporation during PBMC proliferation was measured by scintillation counting using a Wallac Micro Beta TriLux Scintillation Beta Counter (Perkin Elmer,

Waltham, MA, USA). Experiments were carried out repeatedly using five independent pairs of healthy PBMC donors in total.

2.1.16 Immune cell-lysis assay

Peripheral blood lymphocytes (PBL) were isolated from whole blood samples from healthy donors by Ficoll-Hypaque density gradient centrifugation. Natural killer (NK) cells were then isolated from PBL by depletion of non-NK cells using a NK cell isolation kit (Miltenyi Biotec, Bergisch Gladbach, Germany) according to the manufacturer's instructions. Isolated $CD56^+/CD3^-$ NK cells were maintained in Roswell Park Memorial Institute (RPMI) 1640 medium (PAA Laboratories, Pasching, Austria) containing 10% fetal bovine serum (FBS; Perbio, Bonn, Germany) and 1000 U/mL interleukin-2 (Immunotools, Friesoythe, Germany) a known activator of NK cells, for 5 days at 37°C / 5%CO_2.
NK cell cytotoxicity was assessed using the standardized ^{51}Chromium (^{51}Cr)-release assay [129]. Briefly, labeled glioma cells ($5x10^3$/well) were seeded in triplicates into a U-shaped 96-well microtiter plate and incubated with NK effector cells with effective target-to-effector ratios of 1:30, 1:10 and 1:3. Minimum and maximum ^{51}Cr release was determined by using target cells incubated in medium alone or 10% Triton-X-100 (Applichem, Darmstadt, Germany). After incubation at 37°C/5% CO_2 for 4 h, supernatants were collected from each well and counted in a gamma counter (Packard, Meriden, CT, USA). Specific NK lysis in percent was calculated as follows: [Experimental ^{51}Cr Release - Minimum Release] / [Maximum Release- Minimum Release] x100.

2.1.17 Statistical analysis

Quantitative *in vitro* data are expressed as mean ± standard deviation (SD), as indicated. All *in vitro* experiments reported here represent at least three independent replications performed in triplicate. Statistical significance was assessed by two-sided Student's t-Test (Excel, Microsoft, Seattle, WA, USA). Values of $p < 0.05$ were considered significant and asterisked. A two-sided Fisher-Yates test was applied to correlate the PTEN and AKT activation status with the IC_{50} of CCI-779 in different glioma cell lines.

2.2 Reagents and methods for *in vivo* studies

All animal work was approved by the governmental authority (Regierungspräsidium Karlsruhe, Germany) and supervised by institutional animal protection officials in accordance with the NIH 'Guide for the Care and Use of Laboratory Animals'.

2.2.1 Orthotopic xenograft mouse glioma model

I. Implantantion of RGS4 overexpressing human glioma cells

A total of 1 x 10^5 PBS-suspended LN-308 glioma cells stably transfected with pCR3.0 and pCR3.0-RGS4, respectively, were stereotactically implanted into the right striatum of CD1 *nu/nu* mice (Charles River Laboratories, Sulzfeld, Germany) with *n* = 4 mice in each group. Tumor volume was assessed on day 48 after tumor cell inoculation by magnetic resonance imaging (MRI) using a transversal T2-weighted turbo-spin echo sequence (see below). Histological analysis was conducted in all animals the same day by staining coronally cryosectioned brains (8 µm) with hematoxylin/eosin.

II. Implantation of human T269 4IgB7H3 glioma knock-down cells

A total of 1x10^5 human T269 4IgB7H3 knock-down cells or T269 control knock down cells were stereotactically implanted into the right striatum of five 6-12-week-old athymic mice (CD1 *nu/nu*; Charles River Laboratories, Wilmington, MA, USA). Ten weeks after implantation, animals were sacrificed, brains removed and cryosectioned. To access infiltration immunostainings were conducted with rabbit anti-human nestin antibody (Millipore, Schwalbach, Germany) after fixation of cryosections with acetone. Alexa 488 anti-rabbit antibody (Invitrogen, Karlsruhe, Germany) was used as secondary antibody.

2.2.2 Orthotopic syngeneic mouse model

A total of 5,000 murine SMA-560 glioma cells suspended in PBS were stereotactically implanted into the right striatum of 6-12 week old VM/Dk mice (inhouse breeding facility, German Cancer Research Center, Heidelberg, Germany) at a depth of 3 mm.

I. CCI-779 treatment experiment

Animals were divided into four experimental treatment groups (*n* = 14 each): (i) Control group: daily intraperiteonal (i.p.) injections of vehicle substance (sodium chloride 9 g/L solution containing 12% (v/v) ethanol) from postoperative day 3 to 17. (ii) Radiation group: one-time cranial irradiation (6 Gy) at postoperative day 5 and daily i.p. injections of vehicle substance from postoperative day 3 to 17. (iii) CCI-779 group: daily i.p. injections of CCI-779 (Torisel®) at 20 mg/kg body weight from postoperative day 3 to 17. (iv) Radiochemotherapy group: one-time cranial irradiation (6 Gy) at postoperative day 5 and daily i.p. injections of CCI-779 at 20 mg/kg from postoperative day 3 to day 17. Tumor volume was assessed in three mice per treatment group on day 17 after tumor cell inoculation by magnetic resonance imaging (MRI). For the histological assessment of tumor growth,

these same mice were sacrificed at postoperative day 20, brains were isolated and cryosectioned (8 µm) for further histological analysis.

II. APG101 and Cediranib treatment experiments

Animals were divided into different experimental treatment groups as indicated (*n* = 14 each; *n* = 3 for MRI/histology and *n* = 11 for survival analysis). APG101 (Apogenix GmbH, Heidelberg, Germany) was administered twice a week from postoperative day 5 to 20 by intraperiteonal (i.p.) injection at 100 mg/kg body weight. Appropriate control group animals received PBS vehicle substance i.p. injections. Cediranib (AZD271; Recentin®; Selleck Chemicals, Houston, TX, USA) was daily administered at 6 mg/kg bodyweight by oral gavage from postoperative day 5 to 20. Appropriate control group animals received 5% Tween-80 by oral gavage.

2.2.3 Murine cranial irradiation

For local irradiation, brains of VM/Dk mice were irradiated at 6 Gy on postoperative day 5 using 15 MeV electrons from a standard linac radiation source (Siemens, Munich, Germany). Positioning and shielding of the animal were achieved by a lead/plastic shielding allowing the exact application of ionizing radiation with a 100% isodose to the targeted 7 x 7 mm brain section with a maximal dose of 6 Gy in the center, sparing the throat of the mice. Irradiation experiments were conducted in close collaboration with PD Dr. Stephanie Combs, Department of Radiation Oncology, Heidelberg University Hospital, Germany.

2.2.4 Magnetic resonance imaging

MRI was performed using a 1.5 tesla whole-body MR-scanner (Siemens Symphony, Munich, Germany) in combination with a custom-made radio-frequency coil for excitation and signal reception. Morphologic MR-imaging was performed using a transversal T2-weighted turbo-spin echo sequence (repetition time, TR = 4,000 ms; echo time, TE = 109 ms; field of view, FOV = 40 x 40 mm^2; matrix = 128, slice thickness = 1.0 mm; voxel size = 0.3 x 0.3 x 1.0 mm^3). Kinetics of the contrast agent gadolinium-dieethylenetriaminepentaacetic acid (Gd-DTPA, Magnevist®, Bayer-Schering, Berlin, Germany) in tumors were recorded using a T1-weighted inversion-recovery Turbo FLASH (IRTF) sequence (TR = 13 ms; TE = 5.3 ms; TI = 300 ms; FOV = 60 x 60 mm^2; matrix = 128; slice thickness = 2 mm). In total, 80 dynamic scans were acquired from two sections within 10.24 min. MR-Imaging was performed in close collaboration with Dr. Manfred Jugold at the 'Small Animal Imaging Center' of the German Cancer Research Center, Heidelberg, Germany.

2.2.5 Survival analysis

At least 11 mice per indicated treatment group were used for survival analysis according to the Kaplan-Meier method. Mice were sacrificed by an overdose of anaesthetic at the onset of grade 2 neurological symptoms. Neurological symptoms were assessed daily according to modified neurological scores [130]. Grade 0: normal; Grade 1: tail weakness or tail paralysis; Grade 2: hind leg paraparesis or hemiparesis; Grade 3: hind leg paralysis or hemiparalysis; Grade 4: tetraplegia, moribund stage or dead.

2.2.6 Histology on murine brain samples

For histological assessments at least three mice per group were sacrificed and brains isolated, coronally cryosectioned (8 µm) and hematoxylin/eosin stained to visualize tumor and healthy brain tissue.

I. Blood vessel visualization and quantification

Blood vessel stainings were conducted with a rat anti-mouse CD31 antibody (10 µg/mL; BD Bioscience, Heidelberg, Germany) followed by Alexa Fluor 546 goat anti-rat IgG secondary antibody (1:500; Invitrogen, Karlsruhe, Germany) and 4,6-diamidino-2-phenylindol (DAPI; Vectashield Mounting Medium with DAPI, H1200, Vector Laboratories) counter-staining. At least ten microscopic images (Nikon Eclipse 90i; Nikon, Düsseldorf, Germany) per tumor were taken and fluorescent CD31-positive vessels were automatically counted by the NIH ImageJ software (Bethesda, MD, USA).

II. In situ zymography

Mapping of matrix metalloproteinase (MMP) activity was achieved by *in situ* zymography as described before [127]. Briefly, brain sections were incubated with 40 µg/mL Oregon Green 488 conjugated gelatin (Molecular Probes, Oregon, USA). Addition of 10 mmol/l EDTA, served as a negative control. Sections were counterstained with DAPI and green fluorescent gelatinase activity was visualized using a Nikon Eclipse 90i fluorescence microscope (Nikon, Düsseldorf, Germany).

III. Phosphorylation of RPS6

Phosphorylation of RPS6 was detected using a rabbit anti-phospho-RPS6 antibody (Cell Signaling) at a 1:200 dilution and a biotinylated anti-rabbit IgG secondary antibody (Vector Laboratories, Burlingame, CA, USA) and the Vectastain Elite avidin-biotin complex kit (Vector Laboratories) with cobalt chloride-intensified 3,3'-diaminobenzidine (DAB) as chromagen (Sigma-Aldrich, Taufkirchen Germany).

IV. Expression of RGS4

RGS4 expression was detected by a goat anti-RGS4 antibody (N-16; 4 µg/mL; Santa Cruz Biotechnology) and a secondary Alexa Fluor 488 donkey anti-goat IgG antibody (Invitrogen) followed by counter-staining with DAPI.

2.2.7 Immunohistochemistry of human glioma specimens

I. PTEN immunohistochemistry

PTEN-specific immunohistochemistry was performed in T269 and T325 glioblastoma specimens on 3 µm sections from paraffin-embedded patient tumor tissue. Automated immunostaining was performed using a Ventana BenchMark® XT immunostainer (Ventana, Illkirch, France). The protocol included standard pretreatment with cell conditioner 1 (pH 8) for 60 min, followed by antibody incubation for 32 min at 37°C (AF847; dilution 1:200, R&D Systems, Lille, France). UltraView™ Red Detection Kit was used as chromogen (Ventana). Endothelial cells were used as an internal positive control for PTEN positivity.

II. 4IgB7H3 immunohistochemistry

Formalin-fixed paraffin-embedded tissue of human diffuse astrocytomas (WHO grade II, n = 3), anaplastic astrocytomas (WHO grade III, = 7) and glioblastoma (WHO grade IV, n =5) were provided by the Department of Neuropathology, Institute of Pathology, Heidelberg University Hospital, Germany. Sections cut to 3 µm were processed using a Ventana BenchMark XT® immunostainer (Ventana Medical Systems, Tucson, AZ, USA). The staining procedure included a pretreatment with cell conditioner 1 (pH 8) for 60 min, followed by incubation with a goat anti-human 4IgB7H3 antibody (1:200; R&D, Minneapolis, MN, USA) at 37°C for 32 min and application of rabbit anti-goat immunoglobulins (P0446, Dako, Glostrup, Denmark) for 32 min at room temperature. The incubation was followed by a Ventana standard signal amplification, UltraWash, counterstaining with one drop of hematoxylin for 4 min and one drop of bluing reagent for 4 min. For visualization, the ultraView™Universal DAB Detection Kit (Ventana Medical Systems) was used. For quantitative analysis of the staining pattern, the immunoreactive score (IRS) was applied. IRS was calculated as product of staining intensity and percentage of positive cells, determined as follows: staining intensity was subdivided into four groups: 0 (negative), 1 (weak), 2 (moderate) and 3 (strong). Percentage of positive cells was regarded as 0 (none), 1 (<10%), 2 (10-50%), 3 (51-80%) and 4 (>80% positive tumor cells).

4IgB7H3 colocalization studies on cryosections of human T269 and T325 glioblastoma samples were performed after acetone fixation and staining with a goat polyclonal anti-human 4IgB7H3 antibody

(R&D, Minneapolis, MN, USA), a mouse anti-human CD31 antibody (Dako), a mouse anti-human alpha-smooth muscle actin (SMA) antibody (Sigma Aldrich) and a rabbit anti-human nestin (Millipore). As secondary antibodies, a donkey anti-mouse Cy3 antibody (Dianova, Hamburg, Germany) and an Alexa 750 goat anti-rabbit antibody (Invitrogen) were used. Finally, sections were counterstained with 4,6-diamidino-2-phenylindol (DAPI) and analyzed with a Zeiss Axio Observer Z1 immunofluorescence microscope (Zeiss, Oberkochen, Germany).

2.2.8 Clinical survival data

Queries of the Repository of Molecular Brain Neoplasia Data (REMBRANDT, National Cancer Institute, Bethesda, MD) for 4IgB7H3 (CD276) and CD95 were conducted online in 2010 following the webpage's instructions.

'The important thing is not to stop questioning.
Curiosity has its own reason for existing'

ALBERT EINSTEIN

3. Results

3.1 Suppression of invasion-driving RGS4 by mTOR inhibition optimizes glioma treatment

Taken into account that anti-angiogenic treatment modalities as well as radiation therapy have been identified to promote tumor cell invasion after an initial response, an optimization of modern glioblastoma therapy could imply a combined anti-invasive and anti-angiogenic treatment regimen, ideally in combination with radiation therapy. Activation of the PI3K/AKT/mTOR signalling pathway by ligand binding to EGF-receptor has been demonstrated to play a crucial role in tumorigenesis, since activation of mTOR is involved in pro-invasive and pro-angiogenic signaling mechanisms. Temsirolimus (CCI-779), a rapamycin derivative, is a potent inhibitor of the mTOR-complex.
The aim of the study was therefore to test the radiation-enhanced inhibition of the glioma mTOR-signaling pathway by CCI-779 for its potential to optimize anti-angiogenic treatment through suppression of cell invasion.

3.1.1 mTOR inhibition with CCI-779 synergizes with radiation in causing cytostatic anti-tumor effects

In order to mimic a clinical setting, in which tumors are exposed to radiation mainly in a fractionated fashion, chronic effects of radiation-combined mTOR inhibition with biologically meaningful higher single doses of radiation and CCI-779 were tested in glioma cell cultures. Effective working concentrations of CCI-779 for all further *in vitro* investigations were identified by treatment of different glioma cell lines with increasing concentrations of CCI-779 and analysis for phosphorylation of ribosomal protein S6 (P-RPS6). P-RPS6 is a direct substrate of mTORC1-phosphorylated S6K1 that correlates with mTORC1 activity. Phosphorylation of RPS6 was inhibited by CCI-779 in a concentration-dependent manner in almost all glioma cell lines irrespective of their *PTEN* status, except for the *PTEN* wild-type cell line LNT-229 (Figure 8A).
To exclude immunosuppressive effects of CCI-779, the compound was tested in different mixed leukocyte reactions (MLR) using different pairs of healthy human leukocyte donors. A significant immunosuppression with CCI-779 concentrations starting at 100 nM was observed (Figure 1B). Therefore the non-immunosuppressive but effective CCI-779 concentration of 10 nM was used as a standard concentration in following *in vitro* experiments.

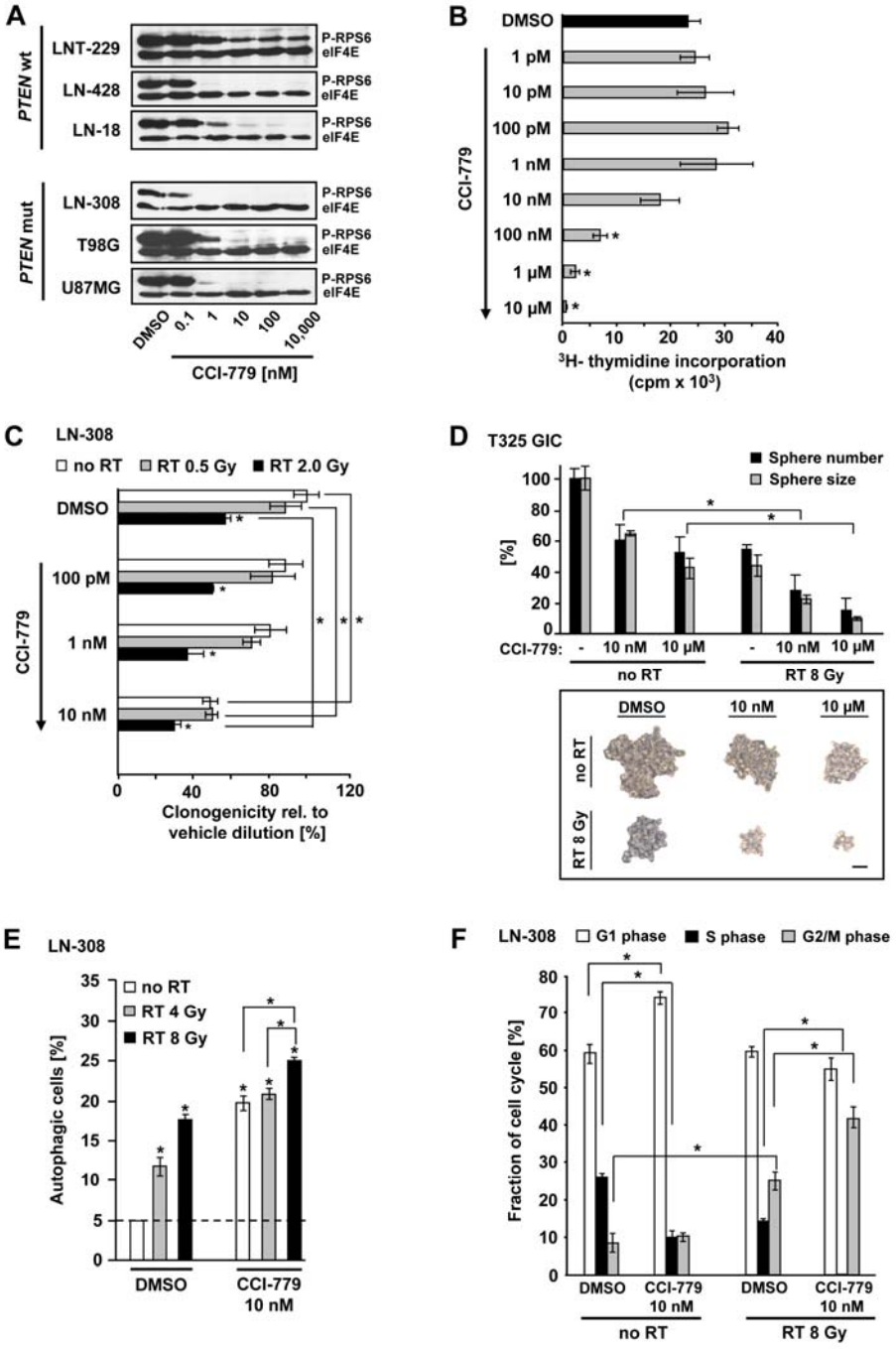

Figure 8. Anti-glioma effects by irradiation-combined mTOR inhibition

(A) Immunoblot analyses of CCI-779-treated glioma cells with different *PTEN* status (*PTEN* wild-type (*PTEN* wt) and *PTEN*-mutated (*PTEN* mut) for RPS6 phosphorylation (P-RPS6). eIF4E served as a loading control. **(B)** Mixed leukocyte reactions evaluating the immunosuppressive properties of CCI-779 at indicated concentrations. Data are expressed as counts per minute (cpm) following incorporation of [^{3}H]-methylthymidine (*$p < 0.05$). **(C)** Cell cycle analysis of DAPI-stained LN-308 glioma cells following indicated treatment (mean ± SD, $n = 3$, *$p < 0.05$). **(D)** Clonogenic survival of LN-308 cells following treatment (mean ± SD, $n = 3$, *$p < 0.05$ relative to unirradiated, vehicle-treated control condition set as 100%). **(E)** Sphere formation capacity of T325 GIC. Top: data are expressed as percentages of sphere number and sphere size, respectively, relative to the unirradiated, vehicle-treated control condition set as 100% (mean ± SD, $n = 3$, *$p < 0.05$). Bottom: Representative T325 GIC-derived glioma spheres are depicted (scale bar, 200 μm). **(F)** Flow cytometry-based analysis of autophagy in LN-308 cells. Data are expressed as percentages of acridine orange-positive cells, and percentage of five was set as the autophagic baseline level in vehicle-treated control cells (mean ± SD, $n = 3$, *$p < 0.05$).

In order to evaluate potential functional effects of irradiation-combined CCI-779 treatment on glioma biology, analyses of clonogenicity, sphere formation of primary GIC, autophagy and cell cycle and were conducted.

The anticlonogenic effect of irradiation was significantly enhanced by CCI-779 (Figure 8C). Analogous results were obtained for primary GIC whose sphere-forming capacity was additively impaired by combined application of CCI-779 and irradiation (Figure 8D).

Since mTOR inhibitors are associated with induction of autophagy, the effects of irradiation-combined CCI-779 treatment on this process were analyzed in LN-308 glioma cells. The autophagy-inducing effect of irradiation both at 4 Gy and 8 Gy was significantly enhanced when combined with CCI-779 (Figure 8 E).

CCI-779, when applied alone, induced a significant G1 cell cycle arrest in LN-308 glioma cells. However, when used as a radiosensitizer, CCI-779 did not affect the G1/S transition but significantly enhanced the G2 cell cycle arrest caused by irradiation alone (Figure 8F).

Taken together, mTOR inhibition with CCI-779 shows additive effects with irradiation in mediating cytostatic anti-glioma effects.

3.1.2 Irradiation-enhanced mTOR-inhibition exerts anti-invasive activity *in vitro*

Matrigel invasion assays were used to test CCI-779 for the potential to influence invasion of glioma cells. CCI-779 applied at 10 nM caused a 50-70% reduction in glioma cell invasiveness irrespective of the *PTEN* status (Figure 9A). Combined with irradiation, CCI-779 significantly reversed the known pro-invasive effect of sublethal irradiation [68] on *PTEN* wild-type LNT-229 glioma cells in a supra-additive way.

Invasion was in addition examined with multicellular LNT-229 glioma spheroids (Figure 9C) and of *PTEN* wild-type primary T269 GIC (Figure 9D) into three-dimensional collagen gel matrices following treatment with radiation, CCI-779 or both. Consistent with the results obtained in the matrigel invasion assays, the combined treatment regimen proved to be significantly better in comparison with respective single treatment in both invasion assays.

In summary, mTOR inhibition with CCI-779 synergizes with irradiation in inhibiting glioma cell invasion.

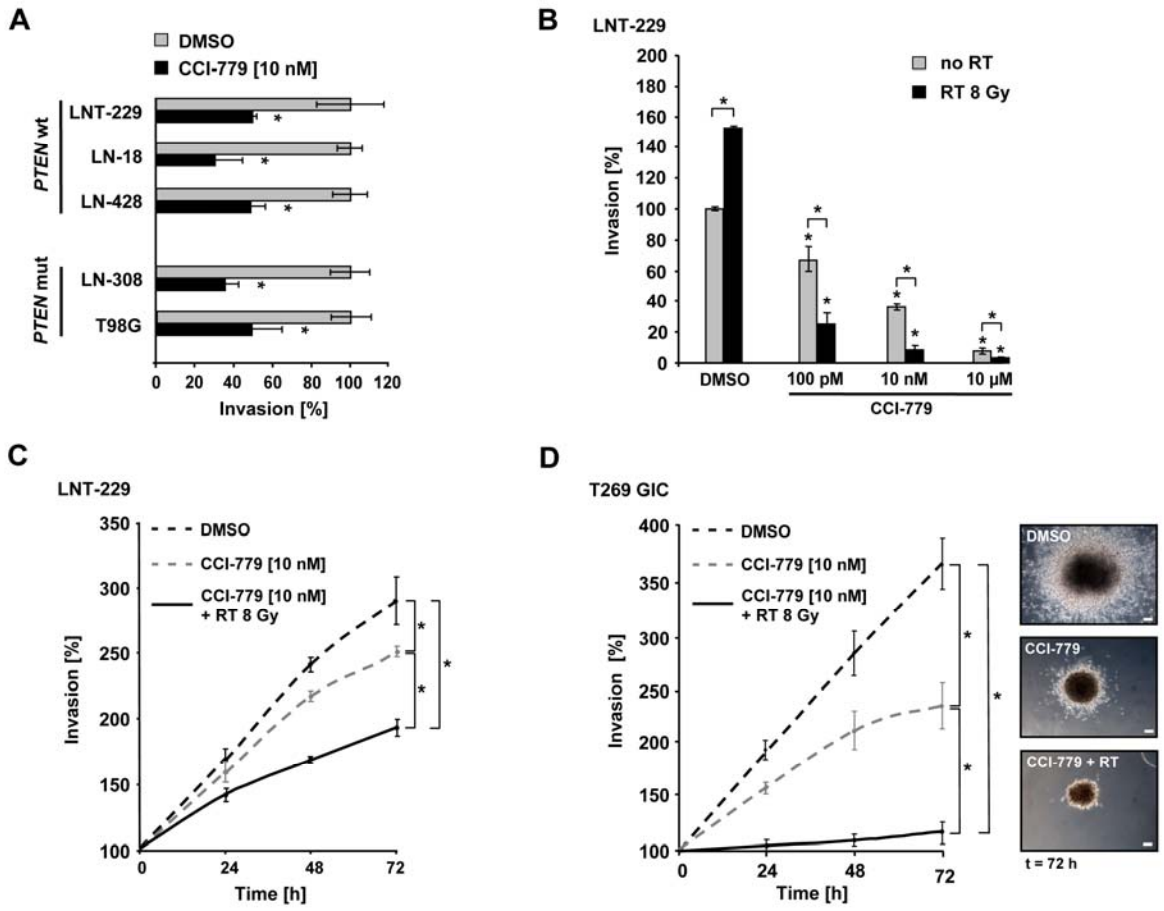

Figure 9. mTOR inhibition counteracts the pro-invasive effect of irradiation irrespective of *PTEN*
(A) Invasion of *PTEN* wild-type (*PTEN* wt) and *PTEN*-mutated (*PTEN* mut) glioma cell lines assayed in matrigel invasion chambers. Data are expressed as percentages of invaded cells relative to the vehicle control. **(B)** Invasion of irradiated LNT-229 cells. Data are expressed as percentages of invaded cells relative to the respective non-irradiated vehicle control. **(C and D)** Spheroids derived from LNT-229 cells (C) and T269 GIC (D) treated as indicated were assayed for invasion into a 3-dimensional collagen matrix. Data are expressed as percentages of the mean migrated distance relative to the initial radius of each individual spheroid at 0 h (n = 3, *p < 0.05). Representative T269 GIC spheroids at 72 h are depicted (scale bars, 100 µm).

3.1.3 Microarray analysis identifies novel candidate molecules transcriptionally downregulated through radiation-combined CCI-779

In order to shed new light on the molecular mechanisms underlying the modes of action of CCI-779 in glioma cells, comparative cRNA microarray analyses were performed to asses the transcript expression profiles of LN-308 cells upon treatment with CCI-779, radiation or both.

As a result, we discovered that CCI-779 lead to a significant upregulation of 64 transcripts and downregulation of 91 transcripts. Combined treatment resulted in upregulation of 85 transcripts and downregulation of 65 transcripts. Both treatment groups showed an overall overlap of 58 deregulated transcripts. Of note, irradiation alone did not significantly alter the expression profile of

LN-308 cells within a time interval of 48 h. This is in line with observations from previous work [131]. Within the transcripts that were regulated by both CCI-779 and irradiation-combined CCI-779, genes known to be associated with angiogenesis and cell motility were considerd to be particularly relevant. Amongst these, two candidate molecules downregulated by both CCI-779 and irradiation-enhanced CCI-779 treatment were selected for further analyses: vascular endothelial growth factor receptor (VEGFR)-2 and regulator of G-protein signaling 4 (RGS4).

3.1.4 RGS4 acts as a potent driver of human glioma cell invasiveness

One of the candidate molecules which were identified to be downregulated by CCI-779 was RGS4. By the use of qRTPCR it was proven that *RGS4* was significantly downregulated in LN-308 glioma cells in response to treatment with CCI-779 irrespective of irradiation (Figure 10A).

In *PTEN*-mutant glioma cell lines, a concentration of 10 nM CCI-779 was sufficient to abrogate RGS4 expression, whereas in *PTEN* wild-type cells this concentration had almost no effect. In these cells a CCI-779 concentration of 10 µM was necessary to downregulate RGS4. This suggests that the protective effect of a wild-type *PTEN* status can be overcome in a concentration-dependent manner (Figure 10B).

Taken into account that RGS4 has been previously mentioned to be associated with tumor cell invasion [132], the influence of RGS4 on invasion was tested by using matrigel invasion assays. Silencing of *RGS4* in LN-308 cells mediated by si-RNA technology (knock-down of 74%) resulted in a 80% decrease in invasion (Figure 10C). Conversely, stable overexpression of RGS4 led to a 62% increase in invasion (Figure 10C). Treatment of RGS4-overexpressing LN-308 cells with CCI-779 at 10 nM displayed a partial rescue mediated by overexpressed RGS4. Taken together, this proves that the anti-invasive effect of CCI-779 treatment is mediated through impaired RGS4 signaling.

To investigate if RGS4 preserves its invasion-promoting function *in vivo*, human LN-308 glioma cells, stably overexpressing RGS4 (Figure 11A), were stereotactically implanted into the right brain hemisphere of nude mice. An influence of RGS4 on cell proliferation was excluded beforehand (Figure 11B).

In order to monitor the orthotopic growth patterns of LN308 gliomas, T2-weighted cranial MRI scans, which are aiming at monitoring invasive growth processes, were conducted. They revealed a five-fold increase in the mean volume of RGS4-overexpressing gliomas compared to empty vector control tumors (Figure 11C). In addition, RGS4-overexpressing gliomas were characterized by a more diffuse growth pattern and by the formation of satellite tumors in comparison with less invading LN-308 gliomas under control conditions (Figure 11G).

In summary, the data demonstrates that RGS4 serves as a driver molecule of glioma cell invasion *in vitro* and *in vivo* and can be suppressed by inhibition of mTOR by CCI-779.

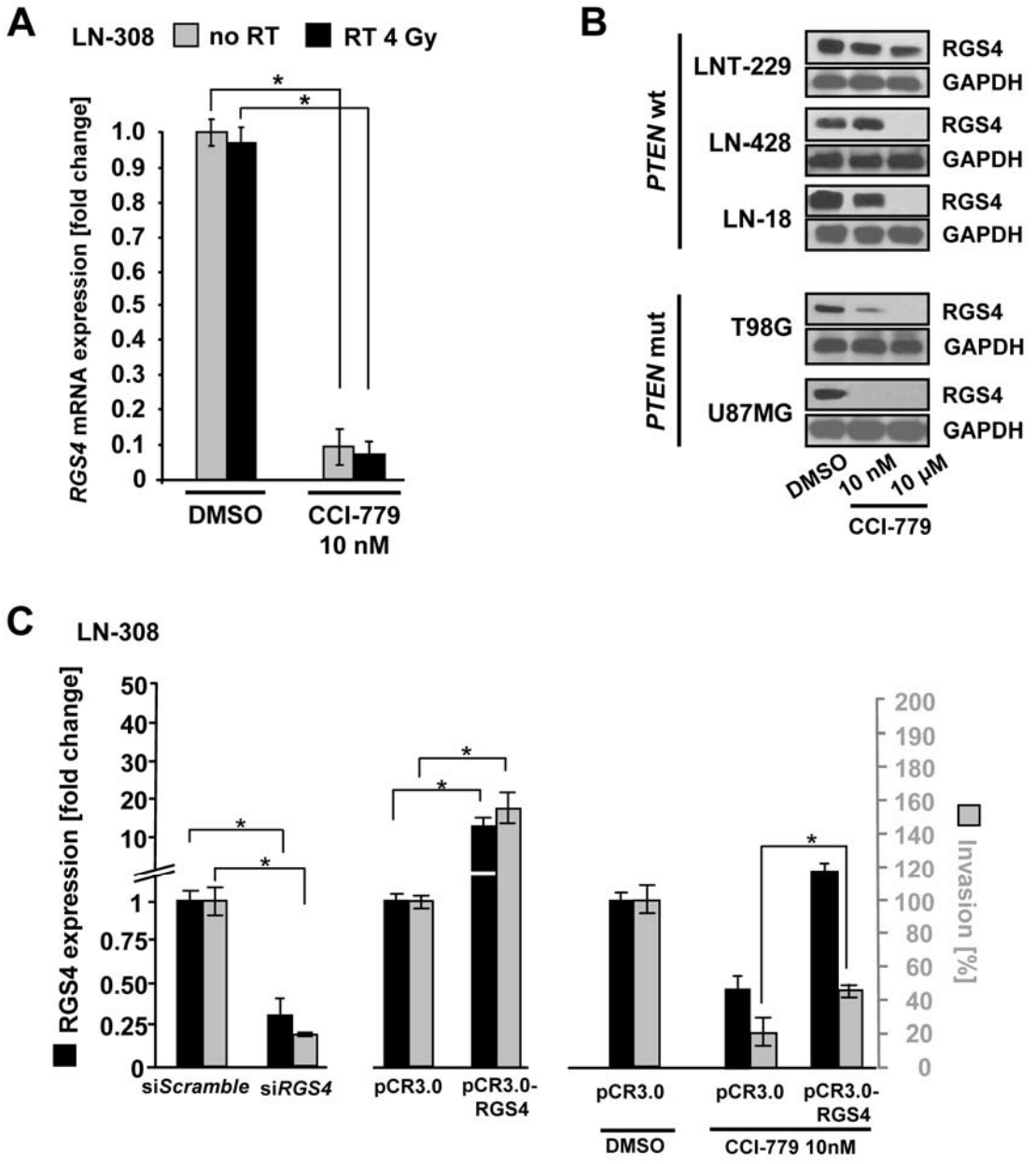

Figure 10. RGS4 is a novel invasion-associated target of mTOR inhibition

(A) Analyses of CCI-779-mediated downregulation of *RGS4* mRNA in LN-308 cells by qRT-PCR (mean ± SD, $n = 3$, $^*p < 0.05$). **(B)** Immunoblot analysis of RGS4 protein expression in different *PTEN* wild-type (*PTEN* wt) and *PTEN*-mutated (*PTEN* mut) glioma cells. GAPDH served as a loading control. **(C)** Comparative analysis of *RGS4* mRNA expression by qRT-PCR and matrigel invasion of LN-308 glioma cells upon siRNA-mediated knock-down (si*RGS4*, left), stable overexpression of RGS4 (pCR3.0-RGS4, middle), and upon treatment with CCI-779 (right). qRT-PCR data are expressed as fold changes relative to respective control-transfected cells (see left y-axis; mean ± SD, $n = 3$, $^*p < 0.05$). Invasion data are expressed as percentages of invaded cells relative to the same controls set as 100% each (see right y-axis; mean ± SD, $n = 3$, $^*p < 0.05$).

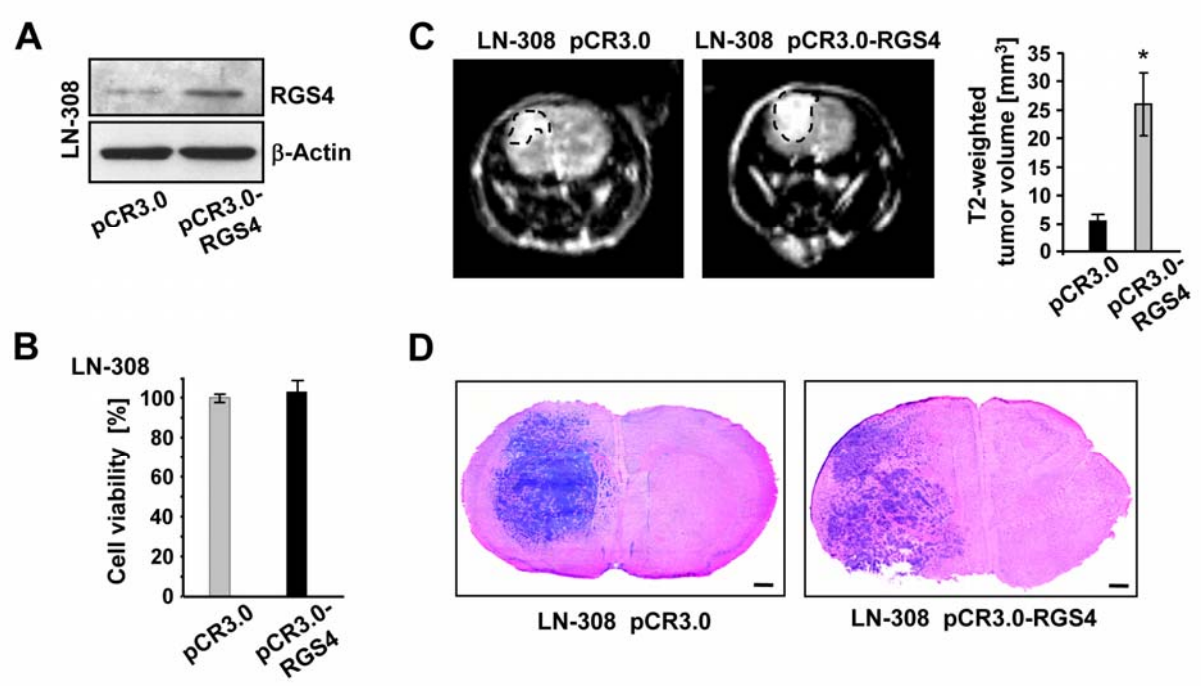

Figure 11. RGS4 exhibits a glioma invasion-promoting function *in vivo*

(A) Immunoblot analyses of control (pCR3.0) and stably RGS4-overexpressing (pCR3.0-RGS4) LN-308 cells. Actin served as a loading control. **(B)** Differences in cell viability between pCR3.0- and pCR3.0-RGS4-transfected LN-308 cells as potential bias of invasion results were excluded by crystal violet staining. Data are expressed as percentages of viable pCR3.0-RGS4-transfected cells relative to empty vector-transfected cells set to 100% (mean ± SD, n = 3). **(C)** Left: Representative T2-weighted MRI on day 48 after orthotopic implantation of pCR3.0- and pCR3.0-RGS4-transfected human LN-308 glioma cells. Right: T2-based tumor volumetry (mean ± SD, n = 4 per group, $*p < 0.05$). **(D)** Histological analysis of coronally cryosectioned and hematoxylin/eosin (H&E)-stained mouse brains harboring RGS4-overexpressing LN-308 gliomas (right) or control tumors (left) (scale bars, 1 mm).

3.1.5 Irradiation-enhanced CCI-779 treatment exerts anti-angiogenic effects in gliomas

Glioblastomas are highly hypoxic tumors and are therefore among the best vascularized human malignancies. Angiogenic processes are based on upregulated HIF-1α-mediated VEGF-signaling processes, provoked by a hypoxic tumor environment. Given that the stimulation and enhancement of VEGF-expression is not only driven by hypoxia but also by irradiation [133, 134] and that radiation therapy is applied as a first-line therapy in glioblastoma, this part of the project aimed at analyzing the potential of CCI-779 to reverse the stimulated release of VEGF.

CCI-779 applied at 10 nM to LN-308 glioma cells led to a significant suppression of VEGF release induced by irradiation (Figure 12A) or hypoxia (1% O_2; Figure 12B). In addition, CCI-779 combined with irradiation demonstrated a synergistic antiangiogenic activity *in vitro,* which was assessed in

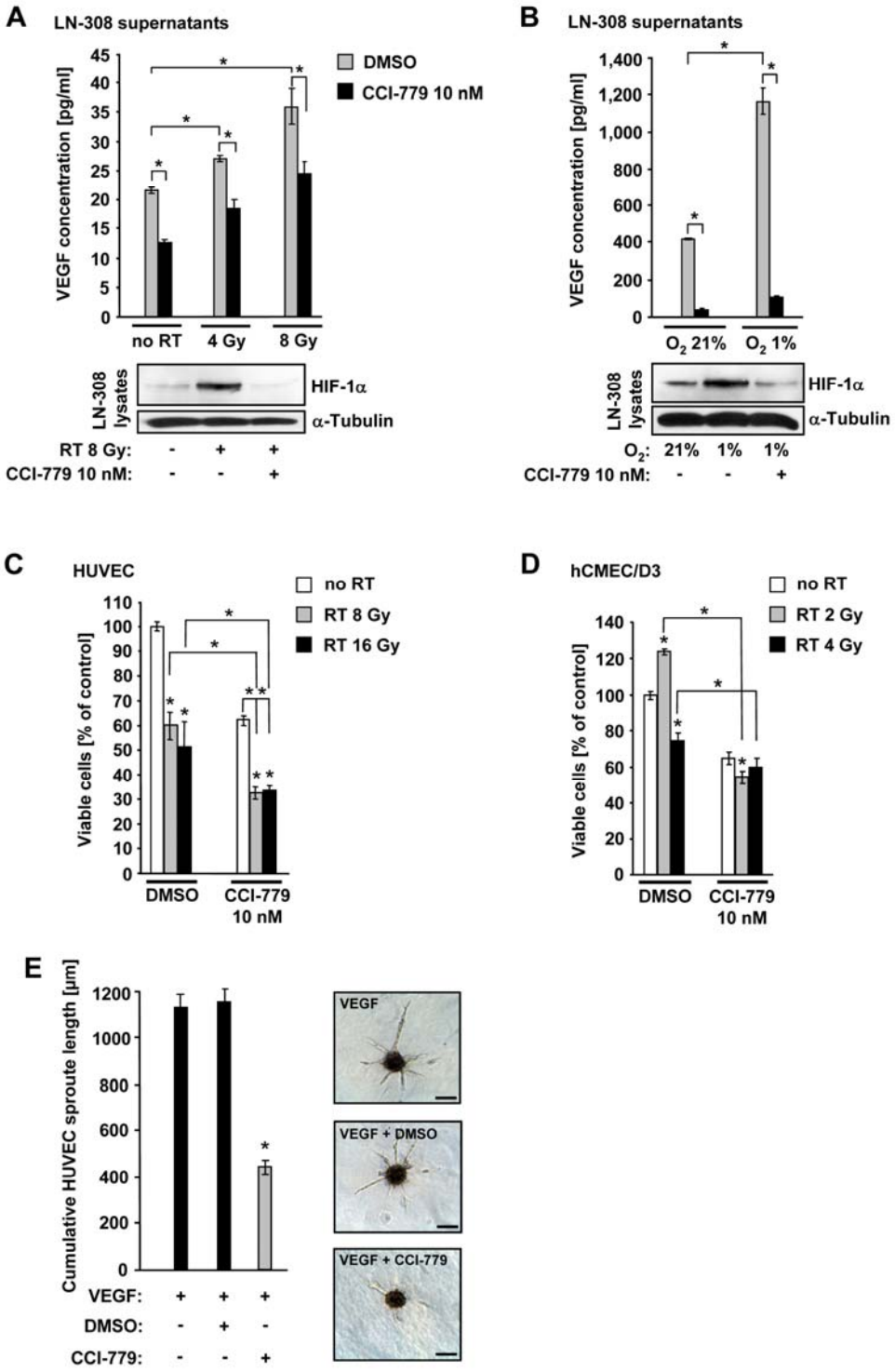

Figure 12. Antiangiogenic effects by irradiation-enhanced mTOR inhibition *in vitro*

(A and B) Effects of CCI-779 on VEGF release promoted by ionizing radiation (A) and hypoxia (B). Top panels: VEGF concentrations in conditioned supernatants from LN308 glioma cells quantified by ELISA (mean ± SD, n = 3, *$p < 0.05$). Bottom panels: Expression analyses of HIF-1α by immunoblot with protein lysates prepared from the same cells. α-tubulin served as a loading control. **(C and D)** Viability of HUVEC (C) and brain-derived hCMEC/D3 (D) in response to treatment with CCI-779 and irradiation.Data are expressed relative to the vehicle-treated control set to 100% (mean ± SD, n = 3, *$p < 0.05$). **(E)** VEGF-induced (25 ng/mL) sprouting of CCI-779 treated HUVEC spheroids (mean ± SD, n = 3, *$p < 0.05$) with depicted representative sprouting HUVEC spheroids (scale bars, 100 µm).

viability assays of primary human umbilical vein endothelial cells (HUVEC; Figure 12C) and human cerebral microvascular endothelial cells (hCMEC/D3; Figure 12D). Furthermore, CCI-779 alone also reduced VEGF-induced sprouting of HUVEC at concentrations of 10 nM (Figure 12E).

Taken together, these results reveal that an inhibition of mTOR counteracts pro-angiogenic signals triggered by radiation and tumor hypoxia, providing a rationale for adding CCI-779 to radiation therapy.

3.1.6 Inhibition of mTOR downregulates VEGFR-2 on glioma and endothelial cells

Besides RGS4, the vascular endothelial growth factor receptor 2 (VEGFR-2) was one of the molecules identified in the microarray analysis to be downregulated by both CCI-779 and irradiation-enhanced CCI-779 treatment.

The VEGFR-2, together with VEGFR-1 and VEGFR-3, belongs to the transmembrane VEGFR tyrosine kinase family, and it's signaling, mediated by binding of its main ligand, VEGF, is essential for various functions of vascular endothelial cells underlying angiogenesis in physiological and pathological conditions [135].

For further analysis, downregulation of *VEGFR-2* in response to 10 nM CCI-779 was first validated by qRT-PCR (Figure 13A). Analyses of VEGFR-2 expression in glioma cell lines with different *PTEN* status revealed that *PTEN*-mutant glioma cells were more susceptible to CCI-779-mediated downregulation of VEGFR-2 (Figure 13B). In contrast to gliomas cells, human endothelial cells displayed an upregulation of *VEGFR-2* mRNA and protein expression in response to irradiation. This induction was counteracted by CCI-779 in a concentration dependent manner (Figure 13C). In summary, mTOR inhibition with CCI-779 leads to a reduced expression of VEGFR-2 on both human glioma and endothelial cells, besides a declined release of glioma-derived VEGF. This suggests a disruption of the pro-angiogenic VEGF/VEGFR-2 signaling axis at both the ligand and receptor levels.

3.1.7 CCI-779-mediated suppression of invasiveness and angiogenesis are regulated through both mTOR-complexes mTORC1 and mTORC2

A phosphorylation-mediated activation of AKT caused by the inhibition of mTOR has been shown in previous reports for a number of cancer cell lines and human tumor samples [136-138]. This AKT feedback-loop activation during mTOR inhibition is associated with the development of cellular resistance to mTOR inhibitors. In order to elucidate whether a treatment with CCI-779 at effective concentrations results in AKT activation and therefore contribute to resistance, CCI-779 treated cells were analyzed for mTOR-, mTORC2- and AKT-activity. CCI-779 applied at 10 nM inhibited mTORC1

activity, which was assessed by decreased phosphorylation levels of RPS6 (Figure 7A), but did not alter mTORC2 activity, indicated by unchanged levels of phospho-mTOR^{S2481}, a recently described marker for an intact mTORC2 [139]. The inhibition of mTOR was in fact paralleled by an increase in phosphorylation of AKT^{S473}, reflecting the above mentioned negative feedback loop activation of AKT (Figure 14A).

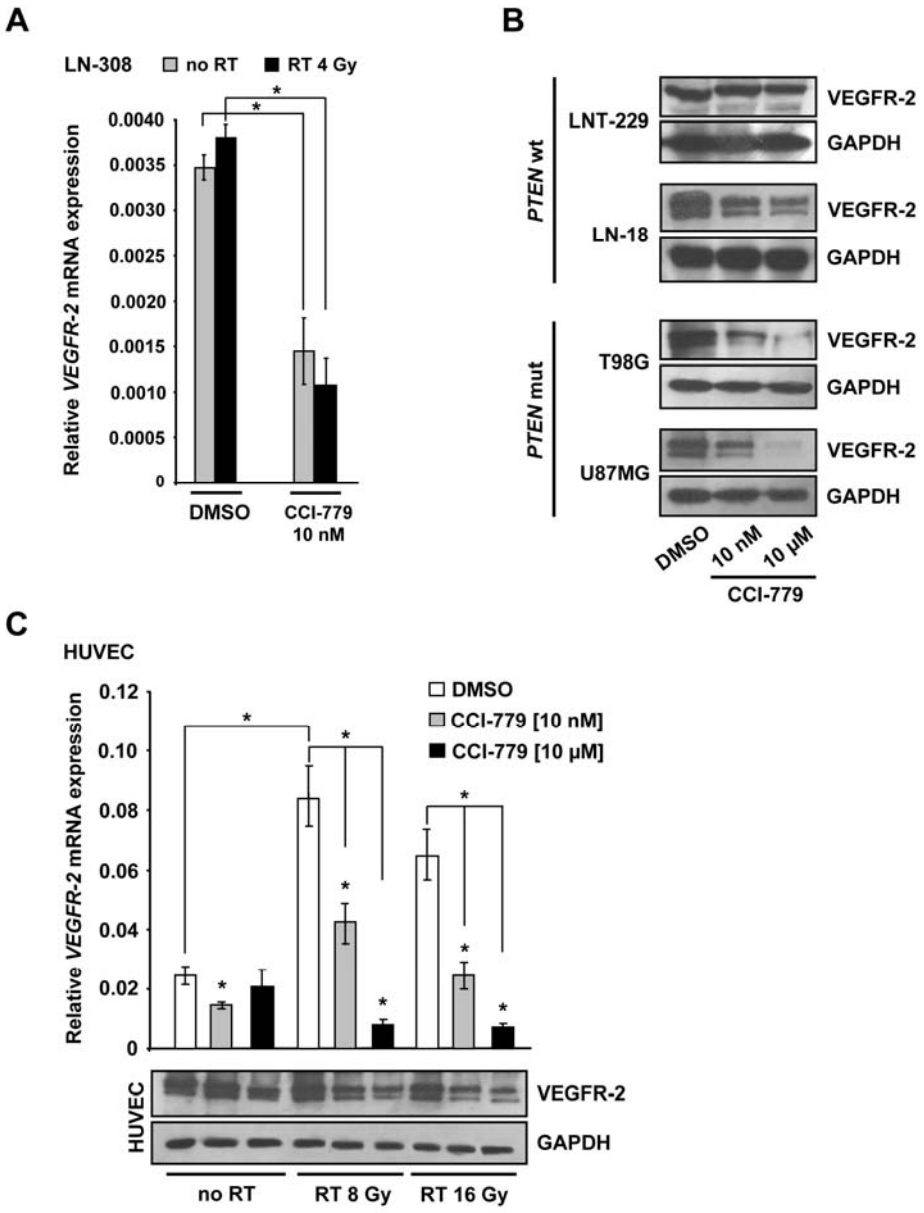

Figure 13. mTOR inhibition downregulates VEGFR-2 on glioma and endothelial cells

(A) CCI-779-mediated downregulation of *VEGFR-2* mRNA in LN-308 cells by qRT-PCR (mean ± SD, $n = 3$, $^*p < 0.05$). **(B)** Immunoblot analysis of VEGFR-2 protein expression in different *PTEN* wild-type (*PTEN* wt) and *PTEN*-mutated (*PTEN* mut) glioma cells. GAPDH served as a loading control. **(C)** Top: qRT-PCR analysis of *VEGFR-2* mRNA expression in HUVEC treated as indicated. Bottom: immunoblot analysis of VEGFR-2 protein expression in HUVEC following treatment as indicated for top panel (mean ± SD, $n = 3$, $^*p < 0.05$). GAPDH served as a loading control.

However, higher CCI-779 concentrations of about 10 µM inhibited mTORC2 activity and led to a reduction of AKT^{S473} phosphorylation back to baseline levels. This suggests that feedback activation of AKT during mTORC1 inhibition was mediated by mTORC2 activity at low CCI-779 concentrations. The mTOR complex mTORC2, is shown here to be sensitive to CCI-779 treatment in glioma, albeit at concentrations, which are above the ones needed to block mTORC1 activity.

Taken together, the data indicates that the feedback activation of AKT induced by CCI-779-mediated mTORC1 inhibition is mediated through mTORC2 signaling and abolished through higher though specific and clinically achievable concentrations of CCI-779 (Peak concentration of CCI-779 in patients following an intravenous infusion of just 25 mg reaches 500 nmol/L). Given the observation that mTORC1 and mTORC2 are inhibited by different concentrations of CCI-779, the question whether regulation of VEGFR-2 and RGS4 are mediated through signaling of mTORC1, mTORC2, or both arises. By using siRNA-mediated knock-down transfectants of LN-308 cells targeting the two interacting proteins mTOR specifically assembles with to form either mTORC1 or mTORC2: Raptor and Rictor, respectively. A silenced expression of both *Raptor* and *Rictor* resulted in a highly significant downregulation of both *VEGFR-2* and *RGS4* on mRNA level (Figure 14B). In addition, both knock-downs resulted in significant less invasion than control transfectants when analyzed in matrigel invasion chambers (Figure 14C).

Data recently published by [140] hint at a regulation of RGS4 expression by the PI3K/AKT/glycogen synthase kinase (GSK)-3β pathway. In contrast to this study, CCI-779 applied at 10 nM did not alter phosphorylation of GSK-3β that becomes inactivated by AKT kinase activity, while RGS4 expression was abolished (Figure 15A). Conversely, activation of GSK-3β by protein dephosphorylation mediated by the protein kinase C-β inhibitor enzastaurin [141] was not accompanied by an increase in RGS4 expression, neither on mRNA nor on protein level (Figure 15B).

In summary, the data led to the conclusion that invasion, depending on signaling through RGS4 and angiogenesis, depending on signaling through VEGFR-2 are controlled by both mTOR complexes, mTORC1 and mTORC2, and are in addition regulated independently from any AKT activity.

3.1.8 CCI-779 inhibits glioma growth, angiogenesis and invasion and prolongs survival in a syngeneic mouse glioma model

In order to integrate the different findings on mTOR-inhibition by CCI-779 obtained *in vitro* and to challenge the differential effects on the immune system (potentially negative) and invasiveness or angiogenesis (potentially positive), irradiation-combined CCI-779 treatment was examined in an immuno-competent *in vivo* model using murine *PTEN* wild-type glioma cells. Sensitivity of these SMA-560 glioma cells to mTOR-inhibition was tested beforehand by immunoblot, analyzing

phoshorylation levels of RPS6 in response to different CCI-779 concentrations (Figure 16A). SMA-560 glioma cells were then stereotactically implanted into the right brain hemisphere of VM/Dk mice and glioma growth was monitored by MRI scans. Animals received combined treatment regimen of CCI-779 (20 mg/kg body weight) and 6 Gy cranial irradiation (RT) at 6 Gy with either alone and a CCI-779-vehicle treatment.

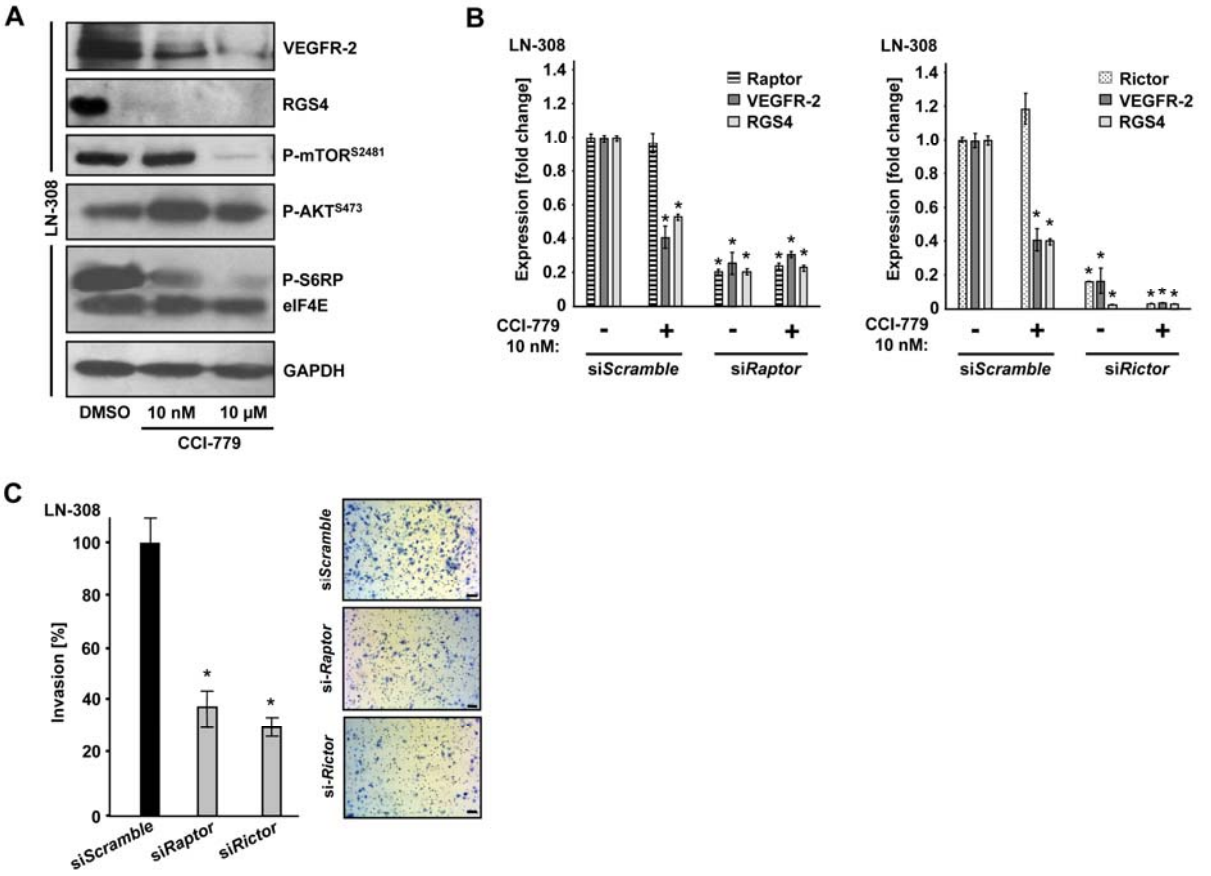

Figure 14. CCI-779 inhibits mTORC1 and mTORC2 both controlling expression of VEGFR-2 and RGS4
(A) Immunoblot analyses of RGS4 and VEGFR-2 expression and phosphorylation of mTOR^{S2481}, AKT^{S473} and RPS6 in LN-308 glioma cells treated with CCI-779 at indicated concentrations. eIF4E and GAPDH served as loading controls. **(B)** qRT-PCR-based analysis of *VEGFR-2* and *RGS4* mRNA expression in *Raptor*-silenced (left) and *Rictor*-silenced (right) LN-308 glioma cells.Non-targeting scramble siRNA (si*Scramble*) served as a control. Data are expressed as fold changes relative to vehicle-treated si*Scramble*-transfected cells set as 1 (mean ± SD, $n = 3$, $^*p < 0.05$). **(C)** Matrigel invasion analysis of Raptor- and Rictor-silenced LN-308 glioma cells. Data are expressed as percentages of invaded cells relative to si*Scramble*-transfected control cells set as 100% (mean ± SD, $n = 3$, $^*p < 0.05$). Representative Boyden chamber membranes are depicted (scale bars, 100 µm).

Of note, clinically relevant doses for humans reach from 25 to 75 mg per week flat dosing which corresponds, in a normally proportioned male (180 cm, 75 kg) to 4.2 to 33 mg/kg mouse weight (www.accessdata.fda.gov/scripts/cder/onctools/animalquery.cfm).

MRI scans taken on day 17 post glioma cell implantation demonstrated that CCI-779, in comparison with vehicle treatment or RT alone, resulted in significantly reduced tumor volumes. In addition, T1-weighted MRI scans revealed less gadolinium contrast enhancement, indicating a reduced vascularization of CCI-779 treated gliomas. This effect was even enhanced when combined with RT (Figure 16B).

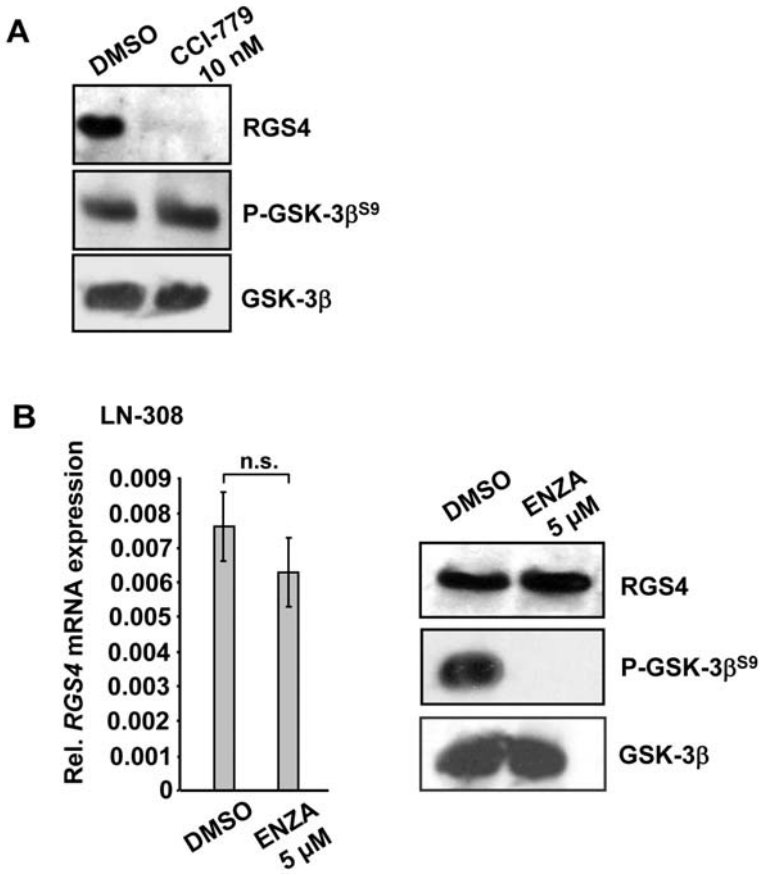

Figure 15. Downregulation of RGS4 by mTOR inhibition is independent from GSK-3β signaling
(A) Immunoblot analysis of RGS4 expression and GSK-3β phosphorylation LN-308 glioma cells treated with CCI-779. Total GSK-3β served as a loading control. **(B)** Left panel: *RGS4* mRNA expression quantified by qRT-PCR in LN-308 cells treated with the protein kinase C-β inhibitor enzastaurin (ENZA) or vehicle control (mean ± SD, *n* = 3; n.s = not significant). Right panel: Immunoblot analysis of RGS4 expression and GSK-3β phosphorylation in LN308 glioma cells treated with ENZA for 24 h. Total GSK-3β served as a loading control.

Histological analyses in forms of H&E stainings, conducted on post-operative day 20, confirmed the MRI-scan based observations about reduced tumor volumes (Figure 16B) and revealed an effective CCI-779-mediated inhibition of mTOR signaling by a reduced phospho-RPS6 immunostaining (Figure 16B). Histology on blood vessels, based on CD31 (PECAM)-specific immunoreactivity (Figure 16B) and quantitative analyses, based on semi-automated vessel quantification (Figure 16C), revealed a weaker vascularization pattern in CCI-779- and CCI-779/RT-treated gliomas compared to control or RT-treated tumors.

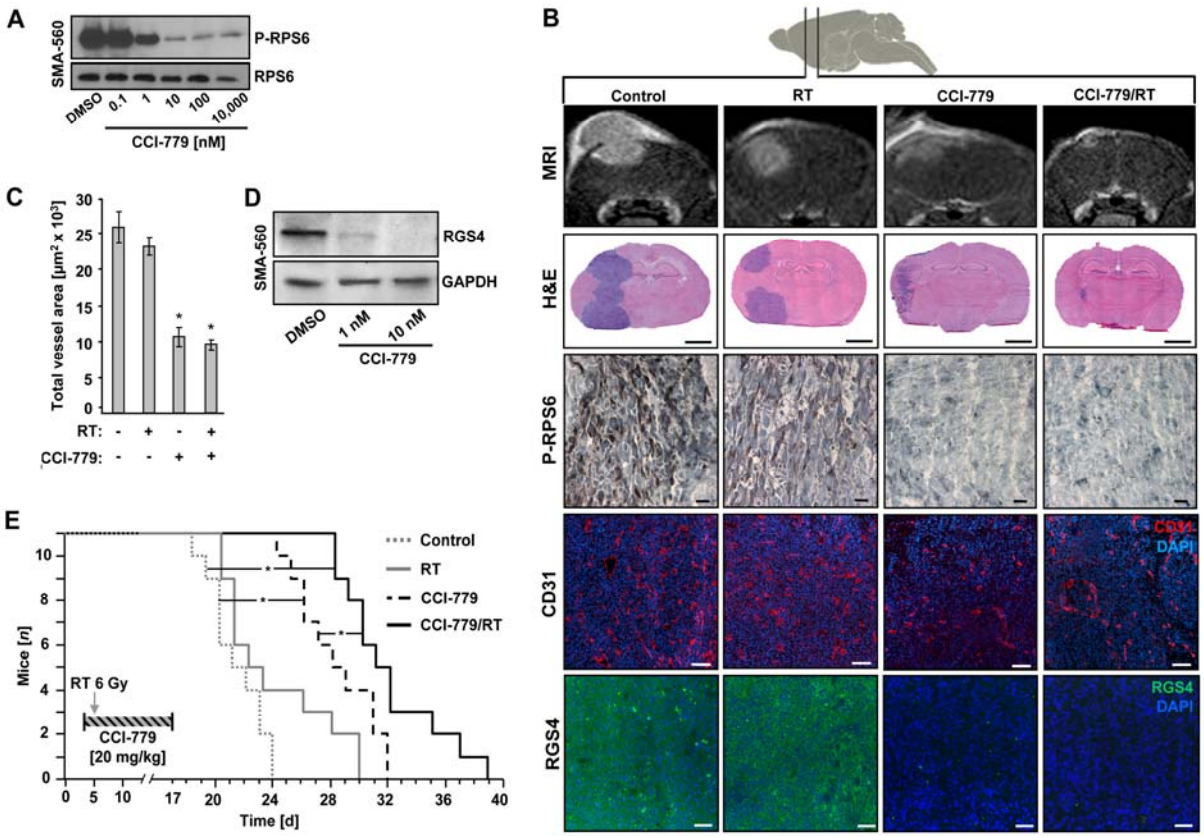

Figure 16. mTOR inhibition disrupts angiogenesis and invasion and prolongs survival in a mouse model

(A) Immunoblot analysis of RPS6 phosphorylation (P-RPS6) in *PTEN* wild-type SMA-560 cells after CCI-779 treatment. **(B)** MRI-monitored orthotopic growth analysis of SMA-560 glioma treated as indicated (Top row). Immunohistochemical evaluation on post-operative day 20 by H&E staining (Second row from top; scale bars = 2 mm), staining of P-RPS6 (third row from top; scale bars, 20 µm) CD31 (second row from bottom; scale bars, 100 µm), and RGS4 (bottom row; scale bars, 50 µm). **(C)** Vascularization of SMA-560 gliomas in each treatment group was assessed by semi-automated quantification of the total CD31-positive vessel area depicted in (B), second row from bottom (mean ± SD, n = 3 per treatment group, *$p < 0.05$). **(D)** Immunoblot analysis of RGS4 in CCI-779-treated SMA-560 cells *in vitro*. GAPDH served as a loading control. **(E)** Survival data of mice treated as indicated plotted by the Kaplan-Meier method and analyzed by the log-rank test (n = 11 per treatment group, *$p < 0.05$).

Aiming at elucidating the impact of mTOR-inhibition on RGS4 expression levels *in vivo,* CCI-779 treated tumors were histochemically analyzed for RGS4-immunoreactivity. Expression of invasion-associated RGS4 was thereby almost eradicated apart from any radiation treatment (Figure 16B). Furthermore, an *in vitro* immunoblot assay confirmed RGS4 downregulation on protein level in murine SMA-560 glioma cells upon treatment with CCI-779 (Figure 16D). As evaluated by Kaplan-Meier survival analyses, the striking anti-tumoral effects mediated by radiation-combined CCI-779 resulted in a significant survival benefit of glioma bearing mice in comparison to vehicle treated control or irradiated animals (Figure 16E). Sole radiation therapy prolonged survival of tumor-bearing

mice in comparison to control animals, but this difference was not significant. Most notably, irradiation enhanced CCI-779 treatment led to a significant survival benefit over CCI-779 treatment alone.

Taken together, the results from this animal experiment clearly demonstrate *in vivo* several advantages of high-dosed CCI-779 treatment in combination with radiotherapy. The combined treatment regimen causes considerable control of tumor growth, angiogenesis and invasion, even in a highly tumorigenic tumor without any observable immune related side-effects.

3.1.9 The PTEN status is of limited predictive value regarding the sensitivity of glioma cells to mTOR inhibition

Based on a functional loss of the PTEN tumor suppressor protein, the EGFR/PI3K/AKT/mTOR signaling pathway is hyperactivated in 30% to 40% of glioblastomas [51]. Previous reports have shown that loss of PTEN results in enhanced sensitivity to mTOR inhibitors, like rapamycin or CCI-779 [142-144]. Contrary to these findings, other reports suggest that the expression of PTEN is not sufficient to predict responsiveness to mTOR inhibition in glioblastoma [145].

In order to evaluate if PTEN-proficient glioma cells respond to the cytostatic activity of CCI-779 as well, the PTEN status of different human and murine glioma cell lines well as of primary human GIC cultures was assessed. Assignment of the PTEN status was accomplished by sequence analysis of *PTEN* cDNA, *PTEN* promoter methylation analysis, immunoblot and immunohistochemical analyses of PTEN expression, and immunoblot analyses of AKT-phosphorylation at T^{308} and S^{473}, since inhibition of AKT-phosphorylation of is a downstream effector mechanism of PTEN (Figure 17A-C and Table 5).

These data on PTEN expression and functionality were then correlated with cell type-specific IC_{50} values of CCI-779 generated in cell viability assays (Figure 17D and Table 5) by using a two-sided Fisher-Yates test of significance. Neither PTEN mRNA expression nor protein levels, *PTEN* promoter methylation, *PTEN* mutational status nor constitutive AKT phosphorylation at T^{308} or S^{473} correlated with the response to CCI-779. In conclusion, these data suggest that PTEN is only of limited value in predicting the sensitivity of glioma cells to mTOR inhibition with CCI-779.

Table 5. **PTEN status of glioma cells and response to CCI-779**

Cells	PTEN				P-AKT ^{T308}	P-AKT^{S473}	IC_{50} (CCI-779)
	cDNA	Promotor	Promotor (WB)	Protein (IHC)			
LNT-229[1]	wt	M	+	N/A	-	-	7.9µmol/L
LN-428[1]	wt	U	+	N/A	+	-	9.7µmol/L
LN-18[1]	wt	M	+	N/A	-	-	0.8nmol/L
LN-308[1]	mut	M	-	N/A	+	+	0.7nmol/L
T98G[1]	mut	U	+	N/A	+	-	0.6nmol/L
U87MG[1]	mut	U	-	N/A	+	+	0.8nmol/L
SMA-560[2]	wt	U	+	N/A	+	-	3.6µmol/L
T269[1]	wt	U	+	+	+	+	5.2µmol/L
T325[1]	mut	U	+	-	-	+	3.2µmol/L

[1]Human; [2]Murine; [3]Truncating frameshift mutation through d165/212 (corresponds to a deletion of exon 6) and subsequent stop codon at 173; [4] In-frame point mutation L42R; [5] In-frame point mutation R55S plus d56/70 (corresponds to an in-frame deletion of exon 3); [6] In-frame point mutation M134I.

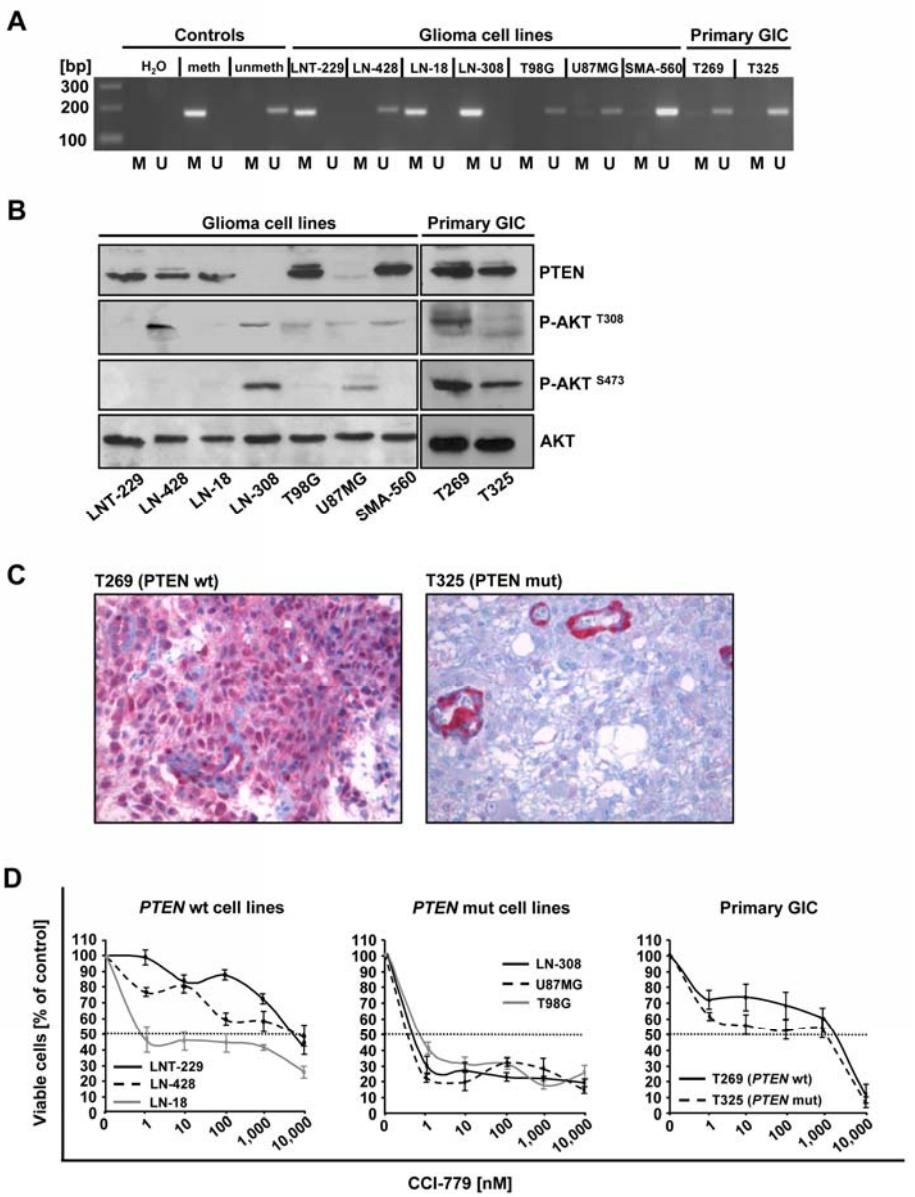

Figure 17. The PTEN status is of limited predictive value regarding the sensitivity to mTOR inhibition
(A) Methylation analysis of the *PTEN* promoter region by methylation-specific PCR (MSP) of bisulfite-converted genomic DNA derived from human and murine glioma cell lines and primary human GIC cultures. PCR bands generated with primers used to detect methylated DNA sequences (M) indicate a methylated *PTEN* promoter region; PCR bands generated with primers used to detect unmethylated DNA sequences (U) indicate an unmethylated *PTEN* promoter region. H_2O as well as bisulfite-treated hypermethylated (meth) and unmethylated (unmeth) genomic DNA probes served as controls. bp, base pairs. Data was contributed by Dr. Markus Weiler. **(B)** Immunoblot analysis of PTEN expression and phosphorylation of AKT at T^{308} (P-AKT^{T308}) and at S^{473} (P-AKT^{S473}) glioma cells. Total AKT served as a loading control. **(C)** PTEN immunohistochemistry of paraffin-embedded human glioblastoma specimens. The PTEN wild-type tumor T269 (left) shows overall PTEN-specific immunoreactivity whereas in the PTEN-mutated specimen T325 (right), only PTEN wild-type vessels are immunoreactive. Magnification, 200x. Data was contributed by the Department of Neuopathology, University Hospital Heidelberg, Germany. **(D)** Viability of *PTEN* wild-type (*PTEN* wt; left) and *PTEN*-mutated (*PTEN* mut; middle) glioma cell lines as well as of two primary human GIC cultures in response to CCI-779 at indicated concentrations assessed by the trypan blue exclusion method. Data are expressed as percentages of trypan blue-unstained cells relative to viable DMSO-treated cells set to 100% (mean ± SD, *n* = 3).

3.2 Inhibition of CD95 signaling by APG-101 enhances efficacy of radiotherapy

Targeting the CD95 death receptor has long been an experimental approach for malignant glioma. However, there is compelling evidence that CD95 receptor activation in non-apoptotic cells leads to invasive tumor growth upon induction of matrix metalloproteinase (MMP)-9 expression. In addition, radiotherapy, despite its proven curative effects and its role as standard of care in glioblastoma therapy, has been shown to act as a driving force for enhanced tumor cell invasion into the surrounding tissue. In order to inhibit the CD95-mediated pro-invasive signaling and radiation therapy induced tumor satellite formation, the CD95 ligand inhibitor APG101 was applied in experimental glioma models *in vitro* and *in vivo*.

3.2.1 CD95L-mediated invasion of glioma cells is inhibited by APG101

Since there is increasing evidence of a growth-promoting role of the CD95/CD95L-system in the biology of glioma, queries of the NIH's REMBRANDT brain tumor database were conducted to reveal potential influences of the CD95 expression on the survival of glioma patients. Analyses based on Affymetrix gene expression data correlated to corresponding patients survival rates indicate a significant correlation between decreased survival and increased gene expression of CD95 in human malignant glioma (Figure 18A). In order to unreveal the influence of radiation on the expression of CD95 and CD95L, mRNA-expression analyses were performed for these candidates upon irradiation with 3Gy. Expression of CD95L was significantly upregulated in response to radiation, whereas the CD95 receptor was not (Figure 18C). In order to proof *in vitro* the capability of the novel CD95L inhibiting compound APG101 (Figure 18B) to block radiation or CD95L induced glioma cell invasion, cells were irradiated or stimulated with CD95L and treatet with APG101 prior and during invasion through a collagen matrix. APG101 significantly blocked radiation and CD95-stimulated invasion of different glioma cell lines (Figure 18D).

3.2.2 Survival of glioma bearing mice is prolonged by APG101 mediated MMP inhibition

In order to validate the *in vitro* findings on the inhibition of glioma cell invasion by APG101, mice bearing a highly tumorigenic murine astrocytoma (SMA-560) were treated with APG101 four days after tumor inoculation. Cranial MRI-based tumor volumetry and histological brain tissue analyses revealed a tendency to smaller tumor sizes in mice treated twice a week with 100 mg/kg body weight APG101 in comparison to vehicle treated only control animals (Figure 19A and B). Importantly, APG101 treatment resulted in a significant survival advantage of about 16 days over untreated

control mice (Figure 19C). Tissue analyses of APG101 treated brain tumors by *in situ* zymography revealed an abrogated activity of invasion related MMPs (Figure 19D). This indicates an effective inhibition of CD95 signaling by APG101 *in vivo,* as expression of MMPs is the key effector of a CD95 stimulation in non-apoptotic settings.

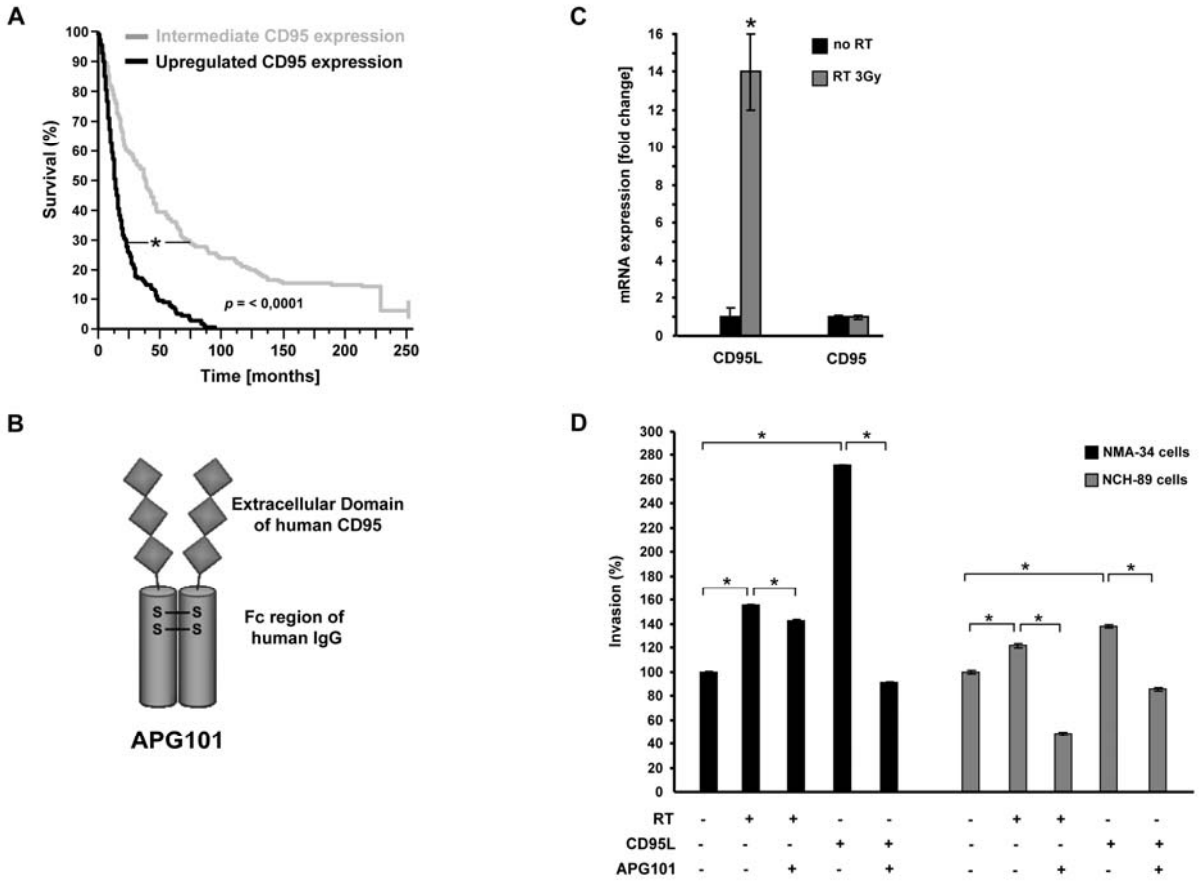

Figure 18. APG101 inhibits CD95L-mediated invasion of glioma cells

(A) Kaplan-Meyer survival plot showing survival of glioma patients with intermediated and upregulated CD95 expression levels according to queries of the NIH's REMBRANDT brain tumor database. **(B)** Schematic drawing of the molecular composition of the fusion protein APG101. **(C)** Quantitative RT-PCR analysis of CD95 ligand and CD95 mRNA expression in NCH-89 glioma cells upon irradiation treatment at 3Gy (mean ± SD, $n = 3$, $^*p < 0.05$). **(D)** Collagen invasion data of NCH-89 and NMA-34 glioma cells expressed as percentages of invaded cells, treated as indicated, relative to untreated control cells set to a 100% (mean ± SD, representative results for $n = 3$, $^*p < 0.05$).

3.2.3 APG-101 enhances the efficacy of radiotherapy in malignant glioma

Since radiotherapy is a fundamental component of first and second-line glioblastoma therapy, CD95L-signaling inhibition by APG101 was combined with irradiation treatment. Following orthotopic implantation of SMA-560 murine astrocytoma cells, VmDk mice were treated with a combined treatment regimen of APG101 (100 mg/kg body weight twice a week) and cranial irradiation (6 Gy on day 4) with either treatment alone. Glioma growth was monitored by cranial MRI on post-operative days 11, 13 and 18. Both, administration of APG101 alone and treatment with APG101 in combination with irradiation resulted in a significant reduction of tumor growth rates compared to irradiation treatment alone (Figure 20A and B). According to previous experimental reports and clinical observations, tumors exhibited an increased invasive potential upon radiation exposure. As shown in Figure 20C, radiation of SMA-560 tumors resulted in the formation of tumor satellites, which accumulate less contrast agent than the highly contrast enhanced core tumor. Importantly, parallel treatment of irradiated tumors with APG101 completely abolished the formation of these infiltrative tumor satellites. These MRI-based observations were largely confirmed by tissue analyses. In addition, neurological symptom-free survival of tumor bearing VmDk-mice that received APG101 additionally to invasion promoting cranial irradiation was significantly increased (Figure 20D).

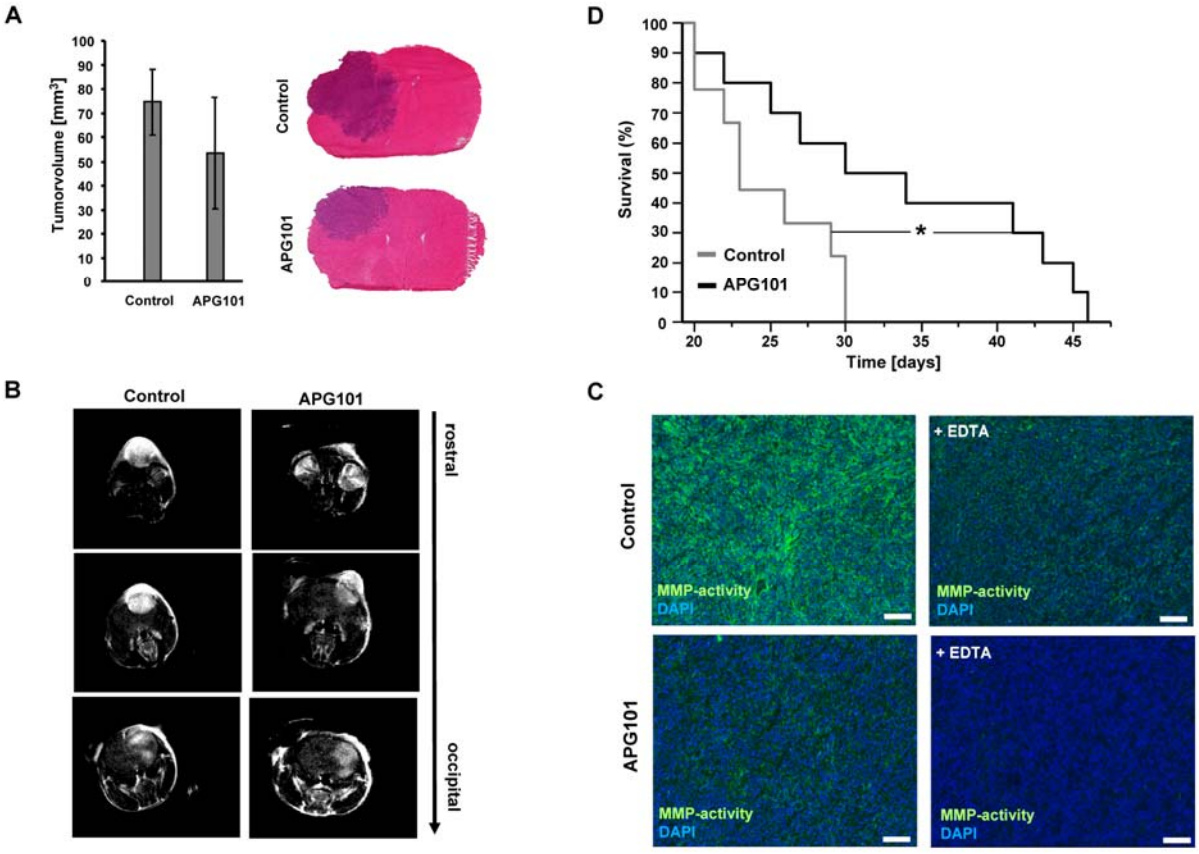

Figure 19. APG101 inhibits MMP activity and prolongs survival in glioma bearing mice

(A) Comparative T1-weighted MRI based volumetry of murine SMA-560 tumors (left panel; mean ± SD, *n* = 6) and histological analysis of coronally cryosectioned and hematoxylin/eosin-stained mouse brains (right panel) of untreated control and APG101 (100 mg/kg BW) treated VmDk-mice on post operative day (POD) 18. **(B)** Representative MRI-monitored orthotopic size analysis of SMA-560 glioma in three different sectional planes. Tumors are marked by white, hyper intense areas within the brain. **(C)** Survival data of glioma bearing mice treated as indicated are plotted by the Kaplan-Meier method and analyzed by log-rank test (*n* = 11 per treatment group, **p* < 0.05). **(D)** Mapping of matrix metalloproteinase (MMP) activity by *in situ* zymography using cryopreserved brain slices of untreated or APG101-treated tumor-bearing VmDk-mice. Inhibition of MMP activity by EDTA served as a negative control; fluorescent counterstaining of cell nuclei was carried out by using DAPI (scale bars, 50 µm).

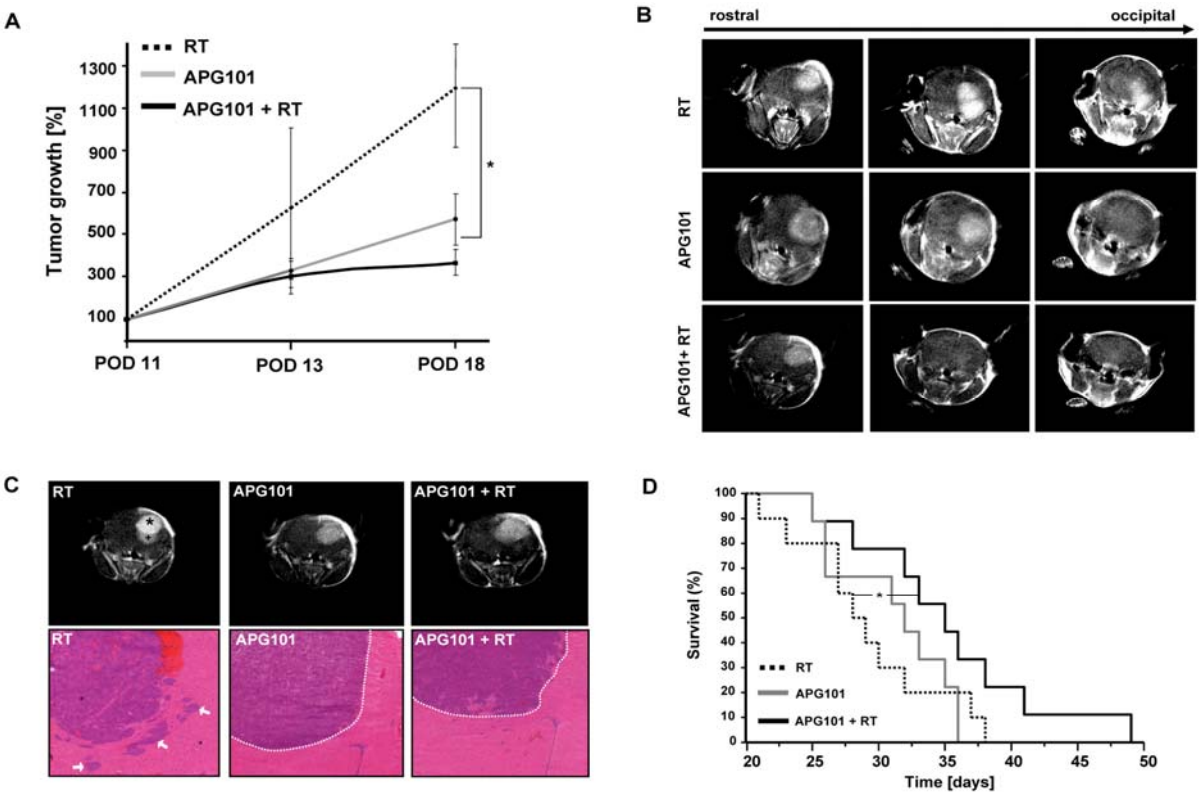

Figure 20. APG-101 enhances the efficacy of radiotherapy

(A) Orthotopic growth of SMA-560 glioma in VmDk-mice treated as indicated monitored by T1-weighted MRI based volumetry. Mean tumor volume in each group on post-operative Day (POD) 11 was set to a 100% (mean ± SD, n = 6 per treatment group, *$p < 0.05$). **(B)** Representative T1-weighted MRI-scans of SMA-560 glioma in three different sectional planes on POD 18 after indicated treatments. **(C)** Upper panel: Representative cranial T1-weighted MR-images of SMA-560 tumor bearing mice 18 days after focal radiation treatment at 6Gy alone (RT), after administration of 100 mg/kg APG101 or after a combination treatment (APG101 + RT). The hyper intense bulky core tumor is marked by an asterisk and the infiltrating less intense part of the glioma is highlighted by the cross symbol. Middle panel: Representative images of coronally cryosectioned and hematoxylin/eosin-stained tumors after indicated treatment with radiation and/or compound. Arrows mark radiation induced tumor satellite formation. **(D)** Survival data of glioma-bearing mice treated as indicated are plotted by the Kaplan-Meier method and analyzed by log-rank test (n = 11 per treatment group, *$p < 0.05$).

3.2.4 Combined CD95- and VEGF-receptor signaling inhibition does not enhance the survival benefit mediated by sole VEGF-receptor blockade

Anti-angiogenic treatment has become an essential part of current glioblastoma therapy but increasing evidence suggests that after an initial therapeutic response, anti-angiogenic treatment strategies, e.g. VEGF-signaling inhibitors, have so far not been able to increase survival of glioma patients. The tumor progression is characterized by enhanced tumor cell invasion into surrounding brain tissue and is commonly referred to as 'evasive escape or resistance'. In order to improve anti-angiogenic treatment strategies for malignant glioma, the anti-invasive acting compound APG101 was combined with the VEGF-receptor-2 (VEGFR-2) tyrosine kinase inhibitor Cediranib (AZD2171) in the SMA-560/VmDk-Mouse model of malignant glioma. Both, daily treatment with 6 mg/kg Cediranib and a combinatorial treatment scheme, consisting of 100 mg/kg APG101 and 6 mg/kg Cediranib, resulted in significantly smaller tumor volumes, compared to untreated or APG101 single treated tumors (Figure 21A). This translated into a significant survival benefit of such treated animals in comparison to untreated control animals (Figure 21B). Histological analysis and a quantitative evaluation based on CD31-positive blood vessel forming endothelial cells revealed drastically weaker vascularization patterns in Cediranib- and Cediranib+APG101- treated SMA-560 tumors (Figure 21C). Interestingly, the combined administration of APG101 and Cediranib did not show any benefit on top of a sole Cediranib treatment, regarding the tumor volume as well as overall survival rates. To further investigate these findings, the blockage of the VEGF-receptor-2 tyrosine kinase activity was analyzed for its impact on the expression of the CD95 ligand, comparable to the induction mediated by sublethal irradiation, as shown in Figure 18C. In this regard, treatment of glioma cell lines with Cediranib did not increase expression of CD95 ligand (data not shown) and hence not providing a reason that there should be an additional benefit by APG-101 in terms of tumor volume and survival on top of sole VEGFR-2 inhibition.

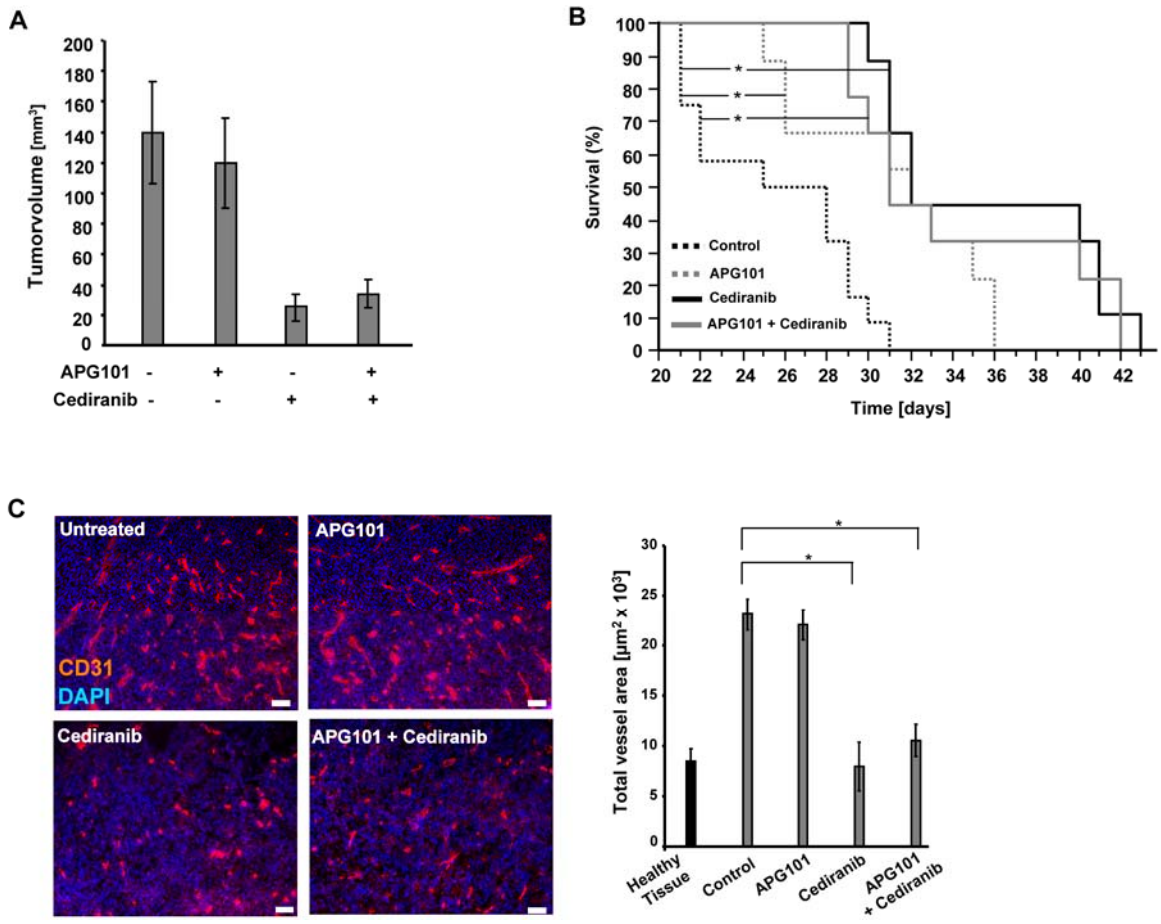

Figure 21. Combined CD95 and VEGF-receptor signaling inhibition does not enhance the survival benefit mediated by sole VEGF-receptor blockade

(A) Comparative T1-weighted MRI based volumetry of murine SMA-560 tumors on POD 18 treated with APG101 or Cediranib alone or in combination with each other. **(B)** Kaplan-Meier survival plot for SMA-560 tumor bearing mice treated as indicated (n = 11 per treatment group, *$p < 0.05$). **(C)** Mean vascularization of SMA-560 gliomas (right panel) in each indicated treatment group assessed by semi-automated quantification of the total CD31-positive vessel area as depicted in the left panel (mean ± SD, n = 3 per treatment group, *$p < 0.05$).

3.3 Co-stimulatory protein B7H3 drives the malignant phenotype of glioblastoma by mediating immune escape and invasiveness

A recently discovered member of the B7-family of co-stimulatory proteins is 4IgB7H3. Increasing evidence suggests that 4IgB7H3 is expressed by various human malignancies and suppresses natural killer cells and cytotoxic T-cells. In addition, the expression of 4IgB7H3 is associated with a poor prognosis in different tumor entities. Hence, the aim of this study was to elucidate a potential role of 4IgB7H3 in mediating the potent immunosuppressive phenotype of glioblastoma.

3.3.1 B7H3 is expressed in human glioma tissue specimens and glioma cell lines

4IgB7H3 was detected in specimens of freshly dissected human glioma tissue by immunohistochemistry (Figure 22A). Here, strong 4IgB7H3 expression is located in close proximity to blood vessels. The amount of 4IgB7H3 expression correlated positively with the grade of malignancy of different gliomas (Figure 22B). In glioblastoma, 10 out of 10 specimens which were stained for immunohistochemistry and immunofluorescence analysis were positive for 4IgB7H3 expression. Queries of the NIH's REMBRANDT brain tumor database, based on Affymetrix gene expression data and corresponding patients survival data, indicate a correlation between decreased survival and increased gene expression of 4IgB7H3 in anaplastic astrocytomas (WHO grade III) and glioblastomas (WHO grade IV; Figure 22C).

To further characterize the localization of the focally enhanced 4IgB7H3-expression, co-stainings with CD31 for endothelial cellls, smooth muscle cell actin (SMA) for pericytes or nestin for glioma cells were done (Figure 23A). These co-localization studies revealed that 4IgB7H3 is expressed by endothelial cells and also weakly by SMA-positive cells but in particular by the glioma cells surrounding the vessels (Figure 23B-D). On a cellular level, 4IgB7H3 protein was expressed in the cytoplasma and on cell membranes.

Moreover, five glioma-initiating cell (GIC) cultures, which were established from human glioblastoma tissue and kept under stem cell conditions, expressed 4IgB7H3 on mRNA level, as did five of five glioma cell lines (Figure 24A). 4IgB7H3 protein of the predicted size of ~ 100 kDa was present in all glioma cultures tested, too (Figure24B upper panel). Finally, 4IgB7H3 was detected on the surface of glioma cell lines and GIC cultures as assessed by flow cytometry (Figure 24B lower panel). There was no significant difference in 4IgB7H3 expression between GIC cultures and cell lines (Figure 24C).

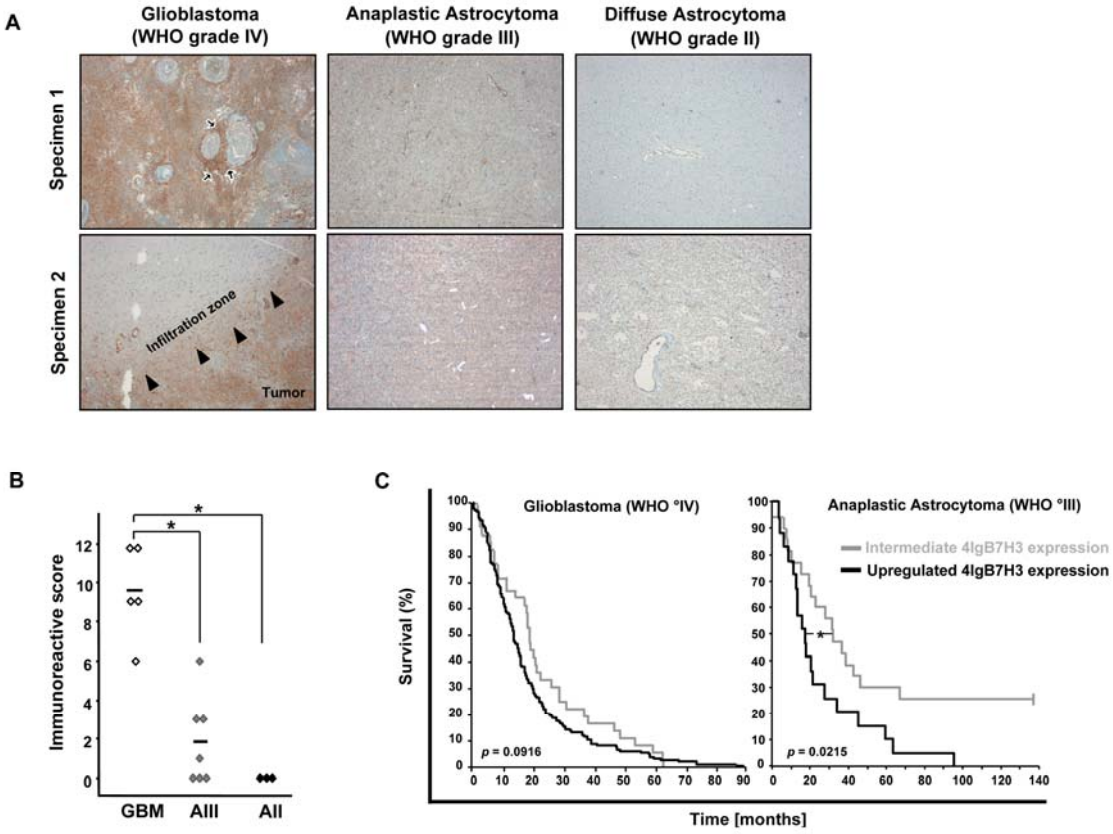

Figure 22. Expression of 4IgB7-H3 correlates with the grade of malignancy of different human gliomas
(A) Gliomas of different WHO grades were analyzed for their 4IgB7H3 expression by immunohistochemistry. In glioblastoma 4IgB7H3 expression is enhanced in proximity to the blood vessels (specimen 1, arrows). Specimen 2 demonstrates upregulated 4IgB7H3 in the tumor compared with the surrounding brain tissue (arrow heads). **(B)** Statistical analysis of 4IgB7H3 expression in gliomas of different WHO grade. **(C)** Kaplan-Meier survival plot showing survival of glioma patients with intermediate and upregulated 4IgB7H3 expression levels.

In an attempt to detect the recently published [122] 16.5 kDa fragment of 4IgB7H3 in cell supernatants, two different antibodies were used: one directed against a peptide sequence in the first N-terminal immunoglobuline-like extracellular domain, the other one capable of detecting the whole extracellular protein. With none of them the existence of a 16.5 kDa fragment could be substantiated in supernatant of glioma cell line cultures or GIC-cultures (Figure 24C).

In order to further analyze soluble 4IgB7H3 secreted by glioma cells, 4IgB7H3 originating from cell lysates was directly compared with its secreted form obtained from cell culturesupernatants. A size difference of about 5 - 7 kDa between supernatant and lysate derived protein was detected by immunoblot analyses (Figure 24D, left panel). In nanoLC electrospray-tandem-massspectrometry analyses this size difference was confirmed, due to a missing peptide sequence of about 7 kDa in the supernatant probe. This part represents the intracellular and transmembrane fragment of 4IgB7H3 (Figure 24D, right panel), which is not present in the supernatant fraction. From this a 93 kDa fragment of 4IgB7H3 can be assumed to be secreted into the supernatant.

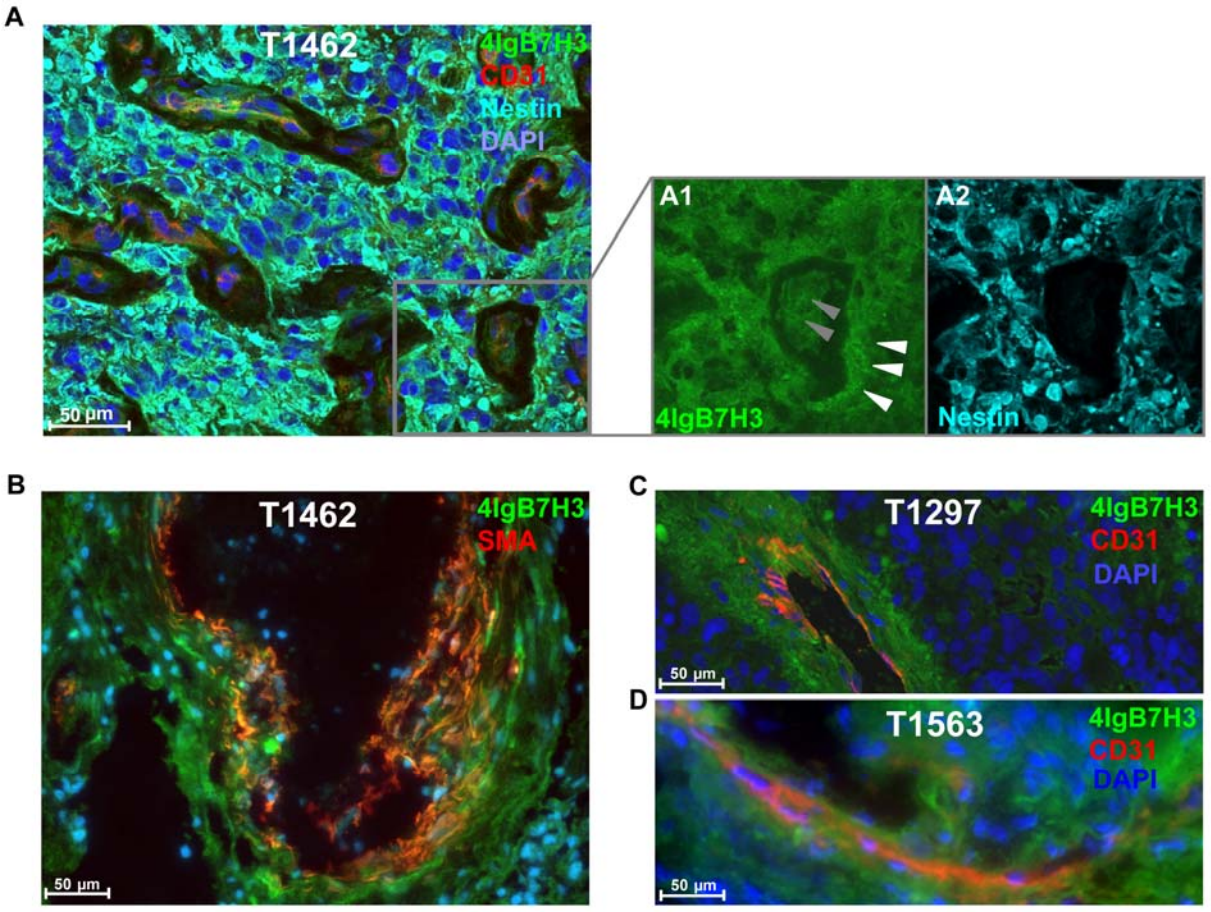

Figure 23. 4IgB7-H3 protein expression in human glioblastoma tissue specimens
(A - D) Immunofluorescence microscopy was applied to detect 4IgB7H3 in three different glioblastoma specimens (T1462, T1297, T1563). Vessels are visualized by CD31 staining, pericytes are stained with α-smooth muscle cell actin (α-SMA), glioma cells are marked by nestin staining, nuclei are counterstained with DAPI. **(B)** Glioblastoma cells surrounding blood vessels exhibit a higher expression of 4IgB7H3. Data was contributed by Dr. Dieter Lemke.

3.3.2 B7H3 inhibits natural killer cell-mediated lysis of glioma cells

Aiming at the evaluation of the functional activity of 4IgB7H3 expressed in glioma cells, 4IgB7H3 was silenced in the glioma cell line LN-229 by using a lentiviral system. The knock-down was about 80% effective, moreover, after clonal selection the knock-down reached 93% in clone 19 on the mRNA level. Immunoblot and flowcytometry analyses revealed a clear reduction on the protein level of 4IgB7H3 in lysates, supernatant and on the surface of the knock-down cells (Fig. 25A). Natural killer (NK) cell lysis assays revealed that LN-229 sh-4IgB7H3 cells were more susceptible to NK cell-mediated lysis. The clonal knock-down was lysed best with around 60% specific lysis at a target to effector cell ratio of 1 to 30, the less-efficient B7H3-silenced pool transfectants showed an intermediate lysis at 40% while the controls were at 25% (Figure 25B, left panel). Given that 4IgB7H3 is released into the supernatant, we also analyzed whether soluble glioma cell-derived 4IgB7H3

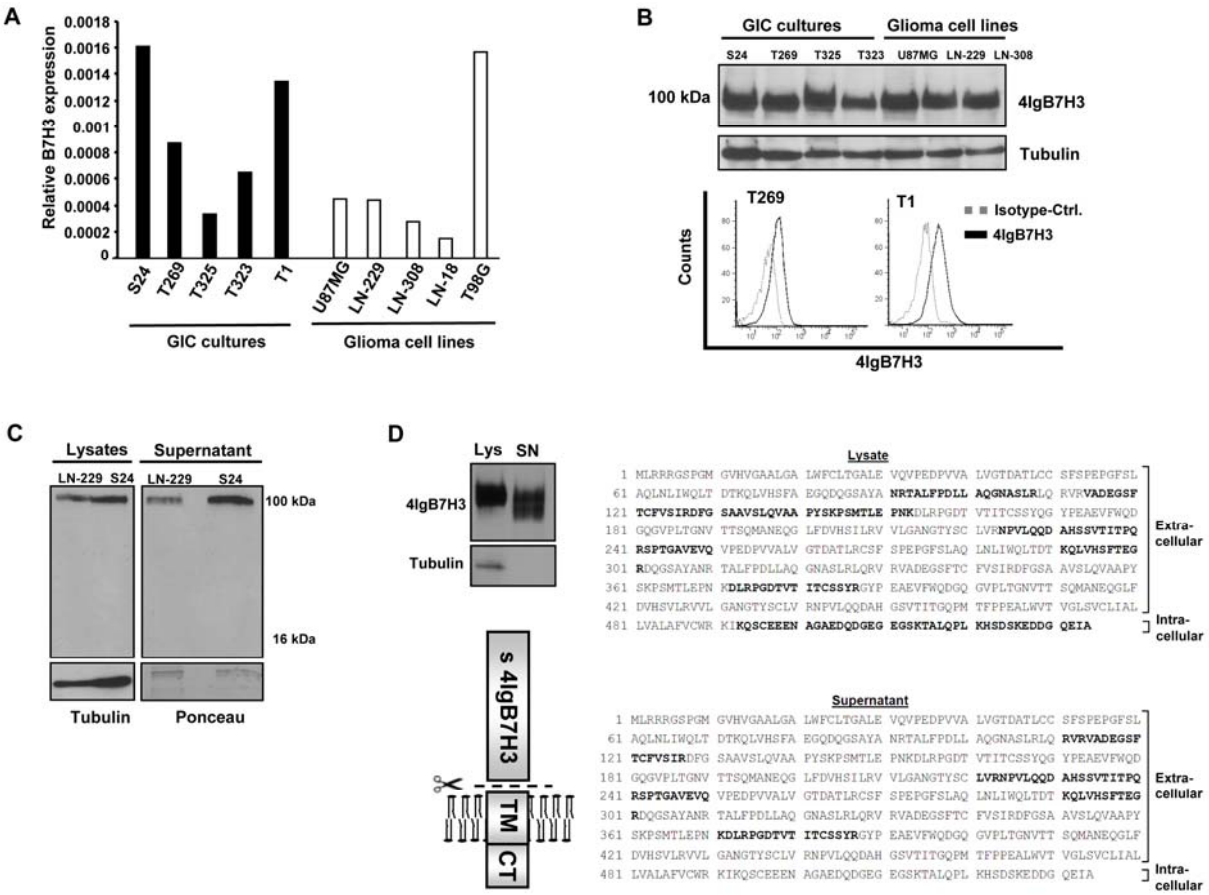

Figure 24. Expression and secretion of 4IgB7H3 by glioma cells.

Expression of 4IgB7H3 in GIC (black bars) and glioma cell lines (white bars) on mRNA level relative to GAPDH determined by qRT-PCR **(A)**, on protein level in Immunoblot analysis **(B, upper panel)** and on the cell surface of GIC cultures measured by flow cytometry **(B, lower panel)**. **(C)** 4IgB7H3 in LN-229 glioma cells and GIC culture S24. α-tubulin was chosen as loading control for cell lysates and Ponceau staining for supernatant **(D)**. Position of identified peptides (bold letters) in human 4IgB7H3 amino acid sequence deriving from lysates and supernatant analyzed by nanoLC-ESI-MSMS (right panel). Protein size analyzes of 4IgB7H3 in LN-229 whole cell lysates (Lys) and supernatant (SN) by immunoblot (left panel). Proteolytic processing of membrane bound 4IgB7H3 by peptidases in a schematic drawing (left panel).

is able to suppress NK-mediated lysis. Hence, we performed NK lysis assays with LN-229 sh-4IgB7H3 clone 19 cells, which were susceptible to lysis, and supplemented supernatant of LN-229 sh-4IgB7H3 clone 19 and control cells. Compared with the specific NK-mediated lysis of LN-229 sh-4IgB7H3 clone 19 cells of around 60%, the specific lysis of these cells was reduced to 20% by coincubation with concentrated supernatant of control cells. This reduction of specific lysis was weaker after diluting the control supernatant 1:100. The supernatant of LN-229 sh-4IgB7H3 clone 19 cells was only marginally capable of reducing the lysis of LN-229 sh-4IgB7H3 clone 19 cells to approximately 50% at a target to effector cell ratio of 1 to 30 (Figure 25B).

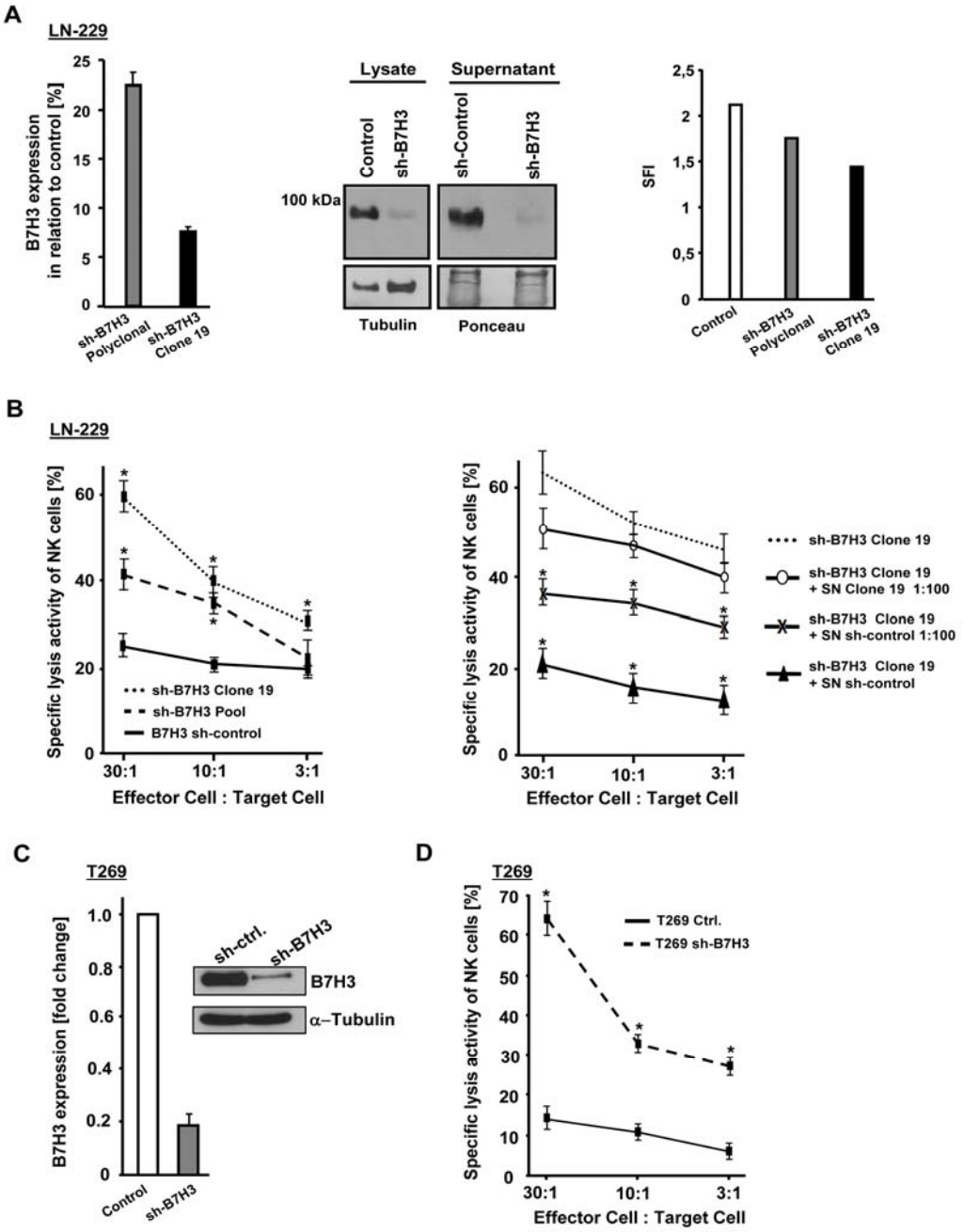

Figure 25. **Increased susceptibility of LN-229 4IgB7H3 sh-cells to NK cell-mediated lysis**

Polyclonal knock-down and clonal selection (clone 19) of 4IgB7H3 in LN-229 cells were performed. Knock-down efficiency on mRNA level **(A**, **left panel)** and protein level (centre and right panel) are illustrated. As a loading control α-tubulin was chosen for cell lysates and Ponceau staining for supernatant. **(B)** LN-229 sh-4IgB7H3 (polyclonal and clone 19), sh-control cells, or LN-229 sh-4IgB7H3 clone 19 cells supplemented with supernatant (SN) derived from clone 19 or control cells were incubated with activated NK cells for 4 h at the indicated effector to target cell ratios. Lysis [%] was calculated as described. **(C)** Knock-down of 4IgB7H3 in GIC culture T269 was performed and efficiency evaluated on mRNA level by qPCR (left panel) and on protein level by Immunoblot analysis (right panel). **(D)** Activated NK cells were incubated with T269 sh-4IgB7H3 or sh-control cells and NK cell mediated lysis [%] of T269 GIC was evaluated. Representative results from 3 independent NK-lysis experiments with similar results are depicted (Data represent mean and standard error of mean (SEM); n=5; *p<0.05 is related to B7H3 sh-control cells in B, left panel and D, and B7H3 clone 19 + SN LN-229 sh-control cells in B,right panel).

There was no significant difference between diluted and undiluted supernatant of LN-229 sh-4IgB7H3 clone 19 (Figure 25B, right panel).
In addition to the elucidation of the functional activity of 4IgB7H3 in glioma cell lines, 4IgB7H3 knock-down cells of the GIC culture T269 were generated, with a knock-down of 80% on mRNA level and a significant reduction on protein level (Figure 25C). NK lysis assays revealed that also T269 sh-4IgB7H3 cells were significantly more susceptible to NK cell-mediated lysis in comparison to T269 control cells still expressing 4IgB7H3 (Figure 25D). Taken together, these data indicate that 4IgB7H3 and its secreted form suppress NK-cell mediated lysis of glioma cells and GICs.

3.3.3 Invasiveness of glioma cells *in vitro* is mediated by B7H3

Increasing evidence suggests that 4IgB7H3 may also be involved in tumor cell migration and invasiveness [146]. Therefore, Boyden chamber matrigel and spheroid invasion assays were performed with LN-229 cells as well as with the GIC culture T269. LN-229 sh-4IgB7H3 cells displayed reduced transmigration compared with control cells in these assays (Figure 26A).
Interestingly, the invasive phenotype was partly restored in LN-229 sh-4IgB7H3 cells when invasion assays were conducted with supplementation of concentrated supernatant of LN-229 control cells. There was also a reduction in the invasiveness of LN-229 control cells when cells were incubated with supernatant from LN-229 sh-4IgB7H3 cells instead of supernatant from control cells during the invasion experiments (Figure 26B). To verify the pro-invasive effect of 4IgB7H3 in primary glioma cells, primary 4IgB7H3-silenced T269 GICs were further used in a functional invasion assay. This spheroid invasion assay demonstrated a significant reduction of the invasive phenotype in T269 cells after 4IgB7H3 gene silencing (Figure 26C).

3.3.4 B7H3 mediates a proinvasive glioma phenotype *in vivo*

In order to confirm the *in vitro* data in an *in vivo* model, T269 sh-4IgB7H3 knock-down or control cells were orthotopically implanted into the brains of CD1 *nu/nu* mice. Ten weeks later, animals were sacrificed and tumor invasion was assessed by staining of the tumor cells with anti-human nestin antibody. Brain sections of mice xenografted with T269 control cells displayed a highly infiltrative tumor growth pattern with tumor cells reaching brain regions in the ipsi- and contralateral hemisphere far off the implantation site (Figure 27, upper panel).
In contrast to this, clearly defined bulky tumors were found in T269 sh-4IgB7H3 xenografted brains without detectable tumor cells in ipsi- or contralateral brain regions distant from the implantation site (Figure 27, lower panel).

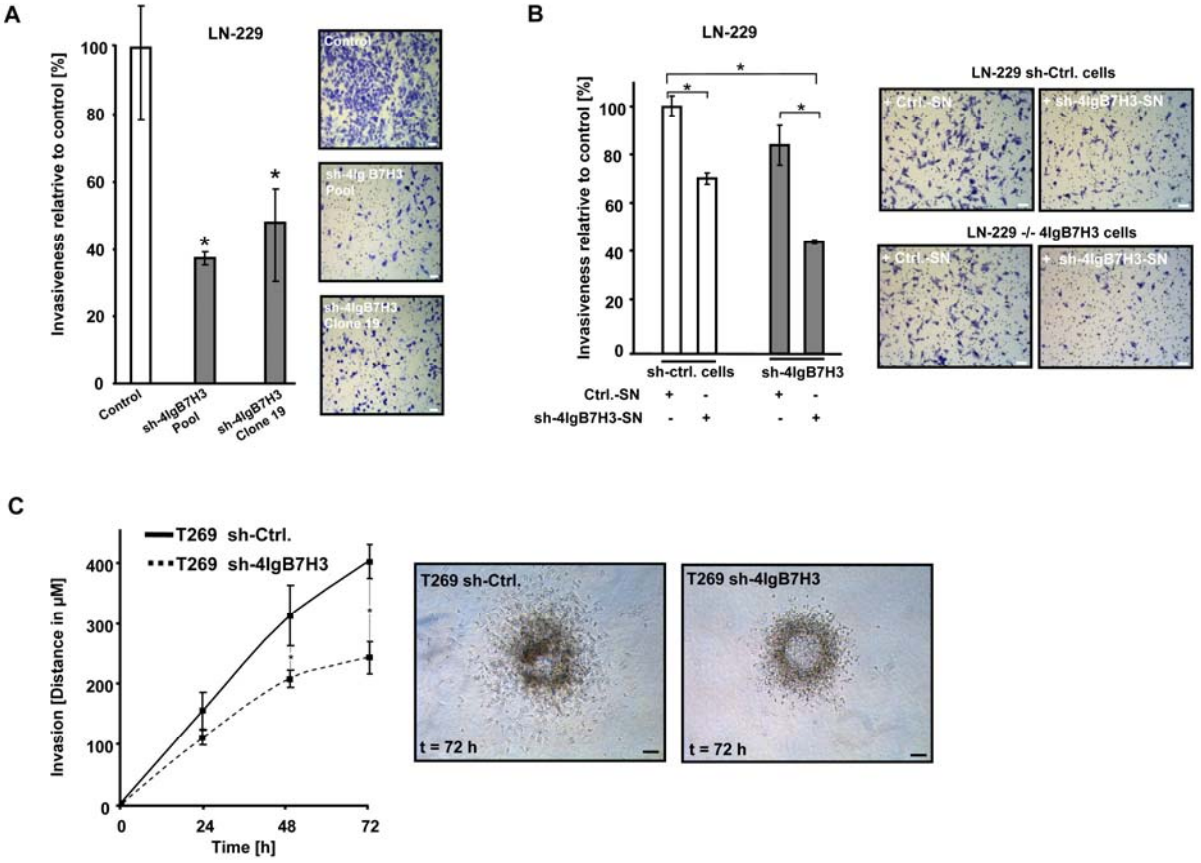

Figure 26. 4IgB7H3 mediates a pro-invasive phenotype in glioma cells *in vitro*

(A) LN-229 sh-4IgB7H3 (polyclonal knock-down and clone 19) and sh-control glioma cells or **(B)** clone 19 and sh-control cells incubated each with concentrated supernatant (SN) of control or clone 19 cells were analyzed for invasiveness in a matrigel invasion chamber assay. Invaded cells were counted in five independent fields. Invasion is expressed as percentage in relation to sh-control cells. (scale bars 100 µm; data represent mean and standard error of mean (SEM); n=3, $p<0.05$). Representative photographs of the Boyden chambers are depicted. **(C)** T269 control and sh-4IgB7H3 cells were analyzed for their invasive properties in a spheroid invasion assay. The area covered by invaded cells from each spheroid was measured in intervals of 24 h. Data represent mean and SEM (n=3,). Representative glioma spheroids at each time are shown (scale bars 100 µM).

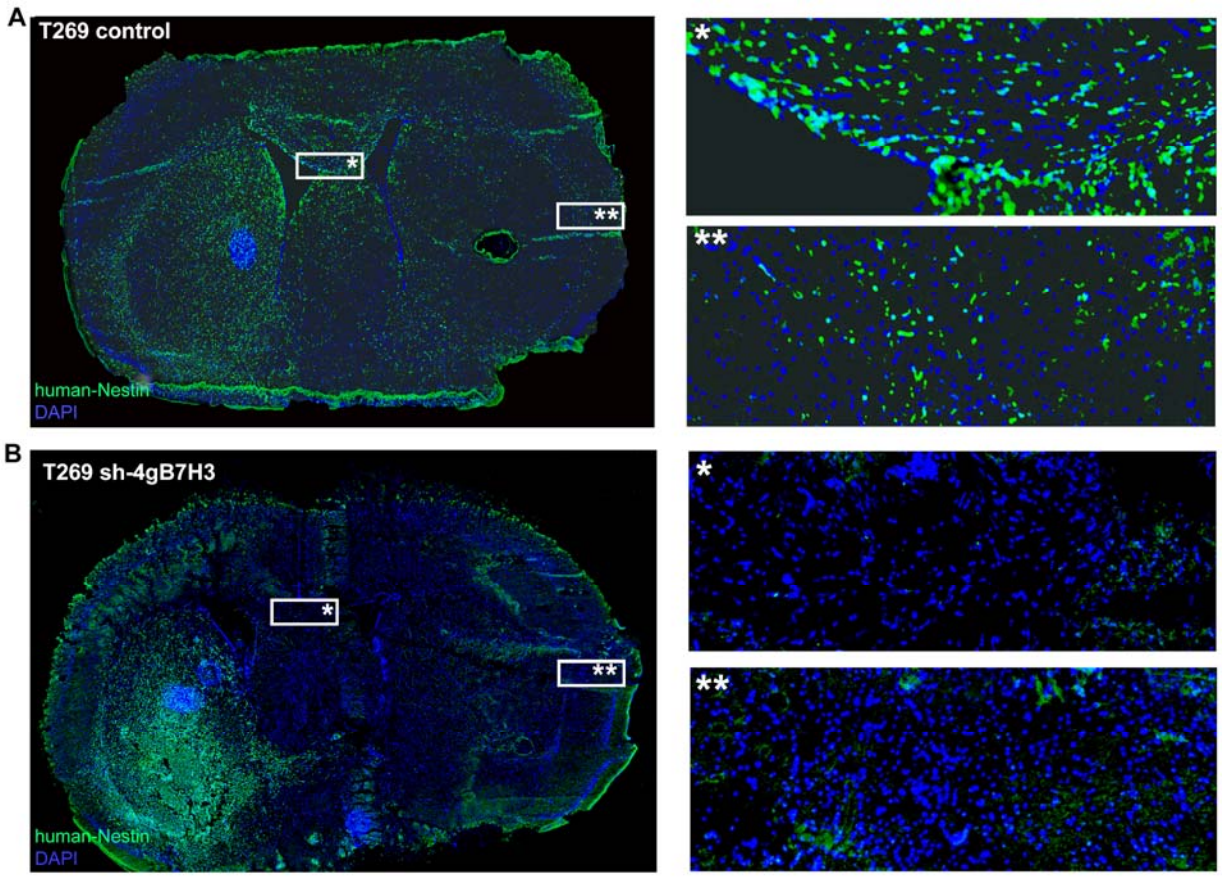

Figure 27. 4IgB7-H3 drives the pro-invasive phenotype of glioblastoma *in vivo*

Immunohistological analysis of **(A)** T269 control and **(B)** T269 sh-4IgB7H3 tumor bearing CD1 *nu/nu* mice. T269 tumor cells were detected by immunoflurescent anti-human nestin staining.

4. Discussion

4.1. Targeting evasive resistance in glioblastoma

Increasing infiltrative tumor growth as an escape mechanism to antiangiogenic compounds and radiotherapy plays an important role on the ineffectiveness of glioblastoma treatment. The pro-invasive growth patterns essentially trigger disease progression, hamper tumor growth control, and have a strong determining influence on patients' survival. Taken this into account, the development of new treatment concepts based on targeting angiogenesis as well as invasion, ideally combined with current radiotherapy standards should have a major impact on this disease. Following this, two different approaches to overcome evasive resistance in glioma were investigated. The first one deals with a dual, radiation enhanced control of invasion and angiogenesis by inhibiting the PI3K/AKT/mTOR signaling axis, whose up regulation is relatively common in human glioblastoma. The second one focuses on a fairly novel model, in which radiation induced CD95 ligand depended signaling mechanisms, contributing to glioma cell invasion, are inhibited by a novel compound.

4.1.1 Optimization of glioma treatment through dual inhibition of RGS4 and VEGFR-2

mTOR inhibition by CCI-779 targets VEGF-mediated angiogenesis on both receptor and ligand level

CCI-779 (Temsirolimus / Torisel®), the compound used in this study to inhibit mTOR signaling, is a rapamycin derivative and was up to now extensively studied [147]. In deed, the observation that CCI-779 has an antiangiogenic potential is not entirely novel. Pre-clinical experiments and clinical investigations in humans, first demonstrated antiangiogenic activity in colon adenocarcinoma cells by VEGF-antagonizing mechanisms [148]. This finding was confirmed for CCI-779 when tested in human multiple myeloma cells [149] or in human breast cancer cells in which the compound inhibited VEGF release through inhibition of HIF-1α expression [150].

The data presented in the current study confirms the VEGF-suppressing action in glioblastoma cells. In addition the inhibitory activity of CCI-779 in brain-derived endothelial cells (hCMEC/D3) was validated. With regards to the data on VEGFR-2, one can postulate two different modes of action of CCI-779 targeting glioma angiogenesis. First, indirectly, by inhibition of transcription of irradiation- or hypoxia-stimulated, HIF-1α-dependent VEGF release and second, directly, through transcriptional downregulation of VEGFR-2 on glioma and endothelial cells. Of note, expression of VEGF and VEGFR-2 is induced as a consequence of radiation and is counteracted in response to treatment with CCI-779. So far, none of the various anti-angiogenic single-agent strategies developed to target the VEGF/VEGFR signaling pathway, is capable to cause such a multilevel blockade of angiogenesis at once. The US-approved anti-VEGF antibody bevacizumab only acts at the ligand level, where as other compounds, currently in clinical testing, only target the VEGF-receptor.

Taken together, the findings presented here implicate that inhibition of mTOR using CCI-779 targets angiogenic processes by interfering with the VEGF/VEGFR-2 signaling axis both at the ligand and the receptor level, and might therefore be more efficaciously.

CCI-779 qualifies as an anti-evasive resistance compound

In order to develop a novel combined anti-invasive and anti-angiogenic glioma treatment strategy, which considers the development of unwanted adaptive evasive responses to a sole anti-angiogenic treatment, potential effects of mTOR-inhibition on glioma invasion were investigated in this study. In this regard, CCI-779 not only efficaciously inhibits VEGF/VEGFR-2 mediated angiogenic signaling but also suppresses glioma cell migration and invasion. This is due to downregulation of RGS4 that is functionally characterized as a potent driver molecule of glioma cell invasiveness. RGS proteins have been discovered in 1996 [151] and have been associated later on with the initiation and progression of cancer [152]. They are regulatory proteins that act as GTPase-activators and thereby shorten the duration of heterotrimeric G-Protein coupled receptors (GPCR) signaling processes. These are involved in a variety of cellular processes including cell motility [153, 154]. RGS4 has previously been identified in playing a role in controlling cancer cell invasiveness. For example in breast cancer, RGS4 was reported to suppress cell migration lamellipodia formation, and downregulation of RGS4 by proteasomal degradation resulted in a more metastatic phenotype [155].

In glioma cells, a screen for activated genes in highly migratory cell clones led to the identification of RGS4. In this regard Tatenhorst and co-workers [132] demonstrated an enhanced adhesion and migration of glioma cells upon overexpression of RGS4 *in vitro*. However, this method seems limited in that overexpression of a protein can change the stoichiometry of signaling molecules and may not always reflect endogenous specificity [156]. As shown in the current study, levels of RGS4 expression directly correlate with the extent of invasiveness [157]. Gene silencing of *RGS4* reduces invasion whereas overexpression increases invasion. Notably the findings prove that CCI-779 specifically suppresses RGS4-induced invasiveness of human glioma cells not only *in vitro* but also in an intracerebral mouse model. With respect to the above-mentioned effects in breast carcinoma cells [155], it seems likely that RGS4 functions in cancer cells are tumor type-specific or has a differential function in brain-derived tissue as compared to breast or other tissue origins.

RGS4 has been reported widely expressed in the human brain [158-160] making it relevant for brain tumor research. Furthermore, changes in RGS4 expression or activity have been shown for other CNS disorders, like Parkinson's disease, schizophrenia, and drug addiction [161-163]. Beyond that, additional studies demonstrated a role for RGS4 in modulating modulates various peripheral functions as heart rate, renal blood flow, secretion of catecholamines from adrenal glands, and

glucose metabolism [164-167]. Therefore RGS4 has been recognized as a promising therapeutic target for inhibition, and specific drug development is currently performed [168-172].

Recently, a HIF-1α-dependent mechanism underlying the recruitment of BMDCs which contribute to the restorage of radiation-damaged vasculature by vasculogenesis was described [105]. Given its known HIF-1α-suppressing effect, CCI-779 might additionally interfere with this influx of BMDCs and prevent the post-irradiation development of a functional tumor vasculature. It is therefore conceivable that CCI-779 impairs in glioma not only angiogenesis but also vasculogenesis.

Rationale for high-dosed CCI-779 treatment

The current findings implicate that CCI-779 elicits combined antiangiogenic and antiinvasive effects and triggered the investigation of the underlying signaling mechanisms. Recently, mTORC2 has been identified as an important player in cancer and therefore as a promising target for inhibition. Consequently, a number of mTOR inhibitors, e.g., Torin1, PP242, PP30, have been developed that target both mTOR complexes mTORC1 and 2 [81, 173]. In contrast to rapamycin and its analogs it remains to be elucidated if this new class of mTOR inhibitors will have an impact in clinical use. The data evolving from this study implicates that, in glioblastoma cells not only mTORC1 but also mTORC2 is a target for the CCI-779 in a dose-dependent way: In *PTEN*-mutated glioma cells, CCI-779 applied at low concentrations is sufficient to partially suppress mTORC1 activity resulting in decreased expression of VEGF, VEGFR-2 and RGS4 paralleled by impaired angiogenesis and invasiveness. As a consequence, a feedback loop through mTORC2 signaling activates AKT by phosphorylation leading to adverse effects such as increased cell survival and invasiveness. CCI-779 applied at higher but clinically relevant concentrations overcomes the protective effect of a *PTEN* wild-type status, inhibits both mTOR complexes at a time and thus prevents the induction of resistance through feedback activation of AKT by mTORC2. In addition, the concerted inhibition of both mTOR complexes results in a more efficacious suppression of VEGFR-2 and RGS4 leading to a more efficient control of angiogenesis and invasiveness. Taken together, a combined inhibition of mTORC1 and mTORC2 is beneficial and can be achieved through higher doses of CCI-779.

Rationale for a clinical evaluation of radiation enhanced mTOR inhibition by CCI-779

Therapeutic treatment modalities aiming at mTOR-inhibition applied as single-agents or in combination with EGFR inhibitors failed so far in clinical trials for recurrent glioblastoma [174-179]. One explanation for this could be that, at recurrence molecular alterations caused by previous treatments or activation of alternative signaling pathways prevent mTOR mediated anti-tumor effects. Another reason could be that mTOR-antagonized glioma cells develop a protection against

hypoxia-induced cell death and might therefore better tolerate the adverse conditions of the hypoxic microenvironment within the tumor burdens [180].

Hence complete tumor resection minimizing hypoxia could be favourable for the responsiveness to mTOR inhibition. Finally, it is possible that mTOR-inhibiting strategies are insufficient when they are applied as monotherapies and only affect tumor progression in combination with a cytostatic treatment like radiation therapy or another cytotoxic treatment like alkylating agents. The data presented here suggest that this might be the case since both ionizing radiation and CCI-779 synergize in causing anti-glioma effects while CCI-779 administration holds the proangiogenic and pro-invasive consequences of irradiation in check.

Taken together, mTOR-inhibition with CCI-779 might be successful in newly diagnosed glioblastoma in which complete resection is achievable and radiation therapy is consequently administered. The clinical efficiency of radiation enhanced mTOR inhibition is currently under investigation in a clinical phase II trial on 'CCI-779 in Combination with Radiotherapy *versus* Radiotherapy with Temozolomide as First-Line Treatment of Glioblastoma with Unmethylated *MGMT* Promoter' (ClinicalTrials.gov identifier: NCT01019434) by the European Organization for Research and Treatment of Cancer (EORTC).

4.1.2 Preventing radiation enhanced invasiveness by inhibition of CD95 signaling

CD95 (APO-1/Fas) is a prototype transmembrane death receptor belonging to the TNF superfamily that regulates upon binding of its ligand CD95L tissue homeostasis by the induction of caspase-dependent apoptosis [58, 59, 64]. The accepted model for CD95 stimulation describes binding of preassembled, trimerized CD95 with its ligand CD95L leading to recruitment of several adaptor proteins into the so-called Death-Inducing-Signaling-Complex (DISC; [181]) Several lines of evidence indicate that CD95 is a receptor with pleiotropic functions mediating besides activation of apoptosis as well non-apoptotic signaling mechanism. Depending on tissue type and conditions, diverse non-apoptotic functions are mediated by the CD95 receptor/ligand system, e.g. liver regeneration, neuronal development, inflammation, invasion of tumor cells and tumor promoting activity [182-184]. For glioma, a CD95/CD95L stimulated non-apoptotic mechanism leading to invasive tumor growth was recently described by Kleber *et al.* [65]. In this regard, CD95 stimulation results in the formation of a PI3K-Activation-Complex (PAC), competing with components of DISC and leading to phosphorylation of the PI3K target AKT. Activated AKT in turn mediates via several effector molecules enhanced expression of pivotal glioblastoma invasion-related proteases that is matrix metalloproteinases (MMP). With this perspective, a shift of paradigm emerges from these findings as much effort has been undertaken to induce cell death in gliomas by various CD95 stimuli, like agonistic antibodies to CD95 [185-188]. Of note, CD95L expression has earlier been found to be

endogenous expressed by glioma cells [189, 190] and to be involved in immune suppression by inducing apoptosis in T-cells [191]. In addition, activation of CD95 has earlier been reported to enhance glioma cell-cycle progression [192] and also invasiveness [193].

This concept of CD95-signaling inhibition rather than stimulation is further supported by *in vitro* as well as *in vivo* findings showing a significant inhibition of glioma cell migration and invasion by using a CD95L-neutralizing antibody [65]. To follow this line and to further establish the concept of CD95L neutralization in the glioma microenvironment for a clinical application, the compound used in the study at hand [194] is a fusion protein, consisting of the extracellular domain of the human CD95 receptor and the Fc- region of human immunoglobulin G. Due to this composition an effective receptor signaling blockage can be achieved through specific binding of the CD95 ligand. Furthermore, the compound can be utilized in the clinic due to its ability to reach the tumor site via the blood brain barrier.

Even though radiotherapy has been demonstrated to be effective in the first- and second line treatment of malignant glioma [24] several studies have proven an adaptive evasive response of radiation treatment in form of enhanced tumor cell invasion [67, 68, 195]. In the present study first the enhanced invasive potential of several glioma cell lines following irradiation treatment was confirmed *in vitro.* Furthermore, increased upregulation of CD95 ligand is responsible for this pro-invasive post-radiation phenotype. In subsequent animal studies the administration of APG101 led to a reduction of radiation-induced tumor satellite formation. Therefore, APG101 allows to relevantly counteracting the increased invasive potential and tumor satellite formation upon radiation treatment.

In order to target in addition evasive resistance to antiangiogenic treatment modalities, a treatment approach consisting in an anti-angiogenic and anti-invasive strategy was applied. The combined administration of APG101 and cediranib, a VEGF-receptor tyrosine kinase inhibitor did not show any benefit on top of a sole cediranib treatment. This can be explained by the lack of increasing CD95 ligand expression following treatment with cediranib, as shown by qRT-PCR. The possibility of a sustained blockage of evasive resistance mechanisms by APG101 is therefore restricted to radiation induced upregulation of the CD95 ligand.

Taken together, the findings support the clinical implementation of a combinatorial treatment scheme consisting of radiotherapy and APG101 in the treatment of malignant brain tumors. The clinical efficiency is currently investigated at 30 different sites in Germany, Austria and Russia in a phase-II ‘Randomized, Open-label, Multi-centre Study of Weekly *APG101* + Reirradiation v*ersus* Reirradiation in the Treatment of Patients With First or Second Progression of Glioblastoma’ (ClinicalTrials.gov identifier: NCT01071837).

4.2 Targeting the immune privilege of glioblastoma

4.2.1 Identification of B7H3 as a mediator of glioma immune escape

With the intention to develop and improve immunotherapeutic strategies for glioblastoma, it is necessary to gain a detailed understanding of the immune phenotype of these highly malignant and immunosuppressive tumors. The co-stimulatory molecule B7H3 was recently discovered to mediate immunosuppressive effects and to be associated with poor survival in several tumor entities. In order to achieve substantial progress on the characterization of the immunosuppressive phenotype of glioblastoma, the role of B7H3 was investigated.

In order to characterize the immune phenotype of glioblastoma the current study shows that 4IgB7H3 is expressed in human glioblastoma tissue by both glioblastoma and endothelial cells and is accentuated in the glioma cells, which surround the blood vessels. In addition to that, expression correlates significantly with increasing tumor grade and is associated with poor survival within WHO grade III and IV gliomas. These findings strongly support the association of 4IgB7H3 with poor prognosis found in several other tumors [120, 121, 196]. Taken into account that 4IgB7H3 was originally discovered as a costimulatory molecule to convey T-cell activation [118], the existence of a soluble form is most likely to assume. By mass spectrometry and immunoblot analysis soluble 4lgB7H3 was identified in the current study in supernatant of glioma cells. Interestingly, this soluble 4IgB7H3 is not the 16.5 kDa soluble form of 4IgB7H3 postulated in non-malignant cells before [124]. Here, the soluble fragment was about 7 kDa smaller than 4IgB7H3 originating from cell lysates. Although two different antibodies were used, the one detecting whole extracellular protein, the other one the first immunoglobulin-like domain of the extracellular N-Terminus, the published fragment of about 16.5 kDa could not be detected in the supernatant of glioma cells, but our data suggest that through a proteolytic process the entire extracellular domain of glioma 4IgB7H3 is released into the supernatant. In an attempt to further characterize the regulation and cleavage mechanism of 4IgB7H3 in glioblastoma, the cells were incubated with phorbol myristate acetate (PMA), which was published to induce 4IgB7H3 on immune and tumor cells [118]. This regimen had no effect on 4IgB7H3 expression in glioblastoma cells on mRNA or protein level, neither did the inhibition of MMP (data not shown), which are suggested to cleave 4IgB7H3 from the surface of tumor cells [124]. Finally blockage of TGF-β activation or knock-down of TGF-β was evaluated for its effects on 4IgB7H3 expression and processing, since TGF-β is known to be responsible for a variety of immunosuppressive and pro-invasive effects [53].

Early reports have shown a contribution of tumor derived 4IgB7H3 in suppression of NK-cells [119]. In order to prove such an involvement of 4Ig B7H3 in mediating glioma immune suppression, glioma cell lines and GIC cultures either expressing 4IgB7H3 or not were exposed to NK-cells and analyzed

for Nk-cell ability for tumor cell lysis. Results clearly elucidate a 4IgB7H3 mediated, suppressed NK cell- tumor lysis, and support therefore the role of 4IgB7H3 in mediating glioma immunosuppression. Whether these findings remain valid in an *in vivo* situation needs to be elucidated in an immunocompetent mouse glioma model and by subsequent analyses of 4IgB7H3 mediated effects on the murine anti-glioma immunereactivity.

Besides its role in immunossuppression, 4IgB7H3 was identified to be a potent mediator of the pro-invasive glioblastoma phenotype, as shown in this study by *in vitro* invasion assays and *in vivo* in an orthotopic mouse glioma model. Gliomas lacking 4IgB7H3 expression display a non-invasive phenotype with clearly defined bulky tumors. In contrast, 4IgB7H3 expressing tumors diffusely infiltrated into the brain. Given the limitations in neurosurgical resections of glioblastoma due to the highly invasive phenotype, 4IgB7H3 is a novel candidate to target in regards to the development of promising anti-invasive treatment strategies.

Taken together, glioma-related B7H3 expression and release was identified in the presented study as a strong inhibitor of anti-glioma immune responses and as a mediator of glioblastoma invasion, similar to factors like TGF-β which are relevant not only for immunosuppression but also for invasion processes. The data provide a therapeutic rationale to ameliorate treatment of glioblastoma by blockage of 4IgB7H3. First attempts to use 4IgB7H3 as a therapeutic target have recently been made with an antibody against 4IgB7H3 used to track neuroblastoma cells without intending to block 4IgB7H3 function itself [197]. Further experiments are needed to evaluate 4IgB7H3 as a target in the treatment of 4IgB7H3-expressing tumors. In addition, identification of the so far unidentified counter-receptor, which is according to the data at hand expressed on immune and glioblastoma cells, remains to be realized.

4.3 Conclusive remarks

Despite extensive research and clinical investigation of glioblastoma invasiveness and its underlying mechanisms, the issue of diffuse and infiltrative tumor growth still limits the feasibility of current glioblastoma treatment. This thesis is therefore mainly dealing with the identification and investigation of novel glioma invasion-related candidates and associated signaling mechanisms. This topic becomes even more important if one considers that radiation therapy and treatment modalities targeting angiogenesis elicit adaptive evasive response mechanisms which enhance diffuse tumor cell infiltration.

The clinical evaluation of radiation-enhanced mTOR inhibition by high-dose CCI-779 is currently ongoing in a european-wide trial. The same is true for the investigation of radiation-combined inhibition of CD95-mediated glioma invasion, since the novel compound APG101 is under clinical investigation at present. Irrespective of the clinical outcome and in order to further improve

targeting the non-apoptotic CD95-receptor signaling, further experimental approaches might deal with a specific inhibition of receptor downstream targets. Given that APG101 is currently investigated only for its effects in recurrent glioblastoma, one can also take into consideration to test this compound in combination with Temozolomide in newly diagnosed glioblastoma.

RGS4 was identified in this thesis as being a key regulator of glioma invasion. Merely indirect modulation of RGS4 by inhibition of the mTOR complexes 1 and 2 was investigated so far. Given the fact that several specific RGS4-inhibitors are already available, investigation of these compounds for their ability to modulate glioma invasion by specific RGS4-inhibition could be a promising approach.

The co-stimulatory molecule B7H3 was identified in this thesis to suppress tumor attacks by the immune system as well as to mediate invasiveness of glioblastoma cells. By mediating this dual role in glioma biology, B7H3 emerges as being an interesting target in future glioma therapy. The impact of anti-angiogenesis therapy triggered evasive resistance and the need for novel treatment strategies targeting tumor and vasculature at the same time as done by CCI-779 mediated mTOR-inhibition was widely discussed in this thesis. Recent data demonstrating the capability of glioma stem cells to differentiate into tumor vasculature generating endothelial cells [198, 199] even supports this need. This is even more supported by the finding that blocking of VEGF only inhibits the maturation of endothelial progenitors but not the differentiation of tumor stem-like cells into endothelial cells.

Taken together, from the findings presented in this thesis, several therapeutic options emerge for targeting unwanted adaptive evasive escape and immunosuppression and should be considered for further clinical investigation in glioblastoma therapy.

5. References

1. Buckner JC, Brown PD, O'Neill BP, Meyer FB, Wetmore CJ, Uhm JH (2007). Central nervous system tumors. Mayo Clin Proc 82: 1271-1286.

2. CBTRUS, Central Brain Tumor Registry of the United States (2011). CBTRUS Statistical Report: Primary Brain and Central Nervous System Tumors Diagnosed in the United States in 2004-2007. Central Brain Tumor Registry of the United States, Hinsdale, IL website.

3. Louis DN, Ohgaki H, Wiestler OD, Cavenee WK, Burger PC, Jouvet A, Scheithauer BW, Kleihues P (2007). The 2007 WHO classification of tumours of the central nervous system. Acta Neuropathol 114: 97-109.

4. Newton HB (1994). Primary brain tumors: review of etiology, diagnosis and treatment. Am Fam Physician 49: 787-797.

5. Kleihues P, Sobin LH (2000). World Health Organization classification of tumors. Cancer 88: 2887.

6. Ohgaki H, Kleihues P (2005). Population-based studies on incidence, survival rates, and genetic alterations in astrocytic and oligodendroglial gliomas. J Neuropathol Exp Neurol 64: 479-489.

7. Miller CR, Perry A (2007). Glioblastoma. Arch Pathol Lab Med 131: 397-406.

8. Ohgaki H, Dessen P, Jourde B, Horstmann S, Nishikawa T, Di Patre PL, Burkhard C, Schuler D, Probst-Hensch NM, Maiorka PC, Baeza N, Pisani P, Yonekawa Y, Yasargil MG, Lutolf UM, Kleihues P (2004). Genetic pathways to glioblastoma: a population-based study. Cancer Res 64: 6892-6899.

9. Balss J, Meyer J, Mueller W, Korshunov A, Hartmann C, von Deimling A (2008). Analysis of the IDH1 codon 132 mutation in brain tumors. Acta Neuropathol 116: 597-602.

10. Brown EJ, Albers MW, Shin TB, Ichikawa K, Keith CT, Lane WS, Schreiber SL (1994). A mammalian protein targeted by G1-arresting rapamycin-receptor complex. Nature 369: 756-758.

11. Knobbe CB, Merlo A, Reifenberger G (2002). Pten signaling in gliomas. Neuro Oncol 4: 196-211.

12. Watanabe K, Sato K, Biernat W, Tachibana O, von Ammon K, Ogata N, Yonekawa Y, Kleihues P, Ohgaki H (1997). Incidence and timing of p53 mutations during astrocytoma progression in patients with multiple biopsies. Clin Cancer Res 3: 523-530.

13. Wong AJ, Ruppert JM, Bigner SH, Grzeschik CH, Humphrey PA, Bigner DS, Vogelstein B (1992). Structural alterations of the epidermal growth factor receptor gene in human gliomas. Proc Natl Acad Sci U S A 89: 2965-2969.

14. Weller M, Felsberg J, Hartmann C, Berger H, Steinbach JP, Schramm J, Westphal M, Schackert G, Simon M, Tonn JC, Heese O, Krex D, Nikkhah G, Pietsch T, Wiestler O, Reifenberger G, von Deimling A, Loeffler M (2009). Molecular predictors of progression-free and overall survival in patients with newly diagnosed glioblastoma: a prospective translational study of the German Glioma Network. J Clin Oncol 27: 5743-5750.

15. Phillips HS, Kharbanda S, Chen R, Forrest WF, Soriano RH, Wu TD, Misra A, Nigro JM, Colman H, Soroceanu L, Williams PM, Modrusan Z, Feuerstein BG, Aldape K (2006). Molecular subclasses of high-grade glioma predict prognosis, delineate a pattern of disease progression, and resemble stages in neurogenesis. Cancer Cell 9: 157-173.

16. Gilbertson RJ (2006). High-grade glioma: can we teach an old dogma new tricks? Cancer Cell 9: 147-148.

17. Stupp R, Mason WP, van den Bent MJ, Weller M, Fisher B, Taphoorn MJ, Belanger K, Brandes AA, Marosi C, Bogdahn U, Curschmann J, Janzer RC, Ludwin SK, Gorlia T, Allgeier A, Lacombe D, Cairncross JG, Eisenhauer E, Mirimanoff RO (2005). Radiotherapy plus concomitant and adjuvant temozolomide for glioblastoma. N Engl J Med 352: 987-996.

18. Hegi ME, Diserens AC, Gorlia T, Hamou MF, de Tribolet N, Weller M, Kros JM, Hainfellner JA, Mason W, Mariani L, Bromberg JE, Hau P, Mirimanoff RO, Cairncross JG, Janzer RC, Stupp R (2005). MGMT gene silencing and benefit from temozolomide in glioblastoma. N Engl J Med 352: 997-1003.

19. Wick W, Weller M, M. W, Batchelor TT, Yung WK, Platten M (2011). Pathway inhibition: emerging molecular targets for treating glioblastoma. Neurooncology in press.

20. Burger PC, Heinz ER, Shibata T, Kleihues P (1988). Topographic anatomy and CT correlations in the untreated glioblastoma multiforme. J Neurosurg 68: 698-704.

21. Nakada M Fau - Nakada S, Nakada S Fau - Demuth T, Demuth T Fau - Tran NL, Tran Nl Fau - Hoelzinger DB, Hoelzinger Db Fau - Berens ME, Berens ME Molecular targets of glioma invasion.

22. Teodorczyk M, Martin-Villalba A (2010). Sensing invasion: cell surface receptors driving spreading of glioblastoma. J Cell Physiol 222: 1-10.

23. Aplin AE, Howe A, Alahari SK, Juliano RL (1998). Signal transduction and signal modulation by cell adhesion receptors: the role of integrins, cadherins, immunoglobulin-cell adhesion molecules, and selectins. Pharmacol Rev 50: 197-263.

24. Tabatabai G, Weller M, Nabors B, Picard M, Reardon D, Mikkelsen T, Ruegg C, Stupp R (2010). Targeting integrins in malignant glioma. Target Oncol 5: 175-181.

25. Forsyth PA, Wong H, Laing TD, Rewcastle NB, Morris DG, Muzik H, Leco KJ, Johnston RN, Brasher PM, Sutherland G, Edwards DR (1999). Gelatinase-A (MMP-2), gelatinase-B (MMP-9) and membrane type matrix metalloproteinase-1 (MT1-MMP) are involved in different aspects of the pathophysiology of malignant gliomas. Br J Cancer 79: 1828-1835.

26. Rao JS (2003). Molecular mechanisms of glioma invasiveness: the role of proteases. Nat Rev Cancer 3: 489-501.

27. Rao JS, Steck PA, Mohanam S, Stetler-Stevenson WG, Liotta LA, Sawaya R (1993). Elevated levels of M(r) 92,000 type IV collagenase in human brain tumors. Cancer Res 53: 2208-2211.

28. Wick W, Platten M, Weller M (2001). Glioma cell invasion: regulation of metalloproteinase activity by TGF-beta. J Neurooncol 53: 177-185.

29. Wild-Bode C, Weller M, Wick W (2001). Molecular determinants of glioma cell migration and invasion. J Neurosurg 94: 978-984.

30. Newton HB (2004). Molecular neuro-oncology and development of targeted therapeutic strategies for brain tumors. Part 2: PI3K/Akt/PTEN, mTOR, SHH/PTCH and angiogenesis. Expert Rev Anticancer Ther 4: 105-128.

31. Gabelloni P, Da Pozzo E, Bendinelli S, Costa B, Nuti E, Casalini F, Orlandini E, Da Settimo F, Rossello A, Martini C Inhibition of metalloproteinases derived from tumours: new insights in the treatment of human glioblastoma. Neuroscience 168: 514-522.

32. Groves MD, Puduvalli VK, Hess KR, Jaeckle KA, Peterson P, Yung WK, Levin VA (2002). Phase II trial of temozolomide plus the matrix metalloproteinase inhibitor, marimastat, in recurrent and progressive glioblastoma multiforme. J Clin Oncol 20: 1383-1388.

33. Levin VA, Phuphanich S, Yung WK, Forsyth PA, Maestro RD, Perry JR, Fuller GN, Baillet M (2006). Randomized, double-blind, placebo-controlled trial of marimastat in glioblastoma multiforme patients following surgery and irradiation. J Neurooncol 78: 295-302.

34. Grandal MV, Madshus IH (2008). Epidermal growth factor receptor and cancer: control of oncogenic signalling by endocytosis. J Cell Mol Med 12: 1527-1534.

35. Heimberger AB, Suki D, Yang D, Shi W, Aldape K (2005). The natural history of EGFR and EGFRvIII in glioblastoma patients. J Transl Med 3: 38.

36. Shinojima N, Tada K, Shiraishi S, Kamiryo T, Kochi M, Nakamura H, Makino K, Saya H, Hirano H, Kuratsu J, Oka K, Ishimaru Y, Ushio Y (2003). Prognostic value of epidermal growth factor receptor in patients with glioblastoma multiforme. Cancer Res 63: 6962-6970.

37. Smith JS, Tachibana I, Passe SM, Huntley BK, Borell TJ, Iturria N, O'Fallon JR, Schaefer PL, Scheithauer BW, James CD, Buckner JC, Jenkins RB (2001). PTEN mutation, EGFR amplification, and outcome in patients with anaplastic astrocytoma and glioblastoma multiforme. J Natl Cancer Inst 93: 1246-1256.

38. Mellinghoff IK, Wang MY, Vivanco I, Haas-Kogan DA, Zhu S, Dia EQ, Lu KV, Yoshimoto K, Huang JH, Chute DJ, Riggs BL, Horvath S, Liau LM, Cavenee WK, Rao PN, Beroukhim R, Peck TC, Lee JC, Sellers WR, Stokoe D, Prados M, Cloughesy TF, Sawyers CL, Mischel PS (2005). Molecular determinants of the response of glioblastomas to EGFR kinase inhibitors. N Engl J Med 353: 2012-2024.

39. Lal A, Glazer CA, Martinson HM, Friedman HS, Archer GE, Sampson JH, Riggins GJ (2002). Mutant epidermal growth factor receptor up-regulates molecular effectors of tumor invasion. Cancer Res 62: 3335-3339.

40. Lefranc F, Brotchi J, Kiss R (2005). Possible future issues in the treatment of glioblastomas: special emphasis on cell migration and the resistance of migrating glioblastoma cells to apoptosis. J Clin Oncol 23: 2411-2422.

41. Chakravarti A, Zhai G, Suzuki Y, Sarkesh S, Black PM, Muzikansky A, Loeffler JS (2004). The prognostic significance of phosphatidylinositol 3-kinase pathway activation in human gliomas. J Clin Oncol 22: 1926-1933.

42. Hara K, Maruki Y, Long X, Yoshino K, Oshiro N, Hidayat S, Tokunaga C, Avruch J, Yonezawa K (2002). Raptor, a binding partner of target of rapamycin (TOR), mediates TOR action. Cell 110: 177-189.

43. Jacinto E, Loewith R, Schmidt A, Lin S, Ruegg MA, Hall A, Hall MN (2004). Mammalian TOR complex 2 controls the actin cytoskeleton and is rapamycin insensitive. Nature cell biology 6: 1122-1128.

44. Kim DH, Sarbassov DD, Ali SM, King JE, Latek RR, Erdjument-Bromage H, Tempst P, Sabatini DM (2002). mTOR interacts with raptor to form a nutrient-sensitive complex that signals to the cell growth machinery. Cell 110: 163-175.

45. Sarbassov DD, Ali SM, Kim DH, Guertin DA, Latek RR, Erdjument-Bromage H, Tempst P, Sabatini DM (2004). Rictor, a novel binding partner of mTOR, defines a rapamycin-insensitive and raptor-independent pathway that regulates the cytoskeleton. Curr Biol 14: 1296-1302.

46. Laplante M, Sabatini DM (2009). mTOR signaling at a glance. J Cell Sci 122: 3589-3594.

47. Sabatini DM (2006). mTOR and cancer: insights into a complex relationship. Nat Rev Cancer 6: 729-734.

48. Sarbassov DD, Ali SM, Sabatini DM (2005). Growing roles for the mTOR pathway. Current opinion in cell biology 17: 596-603.

49. Guertin DA, Sabatini DM (2007). Defining the role of mTOR in cancer. Cancer Cell 12: 9-22.

50. Fults D, Pedone C (2000). Immunocytochemical mapping of the phosphatase and tensin homolog (PTEN/MMAC1) tumor suppressor protein in human gliomas. Neuro Oncol 2: 71-79.

51. Wang SI, Puc J, Li J, Bruce JN, Cairns P, Sidransky D, Parsons R (1997). Somatic mutations of PTEN in glioblastoma multiforme. Cancer Res 57: 4183-4186.

52. Platten M, Wick W, Weller M (2001). Malignant glioma biology: role for TGF-beta in growth, motility, angiogenesis, and immune escape. Microsc Res Tech 52: 401-410.

53. Weller M, Fontana A (1995). The failure of current immunotherapy for malignant glioma. Tumor-derived TGF-beta, T-cell apoptosis, and the immune privilege of the brain. Brain Res Brain Res Rev 21: 128-151.

54. Massague J, Wotton D (2000). Transcriptional control by the TGF-beta/Smad signaling system. The EMBO journal 19: 1745-1754.

55. Merzak A, McCrea S, Koocheckpour S, Pilkington GJ (1994). Control of human glioma cell growth, migration and invasion in vitro by transforming growth factor beta 1. Br J Cancer 70: 199-203.

56. Nakano A, Tani E, Miyazaki K, Yamamoto Y, Furuyama J (1995). Matrix metalloproteinases and tissue inhibitors of metalloproteinases in human gliomas. J Neurosurg 83: 298-307.

57. Platten M, Wick W, Wild-Bode C, Aulwurm S, Dichgans J, Weller M (2000). Transforming growth factors beta(1) (TGF-beta(1)) and TGF-beta(2) promote glioma cell migration via Up-regulation of alpha(V)beta(3) integrin expression. Biochem Biophys Res Commun 268: 607-611.

58. Lavrik I, Golks A, Krammer PH (2005). Death receptor signaling. J Cell Sci 118: 265-267.

59. Peter ME, Krammer PH (2003). The CD95(APO-1/Fas) DISC and beyond. Cell death and differentiation 10: 26-35.

60. Debatin KM, Krammer PH (2004). Death receptors in chemotherapy and cancer. Oncogene 23: 2950-2966.

61. Fulda S, Debatin KM (2004). Exploiting death receptor signaling pathways for tumor therapy. Biochim Biophys Acta 1705: 27-41.

62. Mahmood Z, Shukla Y Death receptors: targets for cancer therapy. Exp Cell Res 316: 887-899.

63. Chen L, Park SM, Tumanov AV, Hau A, Sawada K, Feig C, Turner JR, Fu YX, Romero IL, Lengyel E, Peter ME CD95 promotes tumour growth. Nature 465: 492-496.

64. Peter ME, Budd RC, Desbarats J, Hedrick SM, Hueber AO, Newell MK, Owen LB, Pope RM, Tschopp J, Wajant H, Wallach D, Wiltrout RH, Zornig M, Lynch DH (2007). The CD95 receptor: apoptosis revisited. Cell 129: 447-450.

65. Kleber S, Sancho-Martinez I, Wiestler B, Beisel A, Gieffers C, Hill O, Thiemann M, Mueller W, Sykora J, Kuhn A, Schreglmann N, Letellier E, Zuliani C, Klussmann S, Teodorczyk M, Grone HJ, Ganten TM, Sultmann H, Tuttenberg J, von Deimling A, Regnier-Vigouroux A, Herold-Mende C, Martin-Villalba A (2008). Yes and PI3K bind CD95 to signal invasion of glioblastoma. Cancer Cell 13: 235-248.

66. Wisniewski P, Ellert-Miklaszewska A, Kwiatkowska A, Kaminska B Non-apoptotic Fas signaling regulates invasiveness of glioma cells and modulates MMP-2 activity via NFkappaB-TIMP-2 pathway. Cellular signalling 22: 212-220.

67. Martinou M, Giannopoulou E, Malatara G, Argyriou AA, Kalofonos HP, Kardamakis D Ionizing radiation affects epidermal growth factor receptor signalling and metalloproteinase secretion in glioma cells. Cancer Genomics Proteomics 8: 33-38.

68. Wild-Bode C, Weller M, Rimner A, Dichgans J, Wick W (2001). Sublethal irradiation promotes migration and invasiveness of glioma cells: implications for radiotherapy of human glioblastoma. Cancer Res 61: 2744-2750.

69. Park Cm Fau - Park M-J, Park Mj Fau - Kwak H-J, Kwak Hj Fau - Lee H-C, Lee Hc Fau - Kim M-S, Kim Ms Fau - Lee S-H, Lee Sh Fau - Park I-C, Park Ic Fau - Rhee CH, Rhee Ch Fau - Hong S-I, Hong SI Ionizing radiation enhances matrix metalloproteinase-2 secretion and invasion of glioma cells through Src/epidermal growth factor receptor-mediated p38/Akt and phosphatidylinositol 3-kinase/Akt signaling pathways.

70. Kaur B, Khwaja FW, Severson EA, Matheny SL, Brat DJ, Van Meir EG (2005). Hypoxia and the hypoxia-inducible-factor pathway in glioma growth and angiogenesis. Neuro Oncol 7: 134-153.

71. Wang GL, Semenza GL (1995). Purification and characterization of hypoxia-inducible factor 1. The Journal of biological chemistry 270: 1230-1237.

72. Laughner E, Taghavi P, Chiles K, Mahon PC, Semenza GL (2001). HER2 (neu) signaling increases the rate of hypoxia-inducible factor 1alpha (HIF-1alpha) synthesis: novel mechanism

for HIF-1-mediated vascular endothelial growth factor expression. Mol Cell Biol 21: 3995-4004.

73. Zagzag D, Zhong H, Scalzitti JM, Laughner E, Simons JW, Semenza GL (2000). Expression of hypoxia-inducible factor 1alpha in brain tumors: association with angiogenesis, invasion, and progression. Cancer 88: 2606-2618.

74. Ehtesham M, Winston JA, Kabos P, Thompson RC (2006). CXCR4 expression mediates glioma cell invasiveness. Oncogene 25: 2801-2806.

75. Abounader R, Laterra J (2005). Scatter factor/hepatocyte growth factor in brain tumor growth and angiogenesis. Neuro Oncol 7: 436-451.

76. Hoelzinger DB, Demuth T, Berens ME (2007). Autocrine factors that sustain glioma invasion and paracrine biology in the brain microenvironment. J Natl Cancer Inst 99: 1583-1593.

77. Carmeliet P, Jain RK (2000). Angiogenesis in cancer and other diseases. Nature 407: 249-257.

78. Mentlein R, Held-Feindt J (2003). Angiogenesis factors in gliomas: a new key to tumour therapy? Naturwissenschaften 90: 385-394.

79. Folkman J (2006). Angiogenesis. Annu Rev Med 57: 1-18.

80. Folkman J, Merler E, Abernathy C, Williams G (1971). Isolation of a tumor factor responsible for angiogenesis. J Exp Med 133: 275-288.

81. Guertin DA, Sabatini DM (2009). The pharmacology of mTOR inhibition. Sci Signal 2: pe24.

82. Folkman J, Hanahan D (1991). Switch to the angiogenic phenotype during tumorigenesis. Princess Takamatsu Symp 22: 339-347.

83. Bergers G, Benjamin LE (2003). Tumorigenesis and the angiogenic switch. Nat Rev Cancer 3: 401-410.

84. Rundhaug JE (2005). Matrix metalloproteinases and angiogenesis. J Cell Mol Med 9: 267-285.

85. Jain RK, di Tomaso E, Duda DG, Loeffler JS, Sorensen AG, Batchelor TT (2007). Angiogenesis in brain tumours. Nat Rev Neurosci 8: 610-622.

86. Folkman J (2007). Angiogenesis: an organizing principle for drug discovery? Nat Rev Drug Discov 6: 273-286.

87. Louis DN (2006). Molecular pathology of malignant gliomas. Annual review of pathology 1: 97-117.

88. Kerbel R, Folkman J (2002). Clinical translation of angiogenesis inhibitors. Nat Rev Cancer 2: 727-739.

89. Norden AD, Drappatz J, Wen PY (2008). Novel anti-angiogenic therapies for malignant gliomas. Lancet neurology 7: 1152-1160.

90. Norden AD, Drappatz J, Wen PY (2009). Antiangiogenic therapies for high-grade glioma. Nature reviews 5: 610-620.

91. Wick W, Weller M, van den Bent M, Stupp R Bevacizumab and recurrent malignant gliomas: a European perspective. J Clin Oncol 28: e188-189; author reply e190-182.

92. Wick W, Wick A, Weiler M, Weller M Patterns of Progression in Malignant Glioma Following Anti-VEGF Therapy: Perceptions and Evidence. Curr Neurol Neurosci Rep.

93. Batchelor TT, Sorensen AG, di Tomaso E, Zhang WT, Duda DG, Cohen KS, Kozak KR, Cahill DP, Chen PJ, Zhu M, Ancukiewicz M, Mrugala MM, Plotkin S, Drappatz J, Louis DN, Ivy P, Scadden DT, Benner T, Loeffler JS, Wen PY, Jain RK (2007). AZD2171, a pan-VEGF receptor tyrosine kinase inhibitor, normalizes tumor vasculature and alleviates edema in glioblastoma patients. Cancer Cell 11: 83-95.

94. Rahman R, Smith S, Rahman C, Grundy R Antiangiogenic therapy and mechanisms of tumor resistance in malignant glioma. J Oncol 2010: 251231.

95. Winkler F, Kozin SV, Tong RT, Chae SS, Booth MF, Garkavtsev I, Xu L, Hicklin DJ, Fukumura D, di Tomaso E, Munn LL, Jain RK (2004). Kinetics of vascular normalization by VEGFR2 blockade governs brain tumor response to radiation: role of oxygenation, angiopoietin-1, and matrix metalloproteinases. Cancer Cell 6: 553-563.

96. Zuniga RM, Torcuator R, Jain R, Anderson J, Doyle T, Ellika S, Schultz L, Mikkelsen T (2009). Efficacy, safety and patterns of response and recurrence in patients with recurrent high-grade gliomas treated with bevacizumab plus irinotecan. J Neurooncol 91: 329-336.

97. Casanovas O, Hicklin DJ, Bergers G, Hanahan D (2005). Drug resistance by evasion of antiangiogenic targeting of VEGF signaling in late-stage pancreatic islet tumors. Cancer Cell 8: 299-309.

98. Gomez-Manzano C, Holash J, Fueyo J, Xu J, Conrad CA, Aldape KD, de Groot JF, Bekele BN, Yung WK (2008). VEGF Trap induces antiglioma effect at different stages of disease. Neuro Oncol 10: 940-945.

99. Kunkel P, Ulbricht U, Bohlen P, Brockmann MA, Fillbrandt R, Stavrou D, Westphal M, Lamszus K (2001). Inhibition of glioma angiogenesis and growth in vivo by systemic treatment with a monoclonal antibody against vascular endothelial growth factor receptor-2. Cancer Res 61: 6624-6628.

100. Paez-Ribes M, Allen E, Hudock J, Takeda T, Okuyama H, Vinals F, Inoue M, Bergers G, Hanahan D, Casanovas O (2009). Antiangiogenic therapy elicits malignant progression of tumors to increased local invasion and distant metastasis. Cancer Cell 15: 220-231.

101. Rubenstein JL, Kim J, Ozawa T, Zhang M, Westphal M, Deen DF, Shuman MA (2000). Anti-VEGF antibody treatment of glioblastoma prolongs survival but results in increased vascular cooption. Neoplasia 2: 306-314.

102. Bergers G, Hanahan D (2008). Modes of resistance to anti-angiogenic therapy. Nat Rev Cancer 8: 592-603.

103. Lin MI, Sessa WC (2004). Antiangiogenic therapy: creating a unique "window" of opportunity. Cancer Cell 6: 529-531.

104. Lee DF, Hung MC (2007). All roads lead to mTOR: integrating inflammation and tumor angiogenesis. Cell cycle: 3011-3014.

105. Kioi M, Vogel H, Schultz G, Hoffman RM, Harsh GR, Brown JM Inhibition of vasculogenesis, but not angiogenesis, prevents the recurrence of glioblastoma after irradiation in mice. The Journal of clinical investigation 120: 694-705.

106. Greenfield JP, Cobb WS, Lyden D Resisting arrest: a switch from angiogenesis to vasculogenesis in recurrent malignant gliomas. The Journal of clinical investigation 120: 663-667.

107. Vauleon E, Avril T, Collet B, Mosser J, Quillien V Overview of cellular immunotherapy for patients with glioblastoma. Clin Dev Immunol 2010.

108. Grauer OM, Wesseling P, Adema GJ (2009). Immunotherapy of diffuse gliomas: biological background, current status and future developments. Brain Pathol 19: 674-693.

109. Fenstermaker RA, Ciesielski MJ (2004). Immunotherapeutic strategies for malignant glioma. Cancer Control 11: 181-191.

110. Dhein J, Walczak H, Baumler C, Debatin KM, Krammer PH (1995). Autocrine T-cell suicide mediated by APO-1/(Fas/CD95). Nature 373: 438-441.

111. Jansen T, Tyler B, Mankowski JL, Recinos VR, Pradilla G, Legnani F, Laterra J, Olivi A FasL gene knock-down therapy enhances the antiglioma immune response. Neuro Oncol 12: 482-489.

112. Abou-Ghazal M, Yang DS, Qiao W, Reina-Ortiz C, Wei J, Kong LY, Fuller GN, Hiraoka N, Priebe W, Sawaya R, Heimberger AB (2008). The incidence, correlation with tumor-infiltrating inflammation, and prognosis of phosphorylated STAT3 expression in human gliomas. Clin Cancer Res 14: 8228-8235.

113. Rahaman SO, Vogelbaum MA, Haque SJ (2005). Aberrant Stat3 signaling by interleukin-4 in malignant glioma cells: involvement of IL-13Ralpha2. Cancer Res 65: 2956-2963.

114. Katz JB, Muller AJ, Prendergast GC (2008). Indoleamine 2,3-dioxygenase in T-cell tolerance and tumoral immune escape. Immunol Rev 222: 206-221.

115. Miyazaki T, Moritake K, Yamada K, Hara N, Osago H, Shibata T, Akiyama Y, Tsuchiya M (2009). Indoleamine 2,3-dioxygenase as a new target for malignant glioma therapy. Laboratory investigation. J Neurosurg 111: 230-237.

116. Zamanakou M, Germenis AE, Karanikas V (2007). Tumor immune escape mediated by indoleamine 2,3-dioxygenase. Immunol Lett 111: 69-75.

117. Suh WK, Gajewska BU, Okada H, Gronski MA, Bertram EM, Dawicki W, Duncan GS, Bukczynski J, Plyte S, Elia A, Wakeham A, Itie A, Chung S, Da Costa J, Arya S, Horan T, Campbell P, Gaida K, Ohashi PS, Watts TH, Yoshinaga SK, Bray MR, Jordana M, Mak TW (2003). The B7 family member B7-H3 preferentially down-regulates T helper type 1-mediated immune responses. Nat Immunol 4: 899-906.

118. Chapoval AI, Ni J, Lau JS, Wilcox RA, Flies DB, Liu D, Dong H, Sica GL, Zhu G, Tamada K, Chen L (2001). B7-H3: a costimulatory molecule for T cell activation and IFN-gamma production. Nat Immunol 2: 269-274.

119. Luo L, Chapoval AI, Flies DB, Zhu G, Hirano F, Wang S, Lau JS, Dong H, Tamada K, Flies AS, Liu Y, Chen L (2004). B7-H3 enhances tumor immunity in vivo by costimulating rapid clonal expansion of antigen-specific CD8+ cytolytic T cells. J Immunol 173: 5445-5450.

120. Crispen PL, Sheinin Y, Roth TJ, Lohse CM, Kuntz SM, Frigola X, Thompson RH, Boorjian SA, Dong H, Leibovich BC, Blute ML, Kwon ED (2008). Tumor cell and tumor vasculature expression of b7-h3 predict survival in clear cell renal cell carcinoma. ClinCancer Res 14: 5150-5157.

121. Roth TJ, Sheinin Y, Lohse CM, Kuntz SM, Frigola X, Inman BA, Krambeck AE, McKenney ME, Karnes RJ, Blute ML, Cheville JC, Sebo TJ, Kwon ED (2007). B7-H3 ligand expression by prostate cancer: a novel marker of prognosis and potential target for therapy. Cancer Res 67: 7893-7900.

122. Zang X, Thompson RH, Al-Ahmadie HA, Serio AM, Reuter VE, Eastham JA, Scardino PT, Sharma P, Allison JP (2007). B7-H3 and B7x are highly expressed in human prostate cancer and associated with disease spread and poor outcome. ProcNatlAcadSciUSA 104: 19458-19463.

123. Seaman S, Stevens J, Yang MY, Logsdon D, Graff-Cherry C, St CB (2007). Genes that distinguish physiological and pathological angiogenesis. Cancer Cell 11: 539-554.

124. Zhang G, Hou J, Shi J, Yu G, Lu B, Zhang X (2008). Soluble CD276 (B7-H3) is released from monocytes, dendritic cells and activated T cells and is detectable in normal human serum. Immunology 123: 538-546.

125. Svendsen CN, ter Borg MG, Armstrong RJ, Rosser AE, Chandran S, Ostenfeld T, Caldwell MA (1998). A new method for the rapid and long term growth of human neural precursor cells. Journal of neuroscience methods 85: 141-152.

126. Rieger J, Lemke D, Maurer G, Weiler M, Frank B, Tabatabai G, Weller M, Wick W (2008). Enzastaurin-induced apoptosis in glioma cells is caspase-dependent and inhibited by BCL-XL. Journal of neurochemistry 106: 2436-2448.

127. Weiler M, Bahr O, Hohlweg U, Naumann U, Rieger J, Huang H, Tabatabai G, Krell HW, Ohgaki H, Weller M, Wick W (2006). BCL-xL: time-dependent dissociation between modulation of apoptosis and invasiveness in human malignant glioma cells. Cell death and differentiation 13: 1156-1169.

128. Berger B, Capper D, Lemke D, Pfenning PN, Platten M, Weller M, von Deimling A, Wick W, Weiler M (2010). Defective p53 antiangiogenic signaling in glioblastoma. Neuro Oncol 12: 894-907.

129. Friese MA, Wischhusen J, Wick W, Weiler M, Eisele G, Steinle A, Weller M (2004). RNA interference targeting transforming growth factor-beta enhances NKG2D-mediated antiglioma immune response, inhibits glioma cell migration and invasiveness, and abrogates tumorigenicity in vivo. Cancer Res 64: 7596-7603.

130. Fulda S, Wick W, Weller M, Debatin KM (2002). Smac agonists sensitize for Apo2L/TRAIL- or anticancer drug-induced apoptosis and induce regression of malignant glioma in vivo. Nature medicine 8: 808-815.

131. Rimner A, Wischhusen J, Naumann U, Gleichmann M, Steinbach JP, Weller M (2001). Identification by suppression subtractive hybridization of p21 as a radio-inducible gene in human glioma cells. Anticancer research 21: 3505-3508.

132. Tatenhorst L, Senner V, Puttmann S, Paulus W (2004). Regulators of G-protein signaling 3 and 4 (RGS3, RGS4) are associated with glioma cell motility. J Neuropathol Exp Neurol 63: 210-222.

133. Lund EL, Hog A, Olsen MW, Hansen LT, Engelholm SA, Kristjansen PE (2004). Differential regulation of VEGF, HIF1alpha and angiopoietin-1, -2 and -4 by hypoxia and ionizing radiation in human glioblastoma. International journal of cancer 108: 833-838.

134. Tabatabai G, Frank B, Mohle R, Weller M, Wick W (2006). Irradiation and hypoxia promote homing of haematopoietic progenitor cells towards gliomas by TGF-beta-dependent HIF-1alpha-mediated induction of CXCL12. Brain 129: 2426-2435.

135. Olsson AK, Dimberg A, Kreuger J, Claesson-Welsh L (2006). VEGF receptor signalling - in control of vascular function. Nature reviews 7: 359-371.

136. O'Reilly KE, Rojo F, She QB, Solit D, Mills GB, Smith D, Lane H, Hofmann F, Hicklin DJ, Ludwig DL, Baselga J, Rosen N (2006). mTOR inhibition induces upstream receptor tyrosine kinase signaling and activates Akt. Cancer Res 66: 1500-1508.

137. Sun SY, Rosenberg LM, Wang X, Zhou Z, Yue P, Fu H, Khuri FR (2005). Activation of Akt and eIF4E survival pathways by rapamycin-mediated mammalian target of rapamycin inhibition. Cancer Res 65: 7052-7058.

138. Tabernero J, Rojo F, Calvo E, Burris H, Judson I, Hazell K, Martinelli E, Ramon y Cajal S, Jones S, Vidal L, Shand N, Macarulla T, Ramos FJ, Dimitrijevic S, Zoellner U, Tang P, Stumm M, Lane HA, Lebwohl D, Baselga J (2008). Dose- and schedule-dependent inhibition of the mammalian target of rapamycin pathway with everolimus: a phase I tumor pharmacodynamic study in patients with advanced solid tumors. J Clin Oncol 26: 1603-1610.

139. Copp J, Manning G, Hunter T (2009). TORC-specific phosphorylation of mammalian target of rapamycin (mTOR): phospho-Ser2481 is a marker for intact mTOR signaling complex 2. Cancer Res 69: 1821-1827.

140. Hu X, Pandolfi PP, Li Y, Koutcher JA, Rosenblum M, Holland EC (2005). mTOR promotes survival and astrocytic characteristics induced by Pten/AKT signaling in glioblastoma. Neoplasia 7: 356-368.

141. Tabatabai G, Frank B, Wick A, Lemke D, von Kurthy G, Obermuller U, Heckl S, Christ G, Weller M, Wick W (2007). Synergistic antiglioma activity of radiotherapy and enzastaurin. Annals of neurology 61: 153-161.

142. Neshat MS, Mellinghoff IK, Tran C, Stiles B, Thomas G, Petersen R, Frost P, Gibbons JJ, Wu H, Sawyers CL (2001). Enhanced sensitivity of PTEN-deficient tumors to inhibition of FRAP/mTOR. Proc Natl Acad Sci U S A 98: 10314-10319.

143. Podsypanina K, Lee RT, Politis C, Hennessy I, Crane A, Puc J, Neshat M, Wang H, Yang L, Gibbons J, Frost P, Dreisbach V, Blenis J, Gaciong Z, Fisher P, Sawyers C, Hedrick-

Ellenson L, Parsons R (2001). An inhibitor of mTOR reduces neoplasia and normalizes p70/S6 kinase activity in Pten+/- mice. Proc Natl Acad Sci U S A 98: 10320-10325.

144. Shi Y, Gera J, Hu L, Hsu JH, Bookstein R, Li W, Lichtenstein A (2002). Enhanced sensitivity of multiple myeloma cells containing PTEN mutations to CCI-779. Cancer Res 62: 5027-5034.

145. Yang L, Clarke MJ, Carlson BL, Mladek AC, Schroeder MA, Decker P, Wu W, Kitange GJ, Grogan PT, Goble JM, Uhm J, Galanis E, Giannini C, Lane HA, James CD, Sarkaria JN (2008). PTEN loss does not predict for response to RAD001 (Everolimus) in a glioblastoma orthotopic xenograft test panel. Clin Cancer Res 14: 3993-4001.

146. Chen YW, Tekle C, Fodstad O (2008). The immunoregulatory protein human B7H3 is a tumor-associated antigen that regulates tumor cell migration and invasion. Curr Cancer Drug Targets 8: 404-413.

147. Zoncu R, Efeyan A, Sabatini DM mTOR: from growth signal integration to cancer, diabetes and ageing. Nature reviews 12: 21-35.

148. Guba M, von Breitenbuch P, Steinbauer M, Koehl G, Flegel S, Hornung M, Bruns CJ, Zuelke C, Farkas S, Anthuber M, Jauch KW, Geissler EK (2002). Rapamycin inhibits primary and metastatic tumor growth by antiangiogenesis: involvement of vascular endothelial growth factor. Nature medicine 8: 128-135.

149. Frost P, Moatamed F, Hoang B, Shi Y, Gera J, Yan H, Frost P, Gibbons J, Lichtenstein A (2004). In vivo antitumor effects of the mTOR inhibitor CCI-779 against human multiple myeloma cells in a xenograft model. Blood 104: 4181-4187.

150. Del Bufalo D, Ciuffreda L, Trisciuoglio D, Desideri M, Cognetti F, Zupi G, Milella M (2006). Antiangiogenic potential of the Mammalian target of rapamycin inhibitor temsirolimus. Cancer Res 66: 5549-5554.

151. Druey KM, Blumer KJ, Kang VH, Kehrl JH (1996). Inhibition of G-protein-mediated MAP kinase activation by a new mammalian gene family. Nature 379: 742-746.

152. Hurst JH, Hooks SB (2009). Regulator of G-protein signaling (RGS) proteins in cancer biology. Biochemical pharmacology 78: 1289-1297.

153. Cotton M, Claing A (2009). G protein-coupled receptors stimulation and the control of cell migration. Cellular signalling 21: 1045-1053.

154. De Vries L, Zheng B, Fischer T, Elenko E, Farquhar MG (2000). The regulator of G protein signaling family. Annual review of pharmacology and toxicology 40: 235-271.

155. Xie Y, Wolff DW, Wei T, Wang B, Deng C, Kirui JK, Jiang H, Qin J, Abel PW, Tu Y (2009). Breast cancer migration and invasion depend on proteasome degradation of regulator of G-protein signaling 4. Cancer Res 69: 5743-5751.

156. Weiler M, Pfenning P, Thiepold A, Jestaed L, Gronych J, Dittman L, Berger B, Jugold M, Kosch M, Weller M, Combs S, von Deimling A, Bendszus M, Platten M, Wick W (2011). Suppression of invasion-driving RGS4 by mTOR inhibition optimizes glioma treatment. manuscript submitted to Brain.

157. Pfenning P, Weiler M, Thiepold A, Jestaed L, Gronych J, Dittman L, Berger B, Jugold M, Combs S, Platten M, Wick W (2010). Novel antiinvasive and antiangiogenicmechanisms of mTOR inhibition in glioblastoma. Proceedings of the American Association for Cancer Research 101st Annual Meeting April 2010: (abstract 1308).

158. Ebert PJ, Campbell DB, Levitt P (2006). Bacterial artificial chromosome transgenic analysis of dynamic expression patterns of regulator of G-protein signaling 4 during development. I. Cerebral cortex. Neuroscience 142: 1145-1161.

159. Ebert PJ, Campbell DB, Levitt P (2006). Bacterial artificial chromosome transgenic analysis of dynamic expression patterns of regulator of G-protein signaling 4 during development. II. Subcortical regions. Neuroscience 142: 1163-1181.

160. Erdely HA, Lahti RA, Lopez MB, Myers CS, Roberts RC, Tamminga CA, Vogel MW (2004). Regional expression of RGS4 mRNA in human brain. The European journal of neuroscience 19: 3125-3128.

161. Ding J, Guzman JN, Tkatch T, Chen S, Goldberg JA, Ebert PJ, Levitt P, Wilson CJ, Hamm HE, Surmeier DJ (2006). RGS4-dependent attenuation of M4 autoreceptor function in striatal cholinergic interneurons following dopamine depletion. Nature neuroscience 9: 832-842.

162. Hooks SB, Martemyanov K, Zachariou V (2008). A role of RGS proteins in drug addiction. Biochemical pharmacology 75: 76-84.

163. Levitt P, Ebert P, Mirnics K, Nimgaonkar VL, Lewis DA (2006). Making the case for a candidate vulnerability gene in schizophrenia: Convergent evidence for regulator of G-protein signaling 4 (RGS4). Biological psychiatry 60: 534-537.

164. Cifelli C, Rose RA, Zhang H, Voigtlaender-Bolz J, Bolz SS, Backx PH, Heximer SP (2008). RGS4 regulates parasympathetic signaling and heart rate control in the sinoatrial node. Circulation research 103: 527-535.

165. Iankova I, Chavey C, Clape C, Colomer C, Guerineau NC, Grillet N, Brunet JF, Annicotte JS, Fajas L (2008). Regulator of G protein signaling-4 controls fatty acid and glucose homeostasis. Endocrinology 149: 5706-5712.

166. Ruiz de Azua I, Scarselli M, Rosemond E, Gautam D, Jou W, Gavrilova O, Ebert PJ, Levitt P, Wess J RGS4 is a negative regulator of insulin release from pancreatic beta-cells in vitro and in vivo. Proc Natl Acad Sci U S A 107: 7999-8004.

167. Siedlecki A, Anderson JR, Jin X, Garbow JR, Lupu TS, Muslin AJ RGS4 controls renal blood flow and inhibits cyclosporine-mediated nephrotoxicity. Am J Transplant 10: 231-241.

168. Blazer LL, Roman DL, Chung A, Larsen MJ, Greedy BM, Husbands SM, Neubig RR Reversible, allosteric small-molecule inhibitors of regulator of G protein signaling proteins. Molecular pharmacology 78: 524-533.

169. Blazer LL, Zhang H, Casey EM, Husbands SM, Neubig RR A nanomolar-potency small molecule inhibitor of Regulator of G protein Signaling (RGS) proteins. Biochemistry.

170. Roman DL, Blazer LL, Monroy CA, Neubig RR Allosteric inhibition of the regulator of G protein signaling-Galpha protein-protein interaction by CCG-4986. Molecular pharmacology 78: 360-365.

171. Roof RA, Roman DL, Clements ST, Sobczyk-Kojiro K, Blazer LL, Ota S, Mosberg HI, Neubig RR (2009). A covalent peptide inhibitor of RGS4 identified in a focused one-bead, one compound library screen. BMC Pharmacol 9: 9.

172. Roof RA, Sobczyk-Kojiro K, Turbiak AJ, Roman DL, Pogozheva ID, Blazer LL, Neubig RR, Mosberg HI (2008). Novel peptide ligands of RGS4 from a focused one-bead, one-compound library. Chem Biol Drug Des 72: 111-119.

173. Sparks CA, Guertin DA Targeting mTOR: prospects for mTOR complex 2 inhibitors in cancer therapy. Oncogene 29: 3733-3744.

174. Badruddoja MA, Das A, Chu RM, Gabyan E, Trimm H, Trycieky D, Yu J, Hurwitz C, Black KL (2006). Gefitinib and rapamycin for adult patients with recurrent glioblastoma multiforme. Neuro Oncol 8.

175. Chang SM, Wen P, Cloughesy T, Greenberg H, Schiff D, Conrad C, Fink K, Robins HI, De Angelis L, Raizer J, Hess K, Aldape K, Lamborn KR, Kuhn J, Dancey J, Prados MD (2005). Phase II study of CCI-779 in patients with recurrent glioblastoma multiforme. Invest New Drugs 23: 357-361.

176. Doherty L, Gigas DC, Kesari S, Drappatz J, Kim R, Zimmerman J, Ostrowsky L, Wen PY (2006). Pilot study of the combination of EGFR and mTOR inhibitors in recurrent malignant gliomas. Neurology 67: 156-158.

177. Galanis E, Buckner JC, Maurer MJ, Kreisberg JI, Ballman K, Boni J, Peralba JM, Jenkins RB, Dakhil SR, Morton RF, Jaeckle KA, Scheithauer BW, Dancey J, Hidalgo M, Walsh DJ (2005). Phase II trial of temsirolimus (CCI-779) in recurrent glioblastoma multiforme: a North Central Cancer Treatment Group Study. J Clin Oncol 23: 5294-5304.

178. Kreisl TN, Lassman AB, Mischel PS, Rosen N, Scher HI, Teruya-Feldstein J, Shaffer D, Lis E, Abrey LE (2009). A pilot study of everolimus and gefitinib in the treatment of recurrent glioblastoma (GBM). J Neurooncol 92: 99-105.

179. Reardon DA, Desjardins A, Vredenburgh JJ, Gururangan S, Friedman AH, Herndon JE, 2nd, Marcello J, Norfleet JA, McLendon RE, Sampson JH, Friedman HS Phase 2 trial of erlotinib plus sirolimus in adults with recurrent glioblastoma. J Neurooncol 96: 219-230.

180. Ronellenfitsch MW, Brucker DP, Burger MC, Wolking S, Tritschler F, Rieger J, Wick W, Weller M, Steinbach JP (2009). Antagonism of the mammalian target of rapamycin selectively mediates metabolic effects of epidermal growth factor receptor inhibition and protects human malignant glioma cells from hypoxia-induced cell death. Brain 132: 1509-1522.

181. Sancho-Martinez I, Martin-Villalba A (2009). Tyrosine phosphorylation and CD95: a FAScinating switch. Cell cycle (Georgetown, Tex 8: 838-842.

182. Biancone L, Martino AD, Orlandi V, Conaldi PG, Toniolo A, Camussi G (1997). Development of inflammatory angiogenesis by local stimulation of Fas in vivo. J Exp Med 186: 147-152.

183. Desbarats J, Birge RB, Mimouni-Rongy M, Weinstein DE, Palerme JS, Newell MK (2003). Fas engagement induces neurite growth through ERK activation and p35 upregulation. Nature cell biology 5: 118-125.

184. Hohlbaum AM, Saff RR, Marshak-Rothstein A (2002). Fas-ligand--iron fist or Achilles' heel? Clin Immunol 103: 1-6.

185. Eisele G, Roth P, Hasenbach K, Aulwurm S, Wolpert F, Tabatabai G, Wick W, Weller M APO010, a synthetic hexameric CD95 ligand, induces human glioma cell death in vitro and in vivo. Neuro Oncol 13: 155-164.

186. Roth W, Fontana A, Trepel M, Reed JC, Dichgans J, Weller M (1997). Immunochemotherapy of malignant glioma: synergistic activity of CD95 ligand and chemotherapeutics. Cancer Immunol Immunother 44: 55-63.

187. Weller M, Frei K, Groscurth P, Krammer PH, Yonekawa Y, Fontana A (1994). Anti-Fas/APO-1 antibody-mediated apoptosis of cultured human glioma cells. Induction and modulation of sensitivity by cytokines. The Journal of clinical investigation 94: 954-964.

188. Weller M, Malipiero U, Rensing-Ehl A, Barr PJ, Fontana A (1995). Fas/APO-1 gene transfer for human malignant glioma. Cancer Res 55: 2936-2944.

189. Gratas C, Tohma Y, Van Meir EG, Klein M, Tenan M, Ishii N, Tachibana O, Kleihues P, Ohgaki H (1997). Fas ligand expression in glioblastoma cell lines and primary astrocytic brain tumors. Brain Pathol 7: 863-869.

190. Saas P, Walker PR, Hahne M, Quiquerez AL, Schnuriger V, Perrin G, French L, Van Meir EG, de Tribolet N, Tschopp J, Dietrich PY (1997). Fas ligand expression by astrocytoma in vivo: maintaining immune privilege in the brain? The Journal of clinical investigation 99: 1173-1178.

191. Ichinose M, Masuoka J, Shiraishi T, Mineta T, Tabuchi K (2001). Fas ligand expression and depletion of T-cell infiltration in astrocytic tumors. Brain Tumor Pathol 18: 37-42.

192. Shinohara ET, Cao C, Niermann K, Mu Y, Zeng F, Hallahan DE, Lu B (2005). Enhanced radiation damage of tumor vasculature by mTOR inhibitors. Oncogene 24: 5414-5422.

193. Roth W, Isenmann S, Nakamura M, Platten M, Wick W, Kleihues P, Bahr M, Ohgaki H, Ashkenazi A, Weller M (2001). Soluble decoy receptor 3 is expressed by malignant gliomas and suppresses CD95 ligand-induced apoptosis and chemotaxis. Cancer Res 61: 2759-2765.

194. Pfenning PN, Weiler M, Merz C, Jugold M, Gieffers C, Platten M, Fricke H, Wick W (2011). Inhibition of CD95 signalling by APG-101 enhances efficacy of radiotherapy (RT) and reduces RT-induced tumor satellite formation. Proceedings of the American Association for Cancer Research 102st Annual Meeting April 2011: (abstract LB-382).

195. Zhai GG, Malhotra R, Delaney M, Latham D, Nestler U, Zhang M, Mukherjee N, Song Q, Robe P, Chakravarti A (2006). Radiation enhances the invasive potential of primary glioblastoma cells via activation of the Rho signaling pathway. J Neurooncol 76: 227-237.

196. Zhang GB, Chen YJ, Shi Q, Ma HB, Ge Y, Wang Q, Jiang Z, Xu Y, Zhang XG (2004). Human recombinant B7-H3 expressed in E. coli enhances T lymphocyte proliferation and IL-10 secretion in vitro. Acta BiochimBiophysSin(Shanghai) 36: 430-436.

197. Kramer K, Kushner BH, Modak S, Pandit-Taskar N, Smith-Jones P, Zanzonico P, Humm JL, Xu H, Wolden SL, Souweidane MM, Larson SM, Cheung NK Compartmental intrathecal radioimmunotherapy: results for treatment for metastatic CNS neuroblastoma. J Neurooncol 97: 409-418.

198. Ricci-Vitiani L, Pallini R, Biffoni M, Todaro M, Invernici G, Cenci T, Maira G, Parati EA, Stassi G, Larocca LM, De Maria R Tumour vascularization via endothelial differentiation of glioblastoma stem-like cells. Nature 468: 824-828.

199. Wang R, Chadalavada K, Wilshire J, Kowalik U, Hovinga KE, Geber A, Fligelman B, Leversha M, Brennan C, Tabar V Glioblastoma stem-like cells give rise to tumour endothelium. Nature 468: 829-833.

6. List of Abbreviations

4EBP1	Eukaryotic translation initiation factor 4E binding protein 1
AKT/PKB	Protein kinase B
CCI-779	Temsirolimus / Torisel ®
CD31/ PECAM-1	Platelet endothelial cell adhesion molecule
CNS	Central nervous system
CT	Computed X-ray Tomography
DAPI	4',6-diamidino-2-phenylindole
DISC	Death-inducing signaling complex
DMSO	Dimethyl sulfoxide
ECM	Extracellular matrix
EGFR	Epidermal growth factor receptor
eIF4E	Eukaryotic translation initiation factor 4E
ENZA	Enzastaurin
GAPDH	Glyceraldehyde 3-phosphate dehydrogenase
GBM	Glioblastoma multiforme
GIC	Glioblastoma-initiating cells
GSK-3β	Glycogen synthase kinase-β
H&E	Hematoxylin and eosin stain
hCMEC	Human cerebral microvascular endothelial cells
HIF-1α	Hypoxia inducible factor-1α
HUVEC	Human umbilical vein endothelial cells
IC_{50}	Half maximal inhibitory concentration
MGMT	O^6-methyl-guanine-DNA-methyl-transferase
MLR	Mixed leukocyte reactions
MMP	Matrix metalloproteinase
MRI	Magnetic resonance imaging
MSP	Methylation-specific PCR
mTOR	Mammalian target of rapamycin
mTORC1 / mTORC2	mammalian target of rapamycin complex 1 and 2
NIH	National Institutes of Health (USA)
PCR	Polymerase chain reaction
PET	Positron Emission Tomography
PI3K	Phosphatidylinositol 3-kinase
PTEN	Phosphatase and tensin homolog deleted on chromosome 10
qRT-PCR	quantitative reverse transcription polymerase chain reaction
RGS4	Regulator of G protein signaling 4
RPS6	Ribosomal Protein S6
RT	Radiation therapy
S6K1	Ribosomal S6 kinase 1
SMA	Smooth muscle cell actin
TMZ	Temozolomide
VEGF	Vascular endothelial growth factor
VEGFR	Vascular endothelial growth factor receptor
WHO	World Health Organization

Erklärung gemäß §8 der Promotionsordnung der Naturwissenschaftlich-Mathematischen Gesamtfakultät der Universität Heidelberg

Hiermit erkläre ich, dass ich die vorliegende Dissertation selbst verfasst und mich dabei keiner anderen als der von mir ausdrücklich bezeichneten Quellen und Hilfen bedient habe. Des Weiteren erkläre ich, dass ich an keiner Stelle ein Prüfungsverfahren beantragt oder die Dissertation in dieser oder einer anderen Form bereits anderweitig als Prüfungsarbeit verwendet oder einer anderen Fakultät als Dissertation vorgelegt habe.

Heidelberg, den 24. März 2011 Philipp-Niclas Pfenning